

KAUNAS UNIVERSITY OF TECHNOLOGY

GINTARĖ GRYBAUSKAITĖ-KAMINSKIENĖ

SYNTHESIS, STUDIES AND
APPLICATION IN OLEDs OF NEW
CARBAZOLE DERIVATIVES, CONTAINING
10*H*-PHENOTHIAZINE, TRIPHENYLSILANE,
SULFONYL-4-METHYLBENZENE AND
BENZONITRILE MOIETIES

Doctoral dissertation
Technological sciences, Materials engineering (T 008)

2019, Kaunas

This doctoral dissertation was prepared in Kaunas University of Technology, Faculty of Chemical Technology, Department of Polymer Chemistry and Technology during the period of 2014–2018. The studies were supported by the Research Council of Lithuania.

Scientific supervisor:

Assoc. Prof. Dr. Audrius BUČINSKAS (Kaunas University of Technology, Physical sciences, Chemistry N 003; Technological sciences, Materials engineering T 008) (2017-2018).

Prof. Dr. Gintaras BUIKA (Kaunas University of Technology, Technological sciences, Chemistry engineering T 005) (2014-2017).

Doctoral dissertation has been published in:

<http://ktu.edu>

Editor:

Dr. Armandas Rumšas (Publishing Office “Technologija”)

© G. Grybauskaitė-Kaminskienė, 2019

ISBN 978-609-02-1627-9

The bibliographic information about the publication is available in the National Bibliographic Data Bank (NBDB) of the Martynas Mažvydas National Library of Lithuania

KAUNO TECHNOLOGIJOS UNIVERSITETAS

GINTARĖ GRYBAUSKAITĖ-KAMINSKIENĖ

NAUJŲ KARBAZOLO DARINIŲ, TURINČIŲ
10*H*-FENTIAZINO, TRIFENILSILANO,
FOSFONIL-4-METILBENZENO IR
BENZNITRILO FRAGMENTUS, SINTEZĖ,
SAVYBIŲ TYRIMAI IR PRITAIKYMAS
ORGANINIUOSE ŠVIESTUKUOSE

Daktaro disertacija
Technologiniai mokslai, Medžiagų inžinerija (T 008)

2019, Kaunas

Disertacija parengta 2014-2018 metais Kauno technologijos universiteto Cheminės technologijos fakultete, Polimerų chemijos ir technologijos katedroje. Mokslinius tyrimus rėmė Lietuvos mokslo taryba.

Mokslinis vadovas:

Doc. dr. Audrius Bučinskas (Kauno technologijos universitetas, Fiziniai mokslai, Chemija N 003; Technologijos mokslai, Medžiagų inžinerija T 008) (2017-2018 m.).
Prof. Dr. Gintaras Buika (Kauno technologijos universitetas, Technologijos mokslai, Chemijos inžinerija T 005 (2014-2017 m.).

Interneto svetainės, kurioje skelbiama disertacija, adresas: <http://ktu.edu>

Redagavo:

Dr. Armandas Rumšas (leidykla “Technologija”)

© G. Grybauskaitė-Kaminskienė, 2019

ISBN (įrašyti gautą ISBN kodą)

Leidinio bibliografinė informacija pateikiama Lietuvos nacionalinės Martyno Mažvydo bibliotekos Nacionalinės bibliografijos duomenų banke (NBDB).

List of Abbreviations

(PBi) ₂ Ir(acac)	bis(2,N-diphenylbenzimidazolito) iridium(III) acetylacetonate
(PPy) ₂ Ir(acac)	bis(2-phenylpyridinato)iridium(III) acetylacetonate
¹³ C NMR	carbon nuclear magnetic resonance
¹⁹ F NMR	fluorine nuclear magnetic resonance
¹ H NMR	proton nuclear magnetic resonance
AIE	aggregation induced emission
Al	aluminum
BCP	2,9-Dimethyl-4,7-diphenyl-1,10-phenanthroline
BiCz	9 <i>H</i> , 9' <i>H</i> -3,3'-bicarbazole
Bphen	4,7-Diphenyl-1,10-phenanthroline
CIE	International Commission on Illumination
CT	charge transfer
Cu	copper
CV	cyclic voltamperometry
D-A	donor-acceptor
DF	delayed fluorescence
DFT	density functional theory
DMF	<i>N, N</i> -dimethylformamide
DPEPO	bis[2-(diphenylphosphino)phenyl] ether oxide
DSC	differential scanning calorimetry
E _A	electron affinity
EBL	electron blocking layer
E _g	energy band-gap
EL	electroluminescence
EML	emissive layer
EQE	external quantum efficiency
ET	triplet energy
ETL	electron transporting layer
<i>f</i>	oscillator strength
FIrpic	bis[2-(4,6-difluorophenyl)pyridinato-C ² ,N](picolinato) iridium(III)
FMO	frontier molecular orbitals
HIL	hole injection layer
HOMO	highest occupied molecular orbital
HTL	hole transporting layer
HTM	hole transporting material
ICS	intersystem crossing
ICT	intramolecular charge transfer
IP	ionization potential

IP _{CV}	ionization potential estimated by cyclic voltamperometry
IP _{PE}	ionization potential estimated by electron photoemission technique
IQE	internal quantum efficiency
IR	infrared
Ir(piq) ₂ (acac)	bis[2-(1-isoquinoliny- <i>N</i>)phenyl- <i>C</i>](2,4-pentanedionato- <i>O</i> ² , <i>O</i> ⁴)iridium(III)
Ir(ppy) ₃	tris[2-phenylpyridinato- <i>C</i> ² , <i>N</i>]iridium(III)
ISC	intersystem crossing
ITO	indium tin oxide
<i>k</i> _{ISC}	intersystem crossing rate constant
LUMO	lowest unoccupied molecular orbital
mCP	1,3-bis(<i>N</i> -carbazolyl)benzene
m-MTDATA	4,4',4''-tris[phenyl(<i>m</i> -tolyl)amino]triphenylamine
NPB	<i>N,N'</i> -bis(naphthalen-1-yl)- <i>N,N'</i> -bis(phenyl)benzidine
OLED	organic light-emitting diode
PF	prompt fluorescence
PhOLED	phosphorescent organic light-emitting diode
PLQY	photoluminescence quantum yield
PVD	physical vapor deposition
QE	quantum efficiency
RISC	reverse intersystem crossing
s	singlet
S ₀	ground singlet state
S ₁	the first excited singlet state
t	triplet
T ₁	the first excited triplet state
TADF	thermally activated delayed fluorescence
TCTA	tris(4-carbazoyl-9-ylphenyl)amine
TCz1	9'-(2-ethylhexyl)-9'H-9,3':6',9''-tercarbazole
<i>T</i> _d	destruction temperature
TD-DFT	time-dependent density functional theory
<i>T</i> _g	glass transition temperature
TGA	thermogravimetric analysis
TiO ₂	titanium (IV) oxide
TM	transition metals
<i>T</i> _m	melting point
TMEDA	tetramethylethylenediamine molybdenum trioxide MoO ₃
TOF	time of flight technique
TPBi	2,2',2''-(1,3,5-benzinetriyl)-tris(1-phenyl-1 <i>H</i> -benzimidazole)
TSPO1	diphenyl-4-triphenylsilylphenyl-phosphineoxide
TTA	triplet-triplet annihilation
t _{tr}	transit time

UV/Vis	ultraviolet/visible
V_{oc}	open-circuit photovoltage
V_{on}	turn-on voltage
γ	charge-balance factor
ΔE_{ST}	energy gap between singlet and triplet excited states
ε	dielectric constant
η_{ext}	external quantum efficiency
η_{PL}	photoluminescent quantum yield
λ_{max}^{abs}	absorption maximum
λ_{max}^{em}	emission maximum
μ	charge carrier mobility
μ_e	electron mobility
μ_h	hole mobility
μ_o	zero field mobility
τ	excited state lifetime

CONTENTS

1. INTRODUCTION.....	10
2. LITERATURE REVIEW.....	12
2.1. Introduction to the literature review.....	12
2.2. OLED structures.....	12
2.3. Operation principles of OLEDs.....	13
2.4. Basic mechanism of TADF.....	14
2.5. Molecular design of TADF emitters.....	18
2.6. Bicarbazole-based TADF emitters.....	21
2.7. Acridine based emitters for TADF OLEDs.....	25
2.8. Derivatives of phenoxazine as blue emitters for TADF OLEDs.....	32
2.9. Conclusions of the literature review.....	35
3. EXPERIMENTAL PART.....	36
3.1. Instrumentation and methods.....	36
3.1.1. Instrumentation.....	36
3.1.2. Methods.....	36
3.2. Computational details.....	37
3.3. Fabrication of phosphorescent light emitting diodes.....	38
3.4. Preparation of vacuum deposited OLEDs.....	38
3.5. Materials.....	39
4. RESULTS AND DISCUSSION.....	45
4.1 Derivatives with 9-ethyl-9 <i>H</i> -carbazole and 10 <i>H</i> -phenothiazine moieties.....	45
4.1.1. Synthesis.....	45
4.1.2. Theoretical investigation.....	46
4.1.3. Thermal properties.....	47
4.1.4. Optical and photophysical properties.....	47
4.1.5. Electrochemical properties and ionization potentials.....	50
4.1.6. Charge-transporting properties.....	51
4.1.7. Fabrication and characterization of PhOLEDs.....	52
4.2. Triphenylsilane and sulfonyl-4-methylbenzene-substituted bicarbazolyl derivatives.....	55
4.2.1. Synthesis.....	55

4.2.2. Thermal properties.....	56
4.2.3. Optical and photophysical properties	56
4.2.4. Electrochemical and photoelectrical properties	58
4.2.5. Charge-transporting properties	59
4.2.6. Fabrication and characterization of PhOLEDs	60
4.3. Bicarbazole-based derivative with (trifluoromethyl)benzotrile moiety as effective delayed fluorescence emitter	63
4.3.1. Synthesis.....	64
4.3.2. Thermal properties.....	64
4.3.3. Spectroscopic characterization	64
4.3.4. PL decay measurements	67
4.3.5. Ionization potential and charge-transporting properties	67
4.3.6. OLEDs characteristics	68
4.4. Carbazole and benzonitrile-based compounds	74
4.4.1. Synthesis.....	74
4.4.2. Theoretical investigation	75
4.4.3. Thermal properties.....	77
4.4.4. Photophysical properties	78
4.4.5. Electrochemical properties and ionization potentials	82
4.4.6. Charge-transporting properties	84
4.4.7. TADF behaviour.....	87
4.4.8. TADF OLEDs performance	89
5. CONCLUSIONS	95
6. REFERENCES	97
7. LIST OF PUBLICATIONS ON THE SUBJECT OF THE THESIS	111
8. LIST OF PRESENTATIONS AT INTERNATIONAL CONFERENCES....	111
9. ACKNOWLEDGEMENTS	112

1. INTRODUCTION

Organic light-emitting diodes (OLEDs) have been extensively designed and produced in the recent years. The instant popularity of OLEDs in the display and lighting markets was caused by extensive benefits that they offer, such as design flexibility, light weight, thinness, quick response time, and high device performance. Furthermore, OLED fabrication on plastic films has been implemented in many consumption areas because of the design flexibility and possibility to be applied in different forms [1]. However, OLEDs are hampered by some weaknesses, such as rather low efficiencies and short lifetimes. These issues need to be considered, and adaptation of OLEDs can be extended even further.

Consequently, it is relevant to develop emitting materials satisfying the requirements of high efficiency. Recently, it was reported that thermally activated delayed fluorescence (TADF) emitters can be used for the fabrication of high-efficiency OLEDs. Such devices are fabricated by utilizing pure organic materials which can acquire both singlet and triplet excitons for radiative transition [2]. Therefore, TADF emitters are appropriate as high-efficiency emitters for OLEDs and are replacing fluorescent and phosphorescent emitters.

Although considerable progress in the investigation and application of TADF emitters has been made, hosts are crucial in TADF OLEDs. Optimal combinations of emitters and hosts generally yield improved outcomes compared to those of the nondoped films.

Derivatives of carbazole are widely used in OLEDs as emitters and as hosts. However, easily synthesizable, inexpensive and efficient carbazolyl-containing hosts and emitters are still in great demand.

The aim of this work is design, synthesis, evaluation of the properties and estimation of applicability in OLEDs of newly synthesized derivatives of carbazole.

The tasks proposed for the achievement of the above stated aim:

- Synthesis, characterization and analysis of the properties and applicability in PhOLEDs of new bipolar host materials based on carbazole and phenothiazine moieties;
- Synthesis of a new series of functionalized 3,3'-bicarbazole derivatives, containing triphenylsilane, fluorocyanobenzene and 1-hydrosulfonyl-4-methylbenzene moieties on the 9,9'-positions; investigation of their thermal, electrochemical, photophysical, photoelectrical and charge transporting properties, and applicability in OLEDs;
- Synthesis and investigation of the properties of trifluoromethyl-substituted benzonitrile and carbazole derivatives having different substituents on the C-2,C-7-, C-3,C-6 positions of carbazole moiety, and estimation of their applicability in TADF OLEDs.

Novelty of the work:

- Two new low molar mass compounds based on phenothiazine as donor and carbazole as acceptor moieties were synthesized and investigated. The compounds exhibited ionization potentials of 5.10 eV and 5.25 eV and good ambipolar charge transporting properties. They were used as hosts for green and red PhOLEDs, and maximum power and external quantum efficiencies up to 47.5/40.6 lm/W and 20.0/10.5% for green and red PhOLEDs, respectively, were observed.
- New 3,3'-bicarbazole derivatives containing triphenylsilane, fluorocyanobenzene and 1-hydrosulfonyl-4-methylbenzene moieties on the 9,9'-positions were synthesized and studied as emitters exhibiting TADF and exciplex-forming properties. The device obtained by using one synthesized compound is characterized by the warm-white emission and by outstanding lighting characteristics: brightness of 40900 cd/m² (at 15 V), current efficiency of 53.8 cd/A, and power efficiency of 19.3 lm/W as well as external quantum efficiency of 18.8%.
- New carbazole and benzonitrile derivatives exhibiting both TADF and aggregation induced emission enhancement were designed, synthesized and characterized. Effects of methoxy- and *tert*-butyl-substituents attached to carbazole moiety on the photophysical properties were studied. It was established that the attachment of these substituents allows to increase the efficiency of delayed fluorescence (DF). The compounds were used to fabricate efficient non-doped OLEDs with maximum external quantum efficiency and brightness values of 7.2% and 15000 cd/m², respectively.

Contribution of the author

The author has designed, synthesized and purified 9 bipolar compounds. The author has performed and analyzed the results of thermal properties, infrared spectroscopy, absorption, cyclic voltammetry and photophysical measurements. Ionization potential and charge mobility investigations were performed and analyzed in collaboration with dr. Dmytro Volyniuk (Kaunas University of Technology). Organic light emitting diodes were prepared with the help of dr. Khrystyna Ivaniuk, dr. Nataliya Kostiv (Lviv Polytechnic University, Ukraine) and PhD student Oleksandr Bezvikonnyi (Kaunas University of Technology). The theoretical calculations and analysis of all compounds were carried out in contribution with dr. Gintautas Bagdžiūnas and dr. Viktorija Mimaitė.

2. LITERATURE REVIEW

2.1. Introduction to the literature review

The rapid evolution of optoelectronic device technologies justified by organic compounds in the recent decades has been determined both by the demand for light and flexible devices and by progressive absorption in new technologies with fragile environmental influence [3,4,5]. Organic light emitting diodes are among the category of organic based devices, and they contributed to the flourishing of the industry of smart phones, colored light sources and curved TV screens. Such OLED technology is attractive due to their significant superiority, such as full color and large area display, broad viewing angle, transparency and levity, low power consumption and high luminance efficiency [4,5].

Presently, organic electronics is known not only as a promising academic field but also as a prominent industry gaining in market rate every single year. Recently, OLEDs have been demonstrated to possess new utilization opportunities such as windows which emit light by night, or modern applications in home furniture permitting exclusive lighting projections [6].

Furthermore, OLED technologies can be additionally enhanced by investigation in some problematic areas, such as:

- the low stability of the blue light emission;
- short lifetimes of the devices;
- high cost and dependency on limited worldwide resources [6].

Hereby, organic optoelectronics is an intensively developing research field in chemistry, physics and materials engineering. Researchers are improving the performance of OLEDs by operating on materials and optimization of the device structures.

In this literature review, the latest progress in the design, synthesis and properties investigation of organic compounds characterizing bipolar molecular and TADF compounds architecture for optoelectronic applications will be discussed.

2.2. OLED structures

Fundamentally, an organic light emitting diode can be comprised of one organic layer sandwiched between two electrodes [7] proposing a better efficiency and lifetime because the characteristics of the separate layers can be coordinated through the suitable selection of organic materials. A simplified stack layout of a multilayer OLED is shown in **Fig. 2.2.1**.

The positively biased anode is demanded for holes injection into the hole transport layer (HTL), and electrons are injected from the cathode side into the electron transport layer (ETL) [7]. Highly efficient OLEDs usually possess some extra layers, such as blocking/ injection layers or the cathode interfacial layer (CIL) which protects the cathode from oxidation.

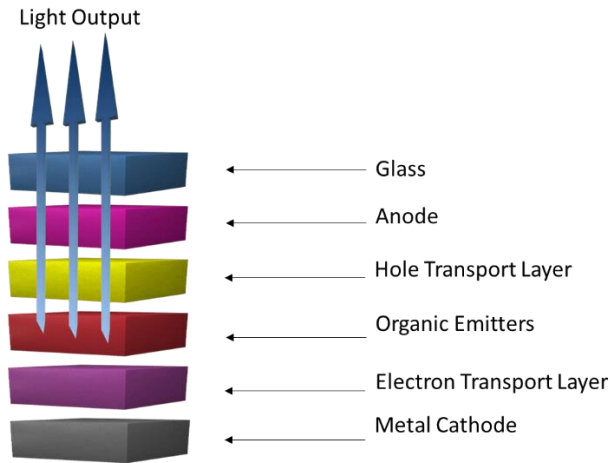


Fig. 2.2.1. A simplified illustration of multilayer OLEDs stack

The OLED is described as a solid-state device that is comprised of carbon-based layers, and the light is generated when electricity is employed by neighboring electrodes. One electrode must be translucent because of the light's exit from the diode. Constantly, the anode of an OLED contains of indium-tin oxide (ITO) which is known for its transparency and high electrical conductability [8]. The reverse situation is that of the cathode because it needs low work function metals, such as calcium or magnesium that are utilized in the formation with very reflective and responsive metals, such as aluminum and silver. Whilst the prevalent substrate material is glass, it is also conceivable to apply polymer or metal foils [9].

Because of the ambient conditions, organic materials are not stable, and for this purpose it is imperative to preserve them with an encapsulation [10]. The most prevalent technique uses a cover glass that is pasted to the substrate and so building a chamber fulfill with inert gas or a desiccant functionalizing as a getter to take up a slight quantity of oxygen and water that infiltrate during the encapsulation. The active zone of the OLED is described as the overlap of cathode and anode [11]. Thus OLEDs can essentially have a different form and size, and accordingly that can be suitable for various customization possibilities. In scientific laboratories, OLEDs are produced in standart scale of a few mm^2 , whereas in a commerce sector OLEDs are scaled-up to formats in $0.1\text{--}1\text{ m}^2$. The thickness of the layers is from 10 nm upwards [12].

2.3. Operation principles of OLEDs

The principal movements in an OLED under action are shown in **Fig. 2.3.1** for a multilayer device. An external voltage source is employed to the OLED, therefore, electrons from the cathode and holes from the anode are injected and flow at each other. In the emissive layer, electrons and holes form excitons that afterwards may split radiatively and emit photons [12]. The complete process can be divided into four

main stages (**Fig. 2.3.1**) [13]:

1. Injection of charge carriers at the electrodes;
2. Transportation of charge carriers over the organic layers;
3. Composition of excitons;
4. Radiative exciton splitting and release of light.

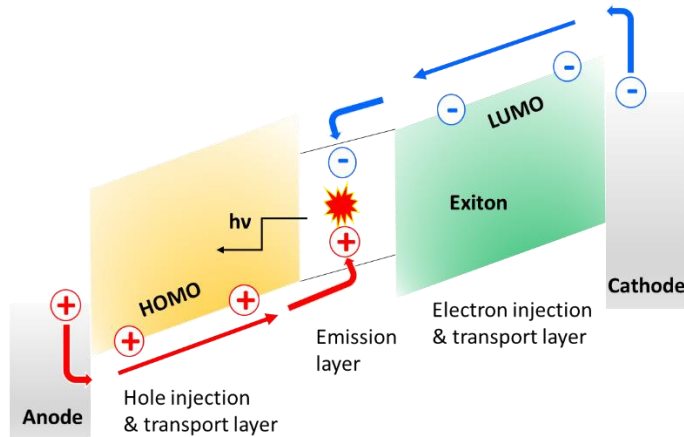


Fig.2.3.1. Illustration of a multilayer OLED demonstrating the main processes of electroluminescence

Electrons are injected from the cathode into the LUMO of the ETL, whereas holes are injected from the anode into HOMO of the HTL. When charge carriers are working in separate work functions Φ_A and Φ_C , built-in voltage Φ_{BI} appears in the diode [12]. The Φ_{BI} has to be managed by an external voltage V before the current can leak over the diode. If organic materials for the layers are suitably selected, recombination of charge carriers will be isolated to the EML, and the flow of profusion carriers which are not recombining will be diminished [14].

In general, in small molecule OLEDs, the generation of light can be isolated by appropriate organic materials with respective energy levels and layer thicknesses to a relatively small area sandwiched between HTL and ETL. Furthermore, if doped hole and electron injection layers are utilized [15], then this area can be situated at a nearly random length away from the electrodes. In order to prevent quenching and afterwards a reduction in efficiency, this system for recombination alongside the electrodes should be fairly conducive.

2.4. Basic mechanism of TADF

In general, fast radiative transition performs a valuable role when fluorescent organic materials emit light by this conversion in nanoseconds from a singlet excited state to a singlet ground state. In recent years, fluorescent organic compounds that provide extra light emission (in microseconds) have already been known; this

phenomenon is named delayed fluorescence (DF). In DF, emission is delayed because of the triplet-singlet transition operation [16].

The delayed fluorescence process is sorted into E-type and P-type DF processes (that depends on the nature of the triplet to singlet conversion process) [17]. The E-type delayed fluorescence stems from eosin, whilst triplet excitons can be transformed into singlet excitons under reverse intersystem crossing (RISC). RISC is mobilized by thermal energy and through a small singlet-triplet energy gap (ΔE_{ST}) [18]. Therefore, these movements are called the TADF effect. Meanwhile, P-type DF originates from pyrene, triplet-triplet annihilation (TTA), or when triplet-triplet connection establishes singlet excitons and supports fluorescent emission [19]. Both TADF emission and TTA emission processes use delayed fluorescence. However, these two emission processes differ in periods of the delayed fluorescence principle dependence on the temperature. The delayed fluorescence principle progressively enhances in the TADF and TTA operation; still, there is an onset temperature simply for the TADF emission when the delayed emission is stimulated by thermal activation in the TADF process [16] (Fig. 2.4.1).

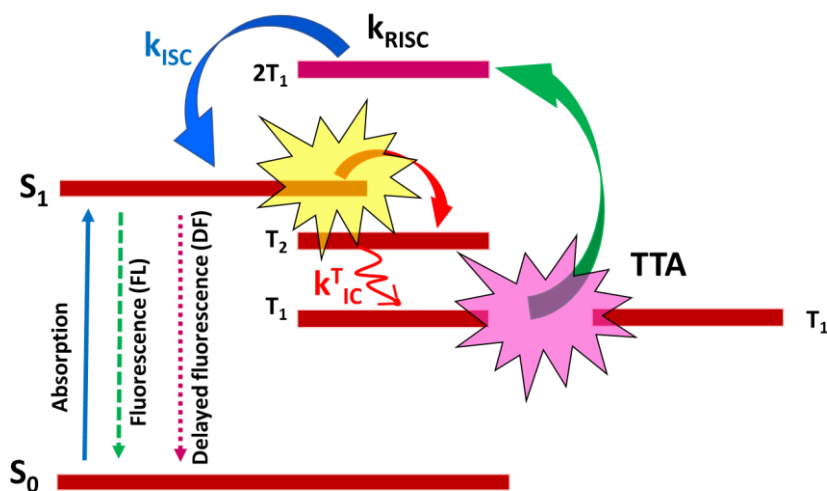


Fig. 2.4.1. Enhanced triplet-triplet annihilation efficiency

From the theoretical point of view, the internal quantum efficiency (QE) of the TADF operation is 100% while all triplet excitons can be converted into singlet excitons. Meanwhile, internal QE of the TTA process is 62.5% because the confrontation of two triplet excitons can cause only one singlet exciton [20]. To conclude, TADF emission is more effective than triplet-triplet annihilation emission.

In the perfect TADF process that is caused by electroluminescence (EL), 25% of light emission is induced from prompt fluorescence, and 75% of light emission is formed by delayed fluorescence by RISC. Such instant fluorescence is provoked by

fast $S_1 \rightarrow S_0$ conversion with excited state lifetime (τ) of a few nanoseconds. DF is delivered by slow $T_1 \rightarrow S_1 \rightarrow S_0$ conversion with longer τ in microseconds [1].

Specific emission processes involving PL and EL processes of TADF compounds are described in **Fig. 2.4.2**. In the PL action, singlet excitons are established by photoexcitation and the fluorescence or internal conversion to the singlet ground state, and some singlet excitons are transformed into triplet excitons by the intersystem crossing (ISC) process. Triplet excitons are also converted into singlet excitons by the RISC process or detained by the internal conversion process. The up-converted triplet excitons split radiatively by singlet emission or nonradiatively by internal conversion [1].

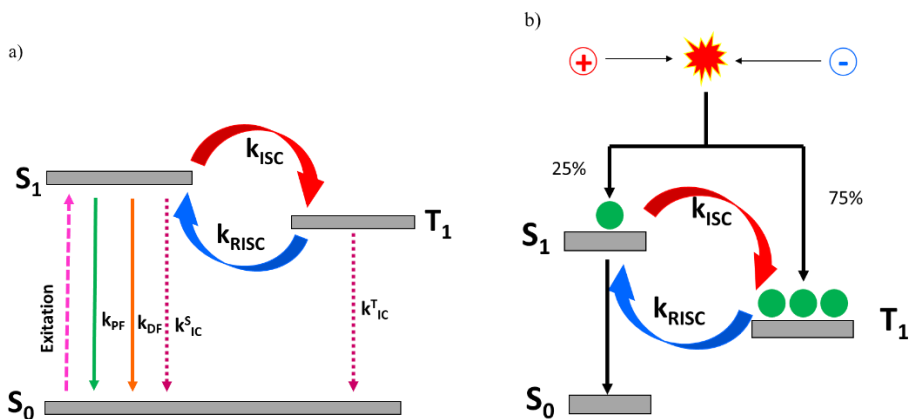


Fig. 2.4.2. Radiative and nonradiative transition process of thermally activated delayed fluorescent emitters by photoluminescence (a) and electroluminescence (b)

In the electroluminescence action of TADF compounds, both singlet and triplet excitons are developed by hole and electron injection. Singlet excitons split radiatively or nonradiatively. Moreover, singlet excitons can be converted into singlet excitons by RISC or be disbanded by internal conversion. However, triplet excitons are ingeniously designed by charge injection decay nonradiatively; or they can be up-converted into singlet excitons complying with radiative singlet emission or nonradiative internal conversion. It could be achieved by high EQE in TADF devices. Singlet emission by up-converted triplet excitons needs to be boosted as 75% of excitons produced by hole and electron injection are triplet excitons. Consequently, the triplet-to-singlet conversion and conducting singlet emission movements are crucial to the EQE of the TADF devices. As the efficacy of the TADF action is determined by the delayed fluorescence action, it is essential to generate TADF organic compounds with high triplet-to-singlet conversion efficiency and high $S_1 \rightarrow S_0$ transition efficiency simultaneously [16].

TADF emitters are relevant for boosting the efficiency and implementation of 3rd-generation heavy-metal-free OLEDs [21]. Furthermore, they are responsible for

the properties of the future display and lighting technologies [22]. Market technologists and researchers are trying to find a way towards the diminishing of the worldwide energy need on Earth, therefore, two physical criterions should be fulfilled for the achievement of efficient TADF emission in the emitters, among which, the most significant criterions are ΔE_{ST} and PL quantum yield (PLQY) that manage the power depletion of OLEDs.

Notably, lightweight and thin devices can be fabricated onto flexible substrates favoring infiltration of OLEDs in these two markets. With the aim of reducing the global energy demand on Earth, two parameters govern the power consumption of OLEDs, namely, the quantum yield of luminescence of the light emitting material, and device stacking [23].

ΔE_{ST} is related with the up-conversion of a triplet exciton into a singlet exciton, while PLQY is connected with the possibility of radiative transition [1].

Small ΔE_{ST} is relevant if we want to maximize the rISC rate constant (k_{rISC}) which is given by Equation (1), hence it is important to realize how this could be decreased in the molecular frame [24].

$$k_{rISC} A \exp - \frac{\Delta E_{ST}}{k_b T} \quad (1)$$

Small ΔE_{ST} enhances the k_{rISC} and triplet-to-singlet transition efficiency, which may enhance the external quantum efficiency of TADF emitters. For this purpose, mainly, TADF emitters were projected to possess small ΔE_{ST} for decent EQE in TADF devices.

Singlet energy (E_S) and triplet energy (E_T) are determined by the following Equations (2) and (3) where E is the orbital energy, and K is the electron repulsion energy:

$$E_S = E + K + J \quad (2)$$

$$E_T = E + K - J \quad (3)$$

Thus the ΔE_{ST} of organic compounds is simply reliant on the interchange energy among the singlet excited state and the triplet excited state:

$$\Delta E_{ST} = E_S - E_T = 2J \quad (4)$$

From Equation (4), it is obvious that detracting the singlet-triplet energy gap demands diminution of exchange energy J . J is calculated by utilizing Equation (5):

$$J = \iint \varphi(r_1)\psi(r_2) \left(\frac{e^2}{r_1-r_2} \right) \varphi(r_2)\psi(r_1) dr_1 dr_2 \quad (5)$$

The HOMO and LUMO wave functions are expressed by using φ and ψ , and e is the electron charge. This equation demonstrates that J can be decreased by diminishing the overlap between the HOMO and LUMO orbitals, which is attained by spatially discerning those frontier orbitals. This feature is fulfilled by organic molecules possessing electron donor (D) and electron acceptor (A) fragments which maintain D-A electron transmission in the excited states. In general, TADF molecules are created by D and A moieties connected through an aromatic bridge, and draw up excited states of a strong charge transporting property. ΔE_{ST} can be then diminished by twisted D and A moieties and receive D-A comparative direction near-orthogonality, or, preferably, by growing the D-A space while utilizing a molecular bridge [25].

The 2nd criterion is related with the light-emitting capacity of the emitter that is concerned with the nature, is the photoluminescence quantum yield (PLQY) of the emitter. With reference to the spin statistics, over electrical excitation, singlet and triplet excitons are concluded in 1:3 ratio [26]. Taking into account fluorescent materials, only singlet excitons can be used for light emission restricting the internal QE of fluorescent OLEDs to 25%. Whilst phosphorescent materials work contrarily, they can be beneficial for both singlet and triplet excitons in terms of emission by ISC for allowing to attain a theoretical IQE of 100% for phosphorescent OLEDs [27]. Among cons, triplet emitters are transition-metal complexes mainly based on Ir, Pt and Os, and the lack of these metals on Earth, their poisonousness and high market price make these materials improper candidates for the manufacturing of OLEDs [28]. Nevertheless, many attempts have also been performed to include emitters involving less toxic metals, supplying soften effects when verified in the devices [29,30].

In 2012, a breakthrough was made by the Adachi group which elaborated purely organic materials that are able to acquire singlet and triplet excitons for emission [2]. Such a novel group of light emitting compounds can be emulated with well-appointed triplet emitters. This indicates comparable efficiency in devices by establishing a new emission system; such emitters were named the 3rd generation of OLEDs emitters; they are thermally activated delayed fluorescence emitters. Hence, these TADF materials can thermally repopulate the singlet state from the triplet state by RISC, commanding an enhancement of the luminescence intensity. From the OLEDs point of view, TADF emitters comply with harvesting both singlet and triplet excitons for radiative transition, except for the fact that emission comes from the singlet state and not from the triplet state and that the TTA generally originating from phosphorescent OLEDs [31] can be considerably diminished (**Fig. 2.4.1**).

2.5. Molecular design of TADF emitters

TADF emitters have been elaborated to fulfill the main needs of small ΔE_{ST} and high PLQY which are closely related with light-emitting properties. Many researches

highlight that the donor-acceptor projection is the best way to generate TADF emitters, and the present emitters are designed on the grounds of the donor-acceptor molecular design strategy with small ΔE_{ST} [2,32,33]. Thus ΔE_{ST} can be decreased if the HOMO and LUMO are spatially seceded. This can be achieved by appropriate steric hindrance that imposes an internal twist and terminates the π -conjugation. This is also aided by an adequate range between the electron-donating and the electron-accepting moieties [34,35].

However, the ordinary donor and acceptor based molecular projection originates from a wide light emission spectrum induced by charge transfer (CT) emissive state and sometimes short lifetime due to the volatility of the chemical structure [16]. The large emission spectrum determines the color purity of the devices, and the instability of the molecular structure is interconnected with the lifetime of the devices. Therefore, the engineering of the ordinary donor-acceptor design has to be adjusted to make it free from these issues.

In the projection strategy of TADF materials, not only small ΔE_{ST} is important, but also the spin-orbit vibronic coupling. In fact, a small ΔE_{ST} is not enough to guarantee that a TADF derivative is an effective RISC that is vibronically coupled. To remain at the effective level, this spin-orbit coupling should also possess a valid rate. Currently, scientific researches studying the correlation between the spin-orbit coupling and RISC are still insufficient [36,37]. Taking into consideration that ΔE_{ST} is one of the most important parameters for verifying the RISC efficiency, that the dihedral angle among the donor (D) and the acceptor (A) can be heavily provided and that an overlap of both HOMO/LUMO energy levels could negatively influence the color purity and ΔE_{ST} , it has to be observed that the photophysical characteristics and the geometry of molecules that are assumed to be TADF emitters are often examined by theoretical calculations upper to the synthesis, optimizing the possibility to achieve eligible energy levels and the desirable ΔE_{ST} [23].

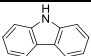
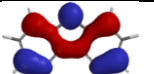
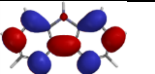
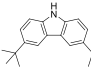
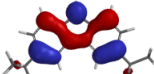
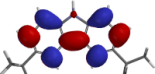
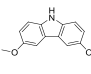
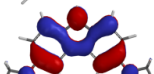
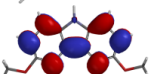
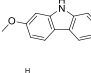
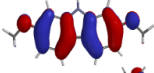
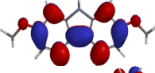
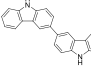
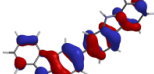
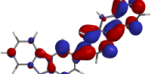
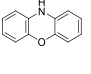
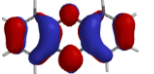
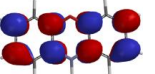
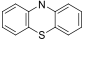
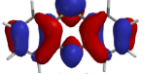
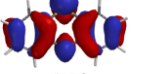
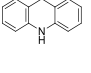
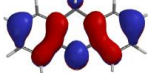
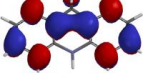
In order to manage the photophysical properties, the D and A fragments should be suitably selected. Intense donors and acceptors orient the HOMO and LUMO on the D and A fragment, respectively, which diminishes the singlet energy of the TADF emitters without major impact on the triplet energy by spatial isolation of the HOMO and LUMO [16]. Differently, weak donors and acceptors cause less important HOMO and LUMO localization, which follows in small reduction of the singlet energy. Consequently, strong D and A fragments are notable to faint D and A fragments to reduce emission energy of TADF emitters.

Thus it has been reported that many D and A moieties have been employed in the development of TADF emitters, and they are characterized by various D and A intensities that can be evaluated from the HOMO and LUMO of each emitter. High HOMO indicates low electron donor power, while superficial HOMO specifies potent electron donor power. When talking about the acceptor fragment, high LUMO implies potent acceptor power, while superficial LUMO proposes mild acceptor strength [16].

Commonly, such electron-donating chromophores were selected as **carbazole**, **bicarbazole**, **acridan**, **phenoxazine**, **phenothiazine**, etc., whereas electron-accepting fragments were chosen from the following moieties: diphenyl sulfone,

triazine, benzonitrile, oxadiazole, anthraquinone [1]. Molecular modeling data demonstrating the HOMO/LUMO localization and HOMO/LUMO levels of the D and A fragments are given in **Table 2.5.1.** and are obtained by utilizing the (TD)-B3LYP/6-31G(d,p) basis set introduced in Gaussian 09 software.

Table 2.5.1. HOMO and LUMO calculation results of donor moieties of thermally activated delayed fluorescent emitters

Donor	Chemical structure	Molecular orbital distribution ^a		HOMO, eV	LUMO, eV	Es/ET, eV
		HOMO	LUMO			
9H-carbazole				-5.46	0.66	4.15/ 3.19
3,6-di- <i>tert</i> -butyl-9H-carbazole				-5.25	-0.59	4.01/ 3.17
3,6-dimethoxy-9H-carbazole				-4.82	-0.67	3.69/ 2.88
2,7-dimethoxy-9H-carbazole				-4.99	-0.39	4.38/ 3.19
9H,9'H-3,3'-bicarbazole				-5.16	-0.83	3.30/ 3.05
10H-phenoxazine				-4.80	-0.22	3.66/ 2.81
10H-phenothiazine				-4.67	-0.44	3.42/ 2.69
9,9-dimethyl-9,10-dihydroacridine				-4.89	-0.08	3.78/ 3.19

^a The frontier molecular orbitals (HOMO/LUMO, isovalue is 0.02 a.u.) and the vertical energies of the lowest singlet and triplet states were computed by using (TD)-B3LYP/6-31G(d,p) methods in gas state, respectively

From the HOMO of the donor, the electron donating nature of the donor fragments can be determined, and the electron accepting nature of the acceptor moieties can be solved by the LUMO of the acceptor as stated earlier [16]. Among many electron-donating moieties, phenoxazine, phenothiazine and acridan are examples of strong donor moieties.

Even though the main investigation has been drawn toward announcing new TADF emitters, the hosts are valid in TADF OLEDs. However, new host materials are tested for their eligibility of serving as suitable hosts for PhOLEDs. What is more, the host material performs more important roles in the photophysics of TADF emitters.

2.6. Bicarbazole-based TADF emitters

In practice, there has been prominent advancement in the development and refinement of the external quantum efficiency (EQE) of the TADF OLEDs over the recent years [1], and the EQE of the TADF OLEDs resembles that of phosphorescent OLEDs. Accordingly, this literature review reveals the molecular design prospects of new TADF emitters and outlines future perspectives of TADF devices. In this literature review, we shall discuss organic-based blue TADF emitters that have been designed based on **bicarbazole**, **acridine** and **phenoxazine** moieties. Photophysical properties and compounds characteristics for the device performance will be analyzed and compared.

Carbazole is broadly used as an electron-donating moiety in the projection of host materials because of its good hole-transport properties and high E_T of ~ 2.95 eV [38,39]. It is observed that organic compounds based on its derivative of 9*H*,9'*H*-3,3'-bicarbazole (BiCz) demonstrate superior donor properties and lower driving voltages in comparison with mono-carbazole counterparts [40]. The meta-linked twisted structure of BiCz sustains high E_T of ~ 2.8 eV regardless of its expanded π conjugation [41]. Moreover, BiCz is characterized with a small ΔE_{ST} which is ~ 0.46 eV, and it is beneficial for energy transfer in PhOLEDs [42]. Additionally, BiCz derivatives demonstrate better electrochemical properties because of the partial blocking in the active C3 and C3' positions, which obviates the electrochemical oxidative polymerization of Cz and useful for the transportation of the positive charges (holes) in OLEDs. Taking into account the 9-*N*-positions of BiCz, hosts are usually blocked by different functional groups to provide their chemical stability and retain particular optoelectronic properties [43].

Tremendous effort was done to investigate various emitting materials for blue TADF OLEDs. The examples and the characteristics of bicarbazole-based donors used in blue or greenish-blue TADF OLEDs are given in **Table 2.6.1**. and **Fig. 2.6.1**. Most of blue TADF OLED devices have been developed by using DPEPO as the host material. Taking into account EQE, the best results were obtained by Kim *et al.* [44] in 2016 with the EQE value reaching 25%. **33TCzTTrz** showed the best external quantum efficiency not only among all TADF emitters introduced in **Table 2.6.1**, but also this material demonstrated one of the best external quantum efficiencies observed in greenish-blue devices [45,46]. Kim *et al.* synthesized three different bicarbazolyl moieties: 2,3'-bicarbazole (**23TCzTTrz**), 3,3'-bicarbazole (**33TCzTTrz**) and 3,4'-bicarbazole (**34TCzTTrz**) which were linked with diphenyltriazine in a twin emitting core type backbone structure. The studies showed that 3,3'-bicarbazolyl derivative was better than other counterparts in reducing its ΔE_{ST} value, which led to delayed fluorescence emission.

Cao *et al.* (2017) [47] synthesized two bicarbazole/dicyanobenzene hybrid compounds (**CF₃CNBCz** and **DCNBCz**). These TADF compounds exhibited the TADF phenomenon of a particularly small ΔE_{ST} of 0.01 eV, and were applied as the

sky-blue and greenish-blue delayed fluorescent emitters, respectively. The EL performance of the emitters was investigated in OLED, where 10wt.% of **CF₃CNBCz** and **DCNBCz** was doped in mCP. At 8 V voltage, these two different devices showed the EL peak in the sky-blue region (479 nm and 493 nm). At the same voltage, the cyano-substituted **DCNBCz** delivered better device performances, with the maximum current efficiency of 30.8 cd/A, power efficiency of 32.0 lm/W, and EQE of 10.0%, and CIE of (0.23, 0.43), while these values for the CF₃-substituted **CF₃CNBCz** containing device were 10.6 cd/A, 4.8 lm/W, 4.9% and (0.18, 0.32).

Kim *et al.* (2016) [48] investigated 3,3'-bicarbazole as a strong donor fragment and produced blue TADF emitters. As acceptors, 1,3,5-triphenyltriazine and benzophenone were used [49,50]. The devices were constructed and optimized for **BPBCz** and **TrzBCz** emitters by dispersing them in DPEPO host with the concentration of 10%. The EQE values of the **BPBCz** and **TrzBCz** doped devices were 23.3% and 23.6%, respectively. EL maxima were detected in the blue region (481 nm and 486 nm) with CIE coordinates of (0.21, 0.34) and (0.21, 0.36), respectively. The authors reported that 3,3'-bicarbazole as the donor performed two functions: the increase of the EQE and the lifetime of the TADF devices [48].

In 2013, Serevičius *et al.* [51] investigated a dicarbazole and triazine-based compound **CzT** (9-(4,6-diphenyl-1,3,5-triazin-2-yl)-9'-phenyl-3,3'-bicarbazole) which was employed as a perspective TADF emitter and showed blue-greenish emission with color coordinates of CIE (0.23, 0.4) and EQE of 6% at low current densities ($>10^{-1}$ mA/cm²).

Li *et al.* (2013) [40] developed A-D-A-type compounds (**26IPNDCz** and **35IPNDCz**), which featured dicyanobenzene (acceptor) and 3,3'-bicarbazole (donor). Bipolar emitters were doped into DPEPO with the concentration of 10 wt.%. The EL maxima of the **26IPNDCz** and **35IPNDCz** based devices were detected at 501 nm and 487 nm, respectively. The EQE values of the devices were 9.2% and 9.6%. It was reported that ortho-substitution of the cyano group on the phenyl ring can induce a larger twisting angle, more efficient separation of the HOMO and LUMO and a smaller ΔE_{ST} , but a shorter TADF lifetime.

Kim *et al.* (2015) [52] developed **34TCzPN** and **44TCzPN** as TADF emitters which were doped (from 5% to 20%) in DPEPO. In both cases, the best results were obtained with the concentration of 10%. EQE values varied from 19.5% to 20.5%. In OLED, both compounds (**34TCzPN** and **44TCzPN**) showed blue emission with the values of 475 nm (CIE_{xy} 0.17; 0.29) and 473 nm (CIE_{xy} 0.16; 0.23), respectively. These OLEDs based on the twin emitter design showed a significant increase of the efficiency of the device.

Shizu *et al.* (2015) [53] designed an efficient sky-blue TADF emitter material **BCzT** (9-(4-(4,6-diphenyl-1,3,5-triazin-2-yl)phenyl)-9'-phenyl-9H,9'H-3,3'-bicarbazole) which was doped into a host layer, and photoluminescence QY reached 95.6%, while EQE reached 21.7%. This OLED produced a sky-blue emission with the peak at 492 nm.

To conclude, 3,3'-bicarbazole is a strong donor fragment that is important for the diminishing ΔE_{ST} of D-A type molecules having separate HOMO and LUMO [54].

As the enhancement of the donor strength of the TADF emitters causes the HOMO shallowness and HOMO-LUMO gap narrowing, the singlet energy can be reduced by the strong 3,3'-bicarbazole donor rather than E_T . In addition, the CT character is strengthened, which also helps to reduce ΔE_{ST} . Therefore, a small ΔE_{ST} is expected from the 3,3'-bicarbazole-derived emitters. Hence, it can equally spread in the HOMO over the whole 3,3'-bicarbazole fragment for high oscillator strength in addition to the broad separation of the HOMO and LUMO [55]. Consequently, the 3,3'-bicarbazole fragment was proposed as the donor fragment of blue TADF emitters.

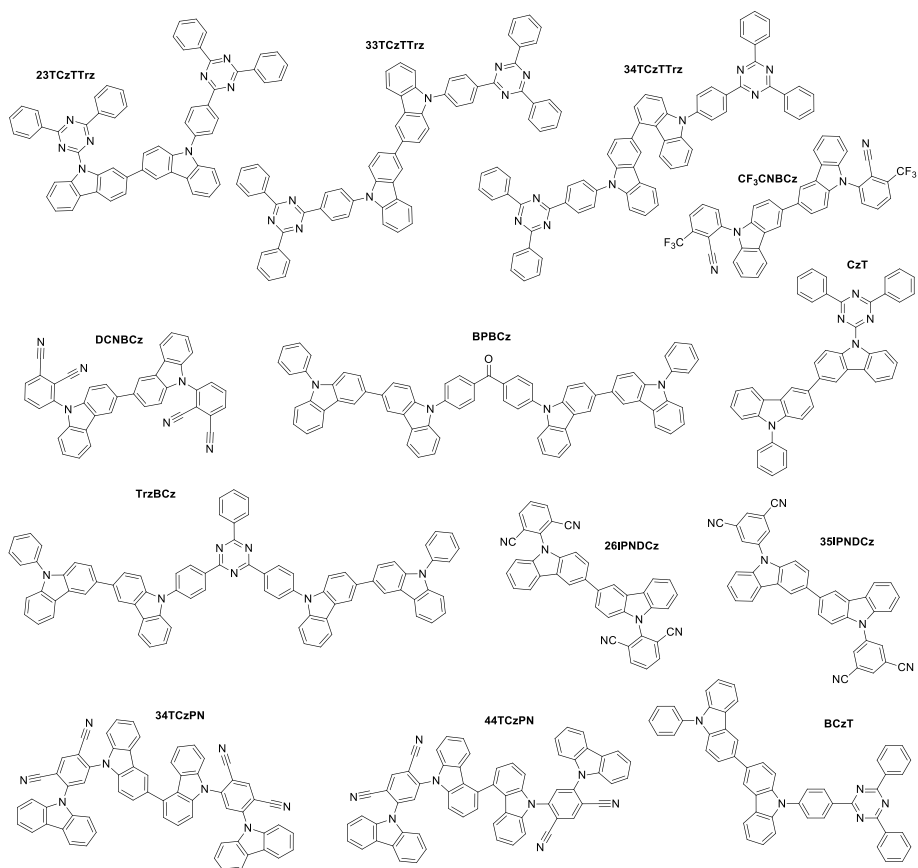


Fig. 2.6.1. Chemical structures of bicarbazole-based emitters for blue TADF OLEDs

Table 2.6.1. Photophysical and electrochemical properties of bicarbazole donor-based TADF emitters

Emitter	HOMO, eV	LUMO, eV	$E_T/\Delta E_{ST}$, eV	T_g , C ^o	T_d , C ^o	Host	V_{out} , V	L , cd m ⁻²	LE_{max} cd A ⁻¹	μ_p , lm W ⁻¹	EQE, %	EL λ_{max}	CIE1931, (x, y)	Ref. No.
23TCzTTrz	5.86	3.19	2.75/ 0.33	-	-	20% in DPEPO	-	-	28.4	22.3	10.7	472	(0.20, 0.26)	[44]
33TCzTTrz	5.74	3.21	2.76/ 0.25	-	-	20% in DPEPO	-	-	64.3	57.7	25.0	490	(0.23, 0.42)	[44]
34TCzTTrz	5.98	3.19	2.79/ 0.35	-	-	20% in DPEPO	-	-	19.1	15.0	10.3	463	(0.16, 0.20)	[44]
CF ₃ CNBCz	5.33	2.37	2.67/ 0.01	160	407	10% in mCP	3.3	8130	10.6	4.8	4.9	479	(0.18, 0.32)	[47]
DCNBCz	5.39	2.50	2.43/ 0.01	194	472	10% in mCP	2.9	28680	30.8	32.0	10.0	493	(0.23, 0.43)	[47]
BPBCz	5.78	-	2.87/ 0.11	-	-	10% in DPEPO	8.7	-	51.5	46.2	23.3	481	(0.21, 0.34)	[48]
TrzBCz	5.79	-	2.74/ 0.16	-	-	10% in DPEPO	10.1	-	53.5	46.8	23.6	486	(0.21, 0.36)	[48]
CzT	5.49	2.77	-	134	425	20% in DPEPO	-	393	-	9.7	6.0	520	(0.23, 0.4)	[51]
26IPNDCz	-	-	0.06/-	-	-	10% in DPEPO	-	-	-	-	9.6	501	-	[40]
35IPNDCz	-	-	0.14/-	-	-	10% in DPEPO	-	-	-	-	9.2	487	-	[40]
34TCzPN	6.30	3.52	2.86/ 0.16	-	-	10% in DPEPO	-	-	37.1	25.9	20.5	475	(0.17, 0.29)	[52]
44TCzPN	6.38	3.54	2.84/ 0.21	-	-	10% in DPEPO	-	-	32.9	23.0	19.5	473	(0.16, 0.23)	[52]
BCzT	-	-	-/ 0.29	-	-	6% in DPEPO	-	-	-	-	21.7	492	-	[53]

2.7. Acridine based emitters for TADF OLEDs

Additionally, external quantum efficiency is an important OLED characteristic that shows how efficient the power utilization is in the newly designed devices. Energy consumption can be optimized by using a properly selected efficient emitter [56]. Recently, an acridine fragment was often used in the D-A or D-A-D as a strong donor [57,58]. Regarding the strong electron-donating ability as well as stability and high triplet state energy, 9,9-dimethyl-9,10-dihydroacridine is used in the search of effective TADF emitters [59]. In this chapter, most promising TADF emitters based on the acridine moiety will be discussed (**Fig.2.7.1** and **Table 2.7.1**).

Yoo *et al.* (2016) [60] synthesized a new TADF emitter (**4DPTIA**) and employed it in the EL device using DPEPO as the host and different concentrations of the guest (10, 20 and 30%). The current density and luminance are increased at high doping concentrations that vary from 15% to 30% [61]. The device reached maximum EQE of 13.7%.

Zhang *et al.* (2014) [33] developed an efficient TADF emitter (**DMAC-DPS**) having pretwisted the intramolecular CT character. Doped in a DPEPO blue emitter was employed in the OLED structure with EQE reaching 19.5%. This device exhibits deep-blue emission with CIE coordinates of (0.16, 0.20).

Lin *et al.* (2016) [62] reported a new series of compounds whose design is based on spiroacridine-triazine (**SpiroAC-TRZ**, **DPAC-TRZ** and **DMAC-TRZ**) and which possess high PLQY of 100%, 82%, and 90%, respectively. The fabricated devices based on **SpiroAC-TRZ**, **DPAC-TRZ** and **DMAC-TRZ** showed EQE values of 36.7%, (94 cd A⁻¹, 98.4 lm W⁻¹), 25.8% (60 cd A⁻¹, 62.7 lm W⁻¹) and 27.4% (77.1 cd A⁻¹, 80.8 lm W⁻¹), respectively. Such a high efficiency (EQE > 30%) is much higher compared with the previously published results [56,63,64,65].

Ganesan *et al.* (2017) [66] synthesized **T1-T4** derivatives possessing dimethyl acridine as the electron donor which was binded to pyrimidine as an electron acceptor. OLEDs based on **T1-T4** exhibit EL peaks of 472, 492, 464 and 476 nm, respectively. The best results were achieved with **T2** TADF with the EQE value reaching 14.2%.

Park *et al.* (2017) [67] synthesized emitters based on a D-A system. By combining acridan-based donors and pyrimidine-based acceptors, five new compounds were produced: **MFAc-PPM**, **MXAc-PPM**, **MFAc-PM**, **MXAc-PM** and **Ac-PM**. The best result was achieved by utilizing **MFAc-PPM** TADF emitter demonstrated bright blue electroluminescence with EQE of 20.4%, maximum current efficiency of 41.7 cd A⁻¹, maximum power efficiency of 37.2 lm W⁻¹, and CIE_{xy} of (0.16, 0.23), (0.16, 0.20), (0.16, 0.21), (0.16, 0.19) and (0.15, 0.15), respectively.

Nakao *et al.* (2017) [68] designed three blue TADF emitters for high-performance TADF OLEDs. 2,4,6-triphenylpyrimidine was utilized as an acceptor, whereas tri-/ penta-substituted acridine was employed as the donor moiety: **Ac-46DPPM**, **Ac-26DPPM** and **CzAc-26DPPM**. The authors successfully developed blue and sky-blue devices with EQE ranging from 15.5% to 23.7%.

Im *et al.* (2017) [69] designed a new electron acceptor unit based on acrylonitrile which was in the deep blue TADF OLED. The electroluminescent device with a **CN-Ac** emitter demonstrated the maximum external quantum efficiency of 1.50% (CIE

(0.16, 0.28)).

Sasabe *et al.* (2017) [70] introduced 9,10-dihydro-9,9-dimethylacridine (Ac) and modified isonicotinitrile (INN) moieties into new compounds: **2AcINN** and **26AcINN**. These TADF emitters showed PLQY of 71% and 79% in the host films for **2AcINN** and **26AcINN**, respectively. A sky-blue emitter, **26AcINN**, showed low turn-on voltage of 2.9 V, high external quantum efficiency of 22%, and high power efficiency of 66 lm W⁻¹ with CIE chromaticity coordinates of (0.22, 0.45). In contrast, the **2AcINN**-based device emitted sky-blue light with CIE chromaticity coordinates of (0.19, 0.36), low turn-on voltage of 3.1 V, EQE of 13%, and power efficiency of 29 lm W⁻¹.

Takahashi *et al.* (2014) [71] reported two new compounds based on the D-A-D structure introducing 1,4-diazatriphenylene (ATP) derivatives with 9,9-dimethylacridane (**ATP-ACR** and **m-ATP-ACR**). The fabricated sky-blue emitting OLEDs containing **ATP-ACR** and **m-ATP-ACR** demonstrated EQE of 7.5% and 8.7%, respectively.

Kitamoto *et al.* (2015) [72] demonstrated a blue light emitting TADF molecule consisting of the π -conjugated system containing a boron atom as an electron-accepting moiety and 9,9-dimethylacridane (**10**) as an electron-donating moiety. The acridane moiety offered suitable twists between the donor and the cross-linking phenylene thus causing a very small ΔE_{ST} . OLED using organic structure **10** exhibited light blue emissions with EQE of 15.1%.

Park *et al.* (2016) [73] synthesized and tested a D-A-D molecule consisting of a phthalonitrile (VPN) acceptor core coupled with 9,9-dimethylacridan (Ac) as the donor moiety. π -Conjugated phenylene linkers were introduced between the donor and acceptor moieties to maintain a small ΔE_{ST} . OLED based on **Ac-VNP** emitter exhibited a high maximum EQE of 18.9% and an extremely small efficiency roll-off.

Komatsu *et al.* (2016) [74] developed an emitter denoted by **Ac-MPM** by introducing a phenylacridine part into the 4,6-position of the pyrimidine core to affect the twisted structure thus causing high photoluminescent QY of ~80%, and a small ΔE_{ST} of <0.20 eV. The optimized device achieved power efficiency of 62 lm W⁻¹, EQE of 24.5%, light-blue emission with the CIE chromaticity coordinates of (0.19, 0.37), and a low turn-on voltage of 2.8 V.

Lee *et al.* (2016) [75] synthesized a TADF emitter, **DMTDAc**, by using rigid 9,9-dimethyl-9H-thioxanthene 10,10-dioxide (DMTD) as the acceptor unit and acridine as the donor unit. They designed a deep blue TADF device with a CIE_{XY} of (0.15, 0.13) and EQE of 19.8%. The rigid DMTD acceptor diminished the emission spectrum of the emitter by interlocking two phenyl moieties of diphenylsulfone and shifted the emission spectrum to deep blue.

Numata *et al.* (2015) [76] developed highly efficient blue TADF molecules possessing 10H-phenoxaborin and acridan moieties (**1-3**). 10H-phenoxaborin was selected as the acceptor unit because of its excellent accepting properties stemming from the electron-withdrawing nature of the boron atom and an expanded π -plane [77]. Furthermore, bulky 2,4,6-triisopropylphenyl was imposed on the boron atom to

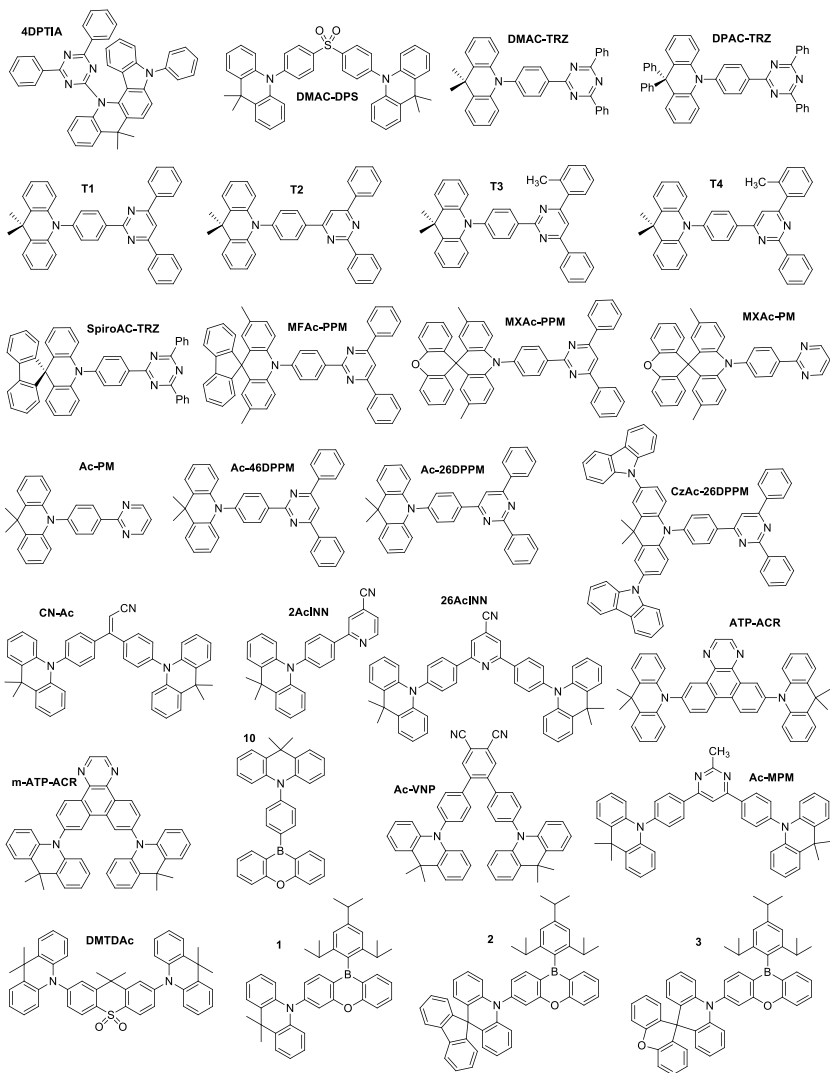
defend the boron center from nucleophilic species such as bases, oxygen, H₂O, and to evade disintegration in the reaction mixture, and regulate the reaction's atmospheric condition [78]. Additionally, in all the compounds, **1-3**, acridan was chosen as a wide-gap donor unit because acridan is characterized as a good donor. In conclusion, the authors designed pure blue TADF with EQE reaching 22% and CIE coordinates of ($\leq 0.16, \leq 0.16$). Furthermore, the authors claimed that utilizing emitter **3** was attained without any particular optimization [79].

Ohkuma *et al.* (2014) [80] synthesized and designed a spiro compound **DPAA-AF** possessing an electron-accepting diazafluorene moiety and an electron-donating bis(diphenylamino)acridane moiety. Employed in TADF OLED, **DPAA-AF** demonstrated blue-greenish electroluminescence with EQE of 9.6%.

Lee *et al.* (2016) [81] notified of two new efficient blue TADF emitters (**Ac-OPO** and **Ac-OSO**) having an angular-linked phenoxaphosphine oxide or phenoxathiin dioxide acceptor moiety linked with a dimethylacridan donor moiety. These D-A emitters were employed in blue TADF-OLED which exhibited EQE of 12.3% and 20.5% with color coordinates of (0.15, 0.14) and (0.16, 0.26) for **Ac-OPO** and **Ac-OSO**, respectively.

Luo *et al.* (2016) [82] established two solution-processed blue TADF emitters, **CzDMAC-DPS** and **DCzDMAC-DPS**. The electron donating part of the core based on 10,10'-(sulfonylbis(4,1-phenylene))bis(9,9-dimethyl-9,10-dihydroacridine) was extended by using *tert*-butyl carbazole moieties introduced for the emissive core. The double-layer blue devices based on these non-doped emitters attained the EQE of 12.2% and 2.2% with the CIE coordinates of (0.22, 0.44) and (0.18, 0.27) for **CzDMAC-DPS** and **DCzDMAC-DPS**, respectively.

To conclude, it is understandable that TADF emitters have a great potential as effective blue emitters, but only some design strategy methods have been reported to develop blue TADF emitters. One of the most promising methods is to couple donor and acceptor fragments by using such a strong donor as acridine. As it can be seen from this chapter, such good results highlighted a great chance for TADF materials to be candidates for achieving pure, effective and stable blue emission in OLEDs.



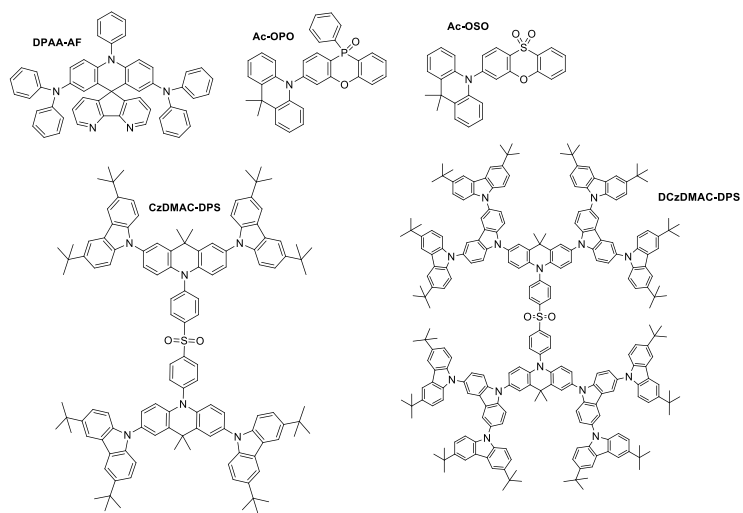


Fig. 2.7.1. Chemical structures of acridine-based emitters for blue TADF OLEDs

Table 2.7.1. Photophysical and electrochemical properties of acridine donor-based TADF emitters

Emitter	HOMO, eV	LUMO, eV	ΔE_{ST} , eV	T_g , C ^o	T_d , C ^o	HOST	V_{on} , V	I_{max} , cd m ⁻²	LE_{max} , cd A ⁻¹	μ_p , lm W ⁻¹	EQE, %	EL λ_{max}	CIE1931, (x, y)	Ref. No.
4DPTIA	6.09	3.20	0.23	-	-	DPEPO	-	-	24.8	17.0	13.7	-	(0.21, 0.31)	[60]
DMAC-DPS	5.92	2.92	0.09	-	-	DPEPO	3.7	-	-	-	19.5	-	(0.16, 0.20)	[33]
DMAC-TRZ	5.70	3.12	0.06	155	353	mCPCN	~2.0	-	77.1	80.8	27.4	-	(0.21, 0.50)	[62]
DPAC-TRZ	5.72	3.12	0.13	136	368	mCPCN	~2.0	-	60	62.7	25.8	-	(0.17, 0.38)	[62]
SpiroAC-TRZ	5.61	3.12	0.07	90	334	mCPCN	~2.0	-	94	98.4	36.7	-	(0.18, 0.43)	[62]
T1	5.34	2.45	-	95	368	DPEPO	3.0	2868	13.4	12.0	7.2	-	(0.17, 0.27)	[66]
T2	5.34	2.48	-	95	382	DPEPO	3.0	7385	34.2	29.8	14.2	-	(0.20, 0.39)	[66]
T3	5.33	2.37	-	93	369	DPEPO	3.0	1269	18.8	19.6	11.8	-	(0.17, 0.21)	[66]
T4	5.34	2.40	-	90	357	DPEPO	3.0	1867	24.0	21.5	11.8	-	(0.18, 0.30)	[66]
MFAc-PPM	5.62	2.67	0.25	-	422	PPF	3.4	-	41.7	37.2	20.4	470	(0.16, 0.23)	[67]
MXAc-PPM	5.65	2.68	0.25	-	422	PPF	3.6	-	22.7	18.8	12.2	462	(0.16, 0.20)	[67]
MFAc-PM	5.60	2.69	0.26	-	351	PPF	3.4	-	34.3	31.7	17.1	469	(0.16, 0.21)	[67]
MXAc-PM	5.65	2.70	0.29	-	354	PPF	3.6	-	25.0	20.7	14.3	460	(0.16, 0.19)	[67]
Ac-PM	5.68	2.70	0.30	-	288	PPF	3.6	-	18.9	16.5	11.4	458	(0.15, 0.15)	[67]
Ac-46DPPM	5.61	2.64	0.25	87	388	DPEPO	6.02	-	2.46	1.29	15.5	-	(0.16, 0.21)	[68]
Ac-26DPPM	5.67	2.70	0.17	90	383	DPEPO	4.92	-	13.5	8.61	19.3	-	(0.18, 0.33)	[68]
CzAc-26DPPM	5.72	2.84	0.12	181	453	DPEPO	4.88	-	21.9	14.1	23.7	-	(0.21, 0.38)	[68]
CN-Ac	5.15	2.62	0.03	-	n.d.	CBP	3.2	4644	2.85	2.43	1.50	460	(0.16, 0.28)	[69]
2AcINN	-	-	0.30	-	319	DPEPO	3.1	-	34.7	38.9	15.2	-	(0.19, 0.36)	[70]
26AcINN	-	-	0.28	141	433	DPEPO	2.9	-	58.4	65.6	21.6	-	(0.22, 0.45)	[70]
ATP-ACR	5.8	3.0	0.16	-	-	mCP	4.8	2300	11.5	5.7	7.5	496	-	[71]
m-ATP-ACR	5.9	3.1	0.13	-	-	mCBP	4.8	3240	13.1	6.2	8.7	486	-	[71]
10	5.81	2.46	0.01	-	-	DPEPO	8.5	8216	-	-	15.1	466	-	[72]
Ac-VNP	5.8	3.1	0.20	-	-	mCBP	4.5	65720	51.7	34.1	18.9	504	(0.23, 0.50)	[73]

Table 2.7.1. (continued)

Emitter	HOMO, eV	LUMO, eV	ΔE_{ST} , eV	T_g , C°	T_d , C°	HOST	V_{on} , V	L_{max} , cd m ⁻²	LE_{max} , cd A ⁻¹	μ_p , lm W ⁻¹	EQE, %	EL λ_{max}	CIE1931, (x, y)	Ref. No.
Ac-MPM	5.66	2.85	0.19	n.d.	432	mCP	2.8	-	-	61.6	24.5	487	(0.19, 0.37)	[74]
DMTDAc	6.10	3.35	-	-	-	TSPO1	<3.0	-	22.6	23.3	19.8	451	(0.15, 0.13)	[75]
1			0.10			PPF		>1500	-	-	21.7	475	(0.14, 0.23)	[76]
2			0.12			PPF		>1500	-	-	19.0	456	(0.14, 0.12)	[76]
3			0.06			PPF		-	-	-	20.1	451	(0.15, 0.09)	[76]
DPAA-AF	-	-	-	-	-	mCP	-	-	-	-	9.6	499	-	[80]
Ac-OPO	5.8	2.6	0.03	-	-	DPEPO	6.0	-	-	-	12.3	445	(0.15, 0.14)	[81]
Ac-OSO	5.7	2.6	0.06	-	-	DPEPO	5.1	-	37.9	20.1	20.5	486	(0.16, 0.26)	[81]
CzDMAC-DPS	5.24	2.31	0.09	272	459	Non-doped	3.6	-	30.6	24.0	12.2	492	(0.22, 0.44)	[82]
DCzDMAC-DPS	5.18	2.09	0.20	274	479	Non-doped	5.2	-	3.8	2.0	2.2	464	(0.18, 0.27)	[82]

2.8. Derivatives of phenoxazine as blue emitters for TADF OLEDs

Major attempts have been dedicated to the design of various TADF materials, particularly for the D-A-type molecules, which showed electroluminescence in the blue emission region [83]. The molecular design of D-A-type and D-A-D-type TADF materials was usually concentrated on different donors, such as carbazole and its linked derivatives [84], phenothiazine [85], phenoxazine [86] and 9,9-dimethyl-9,10-dihydroacridine [64]. In this section, various blue TADF emitters based on phenoxazine derivatives will be discussed (**Fig. 2.8.1** and **Table 2.8.1**).

Zhang *et al.* (2014) [33] designed D-A-D type molecule **PXZ–DPS** possessing diphenylsulphone as the acceptor unit and phenoxazine as the donor unit. Blue TADF OLED was designed by utilizing CBP as the host with a low turn on voltage of 2.7 V. The device with **PXZ–DPS** demonstrated an EQE value reaching 17.5% with a small efficiency roll-off (15.5% at a luminance of 1000 cd/m²).

Liu *et al.* (2016) [87] synthesized two triarylboron-based TADF emitters, denoted as **TB-1PXZ** and **TB-2PXZ**, featuring an electron-donating phenoxazine moiety and an electron-accepting triarylboron moiety. These TADF emitters were applied in solution-processed OLEDs. The devices exhibited blue-green emission peaks (480 nm and 496 nm) in the EL spectrum. Other OLED characteristics are the following: **TB-1PXZ** (CE = 1.7 cd A⁻¹, PE = 0.7 lm W⁻¹ and EQE = 1.0%) and **TB-2PXZ B** (CE = 21.0 cd A⁻¹, PE = 13.8 lm W⁻¹ and EQE = 8.9%).

Lee *et al.* (2013) [46] established a TADF emitter (**2PXZ-TAZ**) which was synthesized by introducing 3,4,5-triphenyl-4*H*-1,2,4-triazole (TAZ) as an acceptor. The **2PXZ-TAZ** based device exhibited sky-blue emission, and the maximum in EL spectra was observed at 456 nm. The respective CIE color coordinates were (0.16, 0.15) at 10 mA cm⁻². OLED based on a D-A-D type triazole-based compound, doped into DPEPO, reached EQE of 6.4%.

Sagara *et al.* (2015) [88] developed highly efficient TADF emitters denoted as **BOX** (D-A-type), **BT** (D-A-type), **BT2** (D-A-D-type), *cis*-**BOX2** (D-A-D-type) and *trans*-**BOX2** (D-A-D-type) with a small ΔE_{ST} (in a range from 0.10 eV to 0.15 eV) and a substantial oscillator strength (in the range from 0.06 to 0.19). Phenoxazine units were employed as electron donors, while benzazole-containing units were employed as electron acceptors. According to the authors, the OLED based on D-A-D structure emitters showed higher maximum EQEs (17.6%) than the ones using D-A-type emitters (12.1%).

Chen *et al.* (2016) [89] synthesized a D-A-type molecule with a phenoxazine moiety as its donor and a benzonitrile moiety as its acceptor, named **mPTC**. The **mPTC**-based TADF device exhibited sky-blue emission with CIE coordinates (0.18, 0.32) and the EL maximum at 484 nm. The maximum current and power efficiencies reached 39.88 cd A⁻¹ and 35.78 lm W⁻¹, respectively, and the EQE value was 17.4%. The authors proved that the increased molecular restriction caused by the additional phenyl group at the meta-position can effectively inhibit the structural relaxation in solid states and, furthermore, improve the color purity of the TADF emitter. Moreover, the intramolecular rotation between D and A could minimize the photonic energy heat [90].

He *et al.* (2018) [91] designed a TADF emitter (**DPE-DPXZ**) by utilizing 10*H*-phenoxazine as the donor segment. The device based on **DPE-DPXZ** doped into CBP showed sky-blue emission with EQE reaching 10.8%.

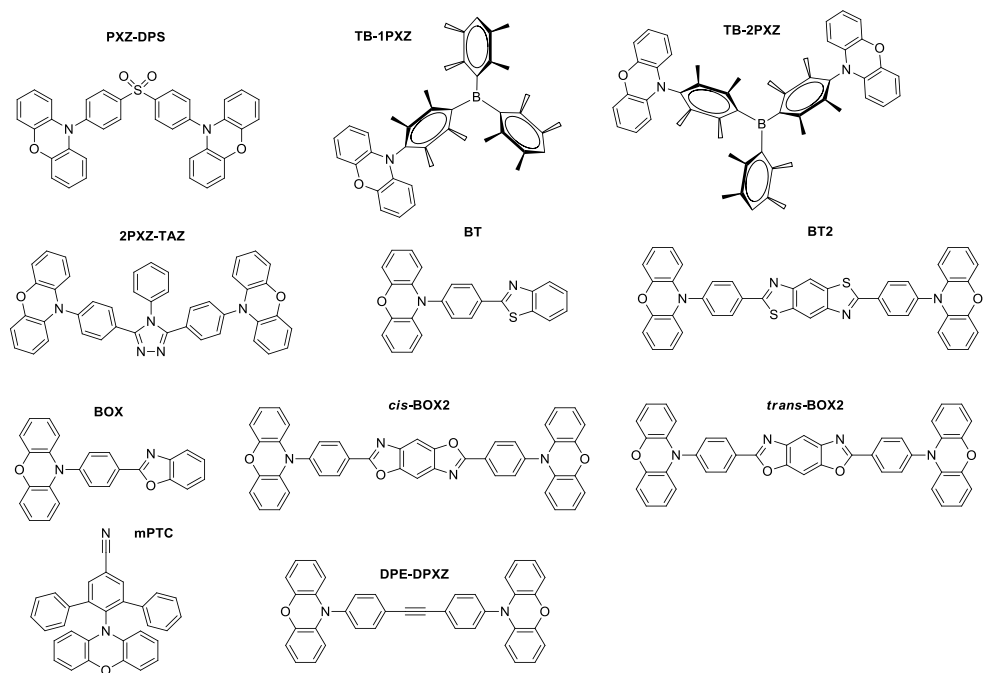


Fig. 2.8.1. Chemical structures of phenoxazine-based emitters for blue TADF OLEDs

Table 2.8.1. Photophysical and electrochemical properties of phenoxazine donor-based blue TADF emitters

Emitter	HOMO, eV	LUMO, eV	$E_T/\Delta E_{ST}$, eV	T_g , C ^o	T_d , C ^o	Dopant conc., %	V_{on} , V	L_{max} , cd m ⁻²	LE_{max} , cd A ⁻¹	μ_p , lm W ⁻¹	EQE, %	EL λ_{max}	CIE1931, (x, y)	Ref. No.
PXZ-DPS	5.59	2.92	-/0.06	-	-	CBP	2.7	-	-	-	17.5	507	-	[33]
TB-1PXZ	5.08	2.24	2.86/ 0.12	-	-	CzSi	8.9	-	1.7	0.7	1.0	480	(0.19, 0.29)	[87]
TB-2PXZ	5.08	2.29	2.84/ 0.05	-	-	CzSi	5.8	-	21.0	13.8	8.9	496	(0.18, 0.40)	[87]
2PXZ-TAZ	-	-	-/ 0.23	-	-	6% in DPEPO	-	-	-	-	6.4	456	(0.16, 0.15)	[46]
BT	-	-	-/ 0.071	-	-	6% in mCBP	-	-	-	-	12.1	-	-	[88]
BT2	-	-	-/ 0.054	-	-	6% in mCBP	-	-	-	-	14.0	-	-	[88]
BOX	-	-	-/ 0.067	-	-	6% in mCBP	-	-	-	-	9.1	-	-	[88]
<i>cis</i> - BOX2	-	-	-/ 0.033	-	-	6% in mCBP	-	-	-	-	17.6	-	-	[88]
<i>trans</i> - BOX2	-	-	-/ 0.05	-	-	6% in mCBP	-	-	-	-	14.4	-	-	[88]
mPTC	5.12	2.84	-/ 0.01	234	300	6.5% in mCBP	-	5800	39.8 8	35.78	17.4	484	(0.18, 0.32)	[89]
DPE-DPXZ	4.98	2.15	-/ 0.40	122	380	CBP	3.4	718	22.8	-	10.8	475	(0.18, 0.31)	[91]

2.9. Conclusions of the literature review

In this literature review, we analyzed the principles of OLEDs and the basic mechanism of the TADF phenomenon. We also reviewed the molecular design of TADF emitters and derivatives of bicarbazole, acridine, phenoxazine as blue emitters for TADF OLEDs. Nowadays, one of the leading approaches of effective conversion of energy into light by using organic compounds is TADF. We described the requirements for the host materials of OLEDs. Furthermore, we conducted a literature review on the latest findings and tendencies concerning the molecular design of TADF emitters for OLED applications.

During the recent years, considerable and sustainable improvement has been witnessed for the lighting characteristics of organic light-emitting devices, primarily reflecting the progress in the design and synthesis of organic materials exhibiting TADF. The TADF phenomenon is usually observed in molecules that are characterized by quasi-degenerate first singlet (S1) and first triplet (T1) excited states, i.e., with singlet-triplet gaps (ΔE_{ST}) being at the kT scale, thus making it possible to activate the spin-forbidden T1→S1 transition by thermal influence. Generally, a small ΔE_{ST} can be achieved through the design of donor-acceptor (D-A) systems with twisted geometry to attain spatial separation between the HOMO and the LUMO, and also by minimizing the exchange integrals between these orbitals. Accordingly, D-A molecular systems with a marked intramolecular charge transfer (ICT) are typical TADF material candidates. Their HOMO and LUMO are mainly localized on the donor and acceptor moieties, respectively. Therefore, the selection of suitable donor and acceptor units is an important aspect for the design of functional TADF materials.

TADF-based OLEDs usually demonstrate high internal quantum efficiency (IQE) by converting nearly 100% of the injected carriers into photons. The design and synthesis of highly efficient TADF materials is, however, quite a difficult task because of the very sensitive balance between the T1→S1 reverse inter-system crossing (RISC) and the radiative decay by the S1→S0 transition. As a general trend, RISC probability increases with the constriction of the ΔE_{ST} gap.

Many highly efficient TADF-based OLEDs have already been reported, but objections regarding design and synthesis of stable blue TADF emitters still remain. There is considerable need to develop new TADF materials that demonstrate top level performance while taking into account the following aspects:

- Mechanism of TADF. It is a conventional aspect that ΔE_{ST} is a valid agent that manages the efficiency of TADF.
- Fabrication cost of TADF OLEDs. The fabrication cost of TADF OLEDs is important in their marketability. The architecture of a simplified device is one of the basic ways to cut production value. The emphasis on the evolution of proper low-molar mass TADF emitters for solution-processable devices is definitely required.
- Emission energy of TADF emitters. There are now sufficient models available of high performance green and yellow emitters. Yet, deficit of blue and red TADF emitters still persists.
- It is significant to determine the eligible structure-properties relationship of TADF materials using different theoretical and experimental techniques.

3. EXPERIMENTAL PART

3.1. Instrumentation and methods

3.1.1. Instrumentation

^1H and ^{13}C nuclear magnetic resonance (NMR) spectra were recorded by using a Bruker Avance III 400 spectrometer (400 MHz (^1H), 100 MHz (^{13}C), 375 MHz (^{19}F)). Chemical shifts (δ) are reported in ppm referenced to tetramethylsilane or the internal solvent signal.

Attenuated total reflection infrared (IR) spectra were recorded by using a Bruker VERTEX 70 spectrometer. MS data was recorded on UPLC-MS Acquity Waters SQ Detector 2.

The melting points of the prepared compounds were estimated by using an *Electrothermal Melt-Temp* apparatus.

UV/Vis absorption spectra of 10^{-4} M solutions and thin films of the compounds were recorded in quartz cells by using an *Aventes AvaSpec-2048XL* spectrometer or a *Perkin Elmer Lambda 35* spectrometer.

TGA was performed on a *Mettler TGA/SDTA851e/LF/1100* apparatus at a heating rate of 20 °C/min under nitrogen atmosphere. Compound decomposition temperatures were determined at the point when the sample loses 5% of its mass ($T_{\text{dec-5\%}}$).

DSC measurements were done on a *DSC Q 100 TA Instrument* at a heating rate of 10 °C/min under nitrogen atmosphere. The melting points (T_{m}) and crystallization temperatures (T_{c}) were taken from the appropriate endo- and exothermic peaks, respectively. The glass transition temperatures (T_{g}) were estimated from the point when the sample heat capacity changed.

3.1.2. Methods

3.1.2.1. Optical and photophysical measurements

Photoluminescence spectra and UV spectra of dilute toluene solutions and of thin films prepared by vacuum deposition were recorded with *Edinburgh Instruments FLS980* and *PerkinElmer Lambda 25* spectrometers, respectively. To separate the phosphorescence spectra of the films from the emission spectra were recorded at 77 °K with the delay time exceeding 50 ms [92,93,94]. An *Edinburgh Instruments FLS980* spectrometer and a *PicoQuant LDH-D-C-375* laser (wavelength 374 nm) as the excitation source were used for recording photoluminescence (PL) decay curves and PL intensity dependencies on the laser flux of the samples at room temperature. Fluorescence quantum yields were measured by using an integrated sphere (inner diameter of 120 mm) spherical cavity calibrated with two analytical standards: quinine sulfate in 0.1 M H_2SO_4 and rhodamine 6G in ethanol.

The phosphorescence spectra were recorded at 77 °K for the solid solutions of the materials in the zeonex matrix by using nanosecond gated luminescence measurements (from 400 ps to 1 s) while using a high energy pulsed Nd:YAG laser

emitting at 355 nm (EKSPLA). The emission was focused onto a spectrograph and detected on a sensitive gated iCCD camera (Stanford Computer Optics) having sub-nanosecond resolution. A model liquid nitrogen cryostat (Janis Research) was used for the experiment.

3.1.2.2. Electrochemical measurements

The cyclic voltammetry (CV) measurements were carried out with a glassy carbon electrode in a three electrode cell. The measurements were performed by using an *Eco Chemie* Company's *AUTOLAB* potentiostat PGSTAT20. Freshly distilled CaH₂ dichloromethane solutions containing 0.1 M tetrabutylammonium hexafluorophosphate (electrolyte) were used. The measurements were performed at room temperature under argon atmosphere at 100 mV/s potential rate. The electrochemical cell included a platinum wire (diameter of 1 mm) serving as the working electrode, an Ag wire calibrated via ferrocene/ferrocinium redox couple (a quasi-reference electrode) and a platinum coil (an auxiliary electrode).

3.1.2.3. Photoelectrical measurements

IP of the layers of the synthesized compounds were measured by employing the electron photoemission method in air [95]. The electron photoemission spectra of the thin solid compound layers deposited on indium tin oxide (ITO) coated glass substrates were recorded under negative voltage of 300 V, deep UV illumination (deuterium light source ASBN-D130-CM), CM110 1/8m monochromator used and 6517B electrometer (Keithley) connected to a counter-electrode.

3.1.2.4. Charge mobility measurements

The time-of-flight (TOF) method was used for the estimation of hole and electron mobilities in the layers of the compounds. TOF experiments were performed on the samples of the structure ITO/ *compound* /Al. The layers were deposited under vacuum of $2-5 \times 10^{-6}$ Pa. The thickness (d) of the compounds' layers was detected as controlled via a quartz resonator in the vacuum deposition process. 355 nm wavelength laser (*EKSPLA NL300*) excitation was used to generate charges in the layers. Positive and negative external voltages (U) were applied to the samples to measure hole and electron mobilities by employing 6517B electrometer (*Keithley*). *TDS 3032C* oscilloscope (*Tektronix*) was used to record the photocurrent transients under different electric fields for holes and electrons. Charge mobilities were evaluated from the equation $\mu = d^2 / (U \times t_{tr})$, where t_{tr} is the transit time.

3.2. Computational details

Computations of the designed compounds were performed by using the Gaussian 16 program. The density functional theory (DFT) [96] employing B3LYP

[97] functional was used in conjunction with the 6-31G(d,p) basis set. The spectroscopic properties of the molecules were calculated by mean of the time dependent density functional theory (TDDFT) [98]. Up to 40 excited states were calculated, and the theoretical absorption bands were obtained by considering the band half-width at half-maximum of 0.3 eV. The adiabatic ionization potentials (I_p^{theor}) were calculated at the B3LYP/6-31G(d,p) level as the energy difference between neutral and cation radical species at the neutral state geometry.

3.3. Fabrication of phosphorescent light emitting diodes

Devices with the structures: ITO/m-MTDATA/host:Ir(ppy)₃ or Ir(piq)₂(acac)/Bphen/Ca:Al were fabricated by deposition of different organic layers and metal electrodes onto pre-cleaned indium tin oxide (ITO) coated glass substrate under vacuum higher than $3 \cdot 10^{-6}$ mBar. 4,4',4''-Tris[phenyl(m-tolyl)amino]triphenylamine (m-MTDATA) was utilized for the preparation of the hole-transporting layer. 4,7-Diphenyl-1,10-phenanthroline (Bphen) served as the electron-transporting and hole-blocking material. Tris[2-phenylpyridinato-C²,N]iridium(III) (Ir(ppy)₃) and bis[2-(1-isoquinolinylnyl-N)phenyl-C](2,4-pentanedionato-O²,O⁴)iridium(III) (Ir(piq)₂(acac)) served as the emitting materials. The top calcium layer was deposited as the cathode which was protected by aluminum because Ca is highly reactive and corrodes quickly in the ambient atmosphere. The structures of PhOLEDs were the following: ITO/CzBisPhen:Ir(ppy)₃ (45 nm)/ Bphen (35 nm)/Ca:Al (Device **IA**); ITO/CzMonoPhen:Ir(ppy)₃ (45 nm)/Bphen(35 nm)/Ca:Al (Device **IB**); ITO/m-MTDATA (30 nm)/CzBisPhen:Ir(ppy)₃ (20 nm)/Bphen (30 nm)/ Ca:Al (Device **IIA**); ITO/m-MTDATA (30 nm)/CzMonoPhen:Ir(ppy)₃ (20 nm)/Bphen(30 nm)/Ca:Al (Device **IIB**); ITO/m-MTDATA(30 nm)/CzBisPhen:Ir(piq)₂(acac) (20 nm)/Bphen(30 nm)/Ca:Al (Device **IIIA**); ITO/m-MTDATA(30 nm)/CzMonoPhen:Ir(piq)₂(acac) (20 nm)/Bphen(30 nm)/Ca:Al (Device **IIIB**).

Density-voltage and luminance-voltage characteristics were recorded by employing a *Keithley 6517B* electrometer, certificated photodiode *PH100-Si-HA-D0* together with the *PC-Based Power and Energy Monitor 11S-LINK* (from *STANDA*) and a *Keithley 2400C* sourcemeter. Electroluminescence (EL) spectra were taken by using an *Aventes AvaSpec-2048XL* spectrometer.

3.4. Preparation of vacuum deposited OLEDs

Selected materials were studied in electroluminescent devices which were fabricated by vacuum deposition of organic and metal layers onto pre-cleaned ITO coated glass substrate under vacuum higher than 2×10^{-6} mBar. ITO-coated glass substrates with a sheet resistance of 15 Ω /sq were pre-patterned for getting independent devices with an area of 6 mm².

Three types of OLEDs were fabricated by means of vacuum deposition of organic semiconductor layers and metal electrodes onto a precleaned ITO-coated glass substrate under vacuum of 10^{-5} Torr:

- A) ITO/CuI/TCTA/**pCNBCzoCF₃**/BCP/Ca:Al
- B) ITO/CuI/m-MTDATA/**pCNBCzoCF₃**/BCP/Ca:Al
- C) ITO/CuI/TCTA/**pCNBCzoCF₃**/m-MTDATA/**pCNBCzoCF₃**/BCP/Ca:Al

The devices were fabricated with step-by-step deposition of the different organic layers. CuI was used as a hole-injection layer [99]. Tris(4-carbazoyl-9-ylphenyl)amine (TCTA) and 4,4',4''-tris[phenyl(*m*-tolyl)amino]triphenylamine (*m*-MTDATA) [100,101] were used for the preparation of hole-transporting layers. **pCNBCzoCF₃** was used as a fluorescent (TADF) material, while 2,9-dimethyl-4,7-diphenyl-1,10-phenanthroline (BCP) [102] was used for the preparation of an electron-transporting layer which alleviates the stepwise electron transfer from the Ca:Al cathode to the emissive layer.

Meanwhile, the following structure was used: ITO/MoO₃(2nm)/TCTA(40nm)/mCP(8nm)/ tested TADF emitter (32nm) /TSPO1(8nm) /TPBi(40nm)/Ca/Al. Molybdenum trioxide (MoO₃) was used for the preparation of the hole injection layer. Tris(4-carbazoyl-9-ylphenyl)amine (TCTA) and 2,2',2''-(1,3,5-benzinetriyl)-tris(1-phenyl-1-H-benzimidazole) (TPBi) were used as hole- and electron-transporting materials. 3-Bis(9-carbazoyl)benzene (mCP) and diphenyl-4-triphenylsilylphenyl-phosphineoxide (TSPO1) with high triplet energies of 2.9 eV for mCP and 3.36 eV for TSPO1 were used as exciton blocking materials.

The density–voltage and luminance–voltage dependences were measured by using a semiconductor parameter analyzer *HP 4145A*. The measurement of brightness was obtained by using a calibrated photodiode [103]. The electroluminescence spectra were recorded with an *Ocean Optics USB2000* spectrometer. Device efficiencies were estimated from the luminance, current density, and EL spectrum.

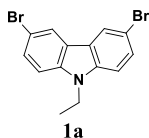
3.5. Materials

The starting compounds, i.e., 9*H*-carbazole (>96.0%, TCI Europe), 9-ethylcarbazole (97%, Aldrich), *N*-bromosuccinimide (NBS, 99%, Aldrich), 10*H*-phenothiazine (C₁₂H₉NS, ≥98%, Aldrich), bis(tri-*tert*-butylphosphine)palladium(0) (Pd(*t*-Bu₃P)₂, 98%, Aldrich), potassium *tert*-butoxide (*t*-BuOK, ≥98%, Aldrich), anhydrous sodium sulfate (Na₂SO₄, Aldrich), iron (III) chloride (FeCl₃, Aldrich), ethylenediaminetetraacetic acid disodium salt dehydrate (EDTA-Na₂·2H₂O, >98%, Aldrich), tetramethylethylenediamine (TMEDA, ≥99%, Aldrich), *tert*-butyllithium solution (*n*-BuLi, 1.7 M in pentane, Aldrich), triphenylchlorosilane ((C₆H₅)₃SiCl, 98%, Aldrich), sodium hydride (NaH, 90%, Aldrich), *p*-toluenesulfonyl chloride (TosCl, Aldrich), iodobenzene (C₆H₅I, Aldrich), copper(I) chloride (CuCl, ≥99%, Aldrich), copper (Cu, 99%, Aldrich), 1,10-phenanthroline (C₁₂H₈N₂, ≥99%, Aldrich), 4-fluoro-3-(trifluoromethyl)benzonitrile (C₈H₃F₄N, 99%, Aldrich), sodium hydroxide

(NaOH, $\geq 97\%$, Aldrich), triethyl phosphite ($\text{P}(\text{OEt})_3$, 98%, Aldrich), dichlorodimethylsilane ($\text{C}_2\text{H}_6\text{Cl}_2\text{Si}$, $\geq 99\%$, Aldrich), 10*H*-phenoxazine ($\text{C}_{12}\text{H}_9\text{NO}$, 97%, Aldrich), 3,7-di-*tert*-butyl-10*H*-phenothiazine ($\text{C}_{20}\text{H}_{25}\text{NS}$, $\geq 98\%$, Aldrich), 9,9-dimethyl-9,10-dihydroacridine ($\text{C}_{15}\text{H}_{15}$, 97%, Aldrich), bis(4-bromophenyl)(dimethyl)silane ($\text{C}_{14}\text{H}_{14}\text{Br}_2\text{Si}$, 99%, Aldrich), palladium(II) acetate ($\text{Pd}(\text{OAc})_2$, 98%, Aldrich), tri-*tert*-butylphosphine ($\text{P}(\text{t-Bu})_3$, 98%, Aldrich), potassium carbonate (K_2CO_3 , $>99\%$, Aldrich), diphenylethanedione ($\text{C}_6\text{H}_5\text{COCOC}_6\text{H}_5$, 98%, Aldrich), 4-aminobenzophenone ($\text{H}_2\text{NC}_6\text{H}_4\text{C}(\text{O})\text{C}_6\text{H}_5$, Aldrich), ammonium acetate ($\text{CH}_3\text{CO}_2\text{NH}_4$, Aldrich), benzaldehyde ($\text{C}_6\text{H}_5\text{CHO}$, $\geq 99\%$, Aldrich), sodium chloride (NaCl , $\geq 99\%$, Aldrich), 3-aminobenzophenone ($\text{H}_2\text{NC}_6\text{H}_4\text{C}(\text{O})\text{C}_6\text{H}_5$, 97%, Aldrich) were purchased from *Sigma-Aldrich* and used as received.

The solvents, i.e., toluene, chloroform, ethyl acetate, *n*-hexane, methanol, acetone, acetonitrile, tetrahydrofuran (Penta), dichloromethane (Poch), isopropanol, *o*-xylene (Sigma-Aldrich) and *N,N*-dimethylformamide (DMF) (Sigma-Aldrich) were dried and distilled according to the conventional procedures [104].

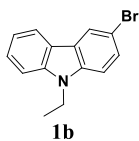
The structure of newly synthesized target compounds was confirmed by ^1H and ^{13}C NMR, ^{19}F NMR and IR spectroscopy.



Chemical formula: $\text{C}_{14}\text{H}_{11}\text{Br}_2\text{N}$

3,6-Dibromo-9-ethyl-9*H*-carbazole (1a), FW=353.05 g/mol, m.p.: lit.: 141 °C [105]) was achieved by the bromination reaction. 9-Ethyl-carbazole (5.00 g, 25.6 mmol) was added to a solution of *N*-bromosuccinimide, NBS (8.89 g, 49.9 mmol), in 50 mL of *N,N*-dimethylformamide (DMF). The reaction mixture was

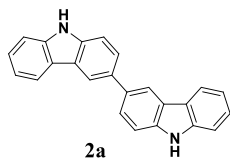
stirred at room temperature for 4 hours. When the reaction was completed, the solution was poured into a large amount of ice water. The yellow precipitate was filtered off and recrystallized from an isopropanol/DMF mixture to yield the product as yellowish needle-like crystals. Yield: 7.38 g (82%), practical melting point 140–142°C.



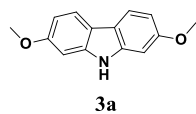
Chemical formula: $\text{C}_{14}\text{H}_{12}\text{BrN}$

3-Bromo-9-ethyl-9*H*-carbazole (1b), FW = 274.16 g/mol, lit. mp.p.: 83 °C [106]) was achieved by the bromination reaction. 9-Ethyl-carbazole (1.00 g, 5.12 mmol) was added to a solution of *N*-bromosuccinimide, NBS (0.911 g, 5.12 mmol), in 10 mL of DMF. The reaction mixture was stirred at room temperature for 24

hours. When the reaction was completed, the solution was poured into a large amount of ice water and extracted with ethyl acetate. The organic layer was dried over anhydrous sodium sulfate followed by solvent evaporation in a rotary evaporator. The product was crystallized in methanol to afford white needle-like crystals. Yield: 0.88 g (62%), melting point 79–82°C.

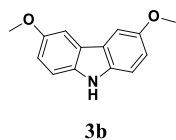


Chemical formula: $C_{24}H_{16}N_2$ **9H,9'H-3,3'-bicarbazole (2a)**, FW = 332.40 g/mol) was synthesized by Friedel-Crafts reaction. A mixture of 9H-carbazole (3.0 g, 17.9 mmol), $FeCl_3$ (11.64 g, 71.8 mmol) and chloroform (75 ml) was stirred for 1 hour at room temperature. The crude product with Celite® inside was concentrated by rotary evaporation. After drying at 40 °C under vacuum, the product was poured into EDTA- $Na_2 \cdot 2H_2O$ (35 g of EDTA/ 350 ml of distilled water). Afterwards, filtration of the compound was carried out, and it was washed with EDTA solution (20 g EDTA/200 ml dist. water), with distilled water and with methanol. After washing, the mixture was extracted from tetrahydrofuran solvent (THF). The product was again concentrated by rotary evaporation, and washed with hot methanol. The product was crystallized in izopropanol/DMF mixture. Yield: 2.53 g (42%), m.p.: 218–220 °C.



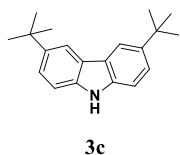
Chemical formula: $C_{14}H_{13}NO_2$

2,7-dimethoxy-9H-carbazole (3a), FW = 227.26 g/mol, m.p.: 271–272 °C, lit.: 272–274 °C) was achieved by Ullmann-coupling and a Cadogan cyclization as reported in the literature [107].



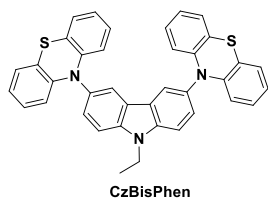
Chemical formula: $C_{14}H_{13}NO_2$

3,6-dimethoxy-9H-carbazole (3b), FW = 227.26 g/mol, m.p.: 131–132 °C, lit.: 131–133 °C) was prepared by bromination and methoxylation reactions according to the procedure described in the literature [108].



Chemical formula: $C_{20}H_{25}N$

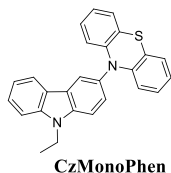
3,6-di-tert-butyl-9H-carbazole (3c), FW = 279.42 g/mol, m.p. = 227–229 °C, lit. 228–230 °C [109]) was synthesized as described in the literature source [110].



Chemical formula: $C_{38}H_{27}N_3S_2$

10,10'-(9-Ethyl-9H-carbazole-3,6-diyl)bis(10H-phenothiazine) (CzBisPhen), FW = 589.16 g/mol). The palladium-catalyzed Buchwald-Hartwig reaction was employed. 3,6-Dibromo-9-ethyl-9H-carbazole (0.4 g, 1.132 mmol), 10H-phenothiazine (0.564 g, 2.83 mmol), bis(tri-*tert*-butylphosphine)palladium(0) (0.012 g, 0.0226 mmol), potassium *tert*-butoxide (0.380 g, 3.40 mmol) dissolved in 9 ml of anhydrous toluene and refluxed 24 hours under nitrogen atmosphere at 100 °C temperature. The mixture was extracted with dichloromethane and water. The organic layer was dried over anhydrous sodium sulfate followed by solvent evaporation in a rotary evaporator. The product was crystallized in izopropanol/DMF mixture. Yield: 0.52 g (78%), m.p.: 278–280°C. 1H NMR (400 MHz, d_6 -DMSO) δ 8.38 (d, J = 2.0 Hz, 2H), 7.98 (d, J = 8.6 Hz, 2H), 7.53 (dd, J =

8.6, 2.1 Hz, 2H), 7.04 (dd, $J = 7.4, 1.5$ Hz, 4H), 6.84 (dtd, $J = 21.5, 7.4, 1.5$ Hz, 8H), 6.16 (dd, $J = 8.1, 1.5$ Hz, 4H), 4.62 (q, $J = 7.0$ Hz, 2H), 1.48 (t, $J = 7.0$ Hz, 3H). ^{13}C NMR (101 MHz, d_6 -DMSO) δ 144.4, 139.5, 131.5, 128.9, 127.2, 126.5, 123.8, 123.4, 122.4, 118.5, 115.8, 111.8, 39.4, 14.0.

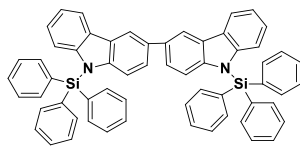


CzMonoPhen

Chemical formula: $\text{C}_{26}\text{H}_{20}\text{N}_2\text{S}$

10-(9-Ethyl-9H-carbazol-3-yl)-10H-phenothiazine (CzMonoPhen, FW = 392.52 g/mol). Palladium-catalyzed Buchwald-Hartwig reaction was carried out. 3-Bromo-9-ethyl-9H-carbazole (0.4 g, 1.46 mmol), 10H-phenothiazine (0.349 g, 1.75 mmol), bis(tri-*tert*-butylphosphine)palladium(0) (0.015 g, 0.0292 mmol), potassium *tert*-butoxide (0.245 g, 2.19 mmol) were dissolved

in 9 ml of anhydrous toluene and refluxed for 24 hours under nitrogen atmosphere at 100 °C temperature. The mixture was extracted with dichloromethane and water. The organic layer was dried over anhydrous sodium sulfate followed by solvent evaporation in a rotary evaporator. The filtrate was then evaporated under vacuum and purified by column chromatography (DCM:Hex = 1:2.5). The product was crystallized in izopropanol/DMF mixture. Yield: 0.36 g (63%), melting point 218–220 °C. ^1H NMR (400 MHz, d_6 -DMSO) δ 8.27 (d, $J = 1.7$ Hz, 1H), 8.23 (d, $J = 7.8$ Hz, 1H), 7.89 (d, $J = 8.6$ Hz, 1H), 7.68 (d, $J = 8.6$ Hz, 1H), 7.54–7.43 (m, 2H), 7.22 (t, $J = 7.4$ Hz, 1H), 7.05 (dd, $J = 7.4, 1.8$ Hz, 2H), 6.89–6.77 (m, 4H), 6.15 (dd, $J = 7.1, 1.2$ Hz, 2H), 4.53 (q, $J = 7.0$ Hz, 2H), 1.40 (t, $J = 7.0$ Hz, 3H). ^{13}C NMR (101 MHz, d_6 -DMSO) δ 144.6, 140.1, 138.9, 131.2, 128.1, 127.3, 126.5, 124.1, 122.6, 122.4, 122.1, 121.0, 119.2, 118.5, 115.8, 111.3, 109.5, 37.4, 13.9.

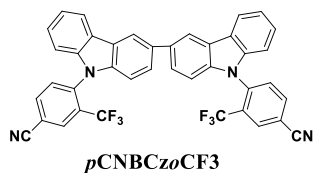


BiCzSiPh₃

Chemical formula: $\text{C}_{60}\text{H}_{44}\text{N}_2\text{Si}_2$

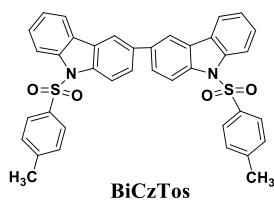
9,9'-Bis(triphenylsilyl)-9H,9'H-3,3'-bicarbazole (BiCzSiPh₃, FW = 849.18 g/mol). N-unsubstituted bicarbazole (0.50 g, 1.5 mmol) was dissolved in THF, treated with tetramethylethylenediamine (TMEDA) (0.68 ml, 4.5 mmol) and with 1.7 M *n*-BuLi (1.95 ml, 3.3 mmol) at -40 °C to give a lithiated intermediate, which, after 30 minutes of stirring, was subsequently quenched

with chlorotriphenylsilane (0.98 g, 3.3 mmol) at -70 °C. The reaction mixture was left overnight for stirring. The target compound of **BiCzSiPh₃** gave a colorless powder after washing with methanol. Yield: 0.30g (24%), melting point > 300 °C from DSC. IR ($\bar{\nu}$, cm^{-1}): 3415 (N-H, 3500–3200 cm^{-1}); 1670 (C-C in Ar, 1600–1585, 1500–1400 cm^{-1}); 1303, 1256 (C-N in Ar, 1350–1250 cm^{-1}); 970–900 (Si-H₃).



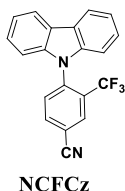
Chemical structure: C₄₀H₂₀F₆N₄

4,4'-(9*H*,9'*H*-[3,3'-bicarbazole]-9,9'-diyl)bis(3-(trifluoromethyl)benzonitrile) (pCNBCzoCF₃, FW = 670.60 g/mol). A mixture of *N*-unsubstituted bicarbazole (0.50 g, 1.5 mmol), sodium hydride (NaH) (0.22g, 9.0 mmol) and 4-fluoro-3-(trifluoromethyl)benzonitrile (0.68g, 3.6 mmol) were dissolved in dimethylformamide (DMF) under argon atmosphere. The reaction mixture was mixed at room temperature for 20 hours. When the reaction was completed, the mixture was poured into water and a small amount of saturated sodium hydroxide (NaOH) was infused because of coagulation. Afterwards, the crude product was filtered and purified by column chromatography (silica, DCM/Hex=1/1 as eluent). The target compound pCNBCzoCF₃ was obtained as a yellowish powder after recrystallization from hot methanol. Yield: 0.30 g (25%), m.p.: 294–295 °C. ¹H NMR (400 MHz, CDCl₃) δ 8.42 (s, 2H), 8.32 (d, *J* = 1.1 Hz, 2H), 8.22 (d, *J* = 7.7 Hz, 2H), 8.09 (dd, *J* = 8.1, 1.5 Hz, 2H), 7.77–7.69 (m, 2H), 7.59 (d, *J* = 8.1 Hz, 2H), 7.42 (t, *J* = 7.2 Hz, 2H), 7.36 (t, *J* = 7.2 Hz, 2H), 7.02 (d, *J* = 8.4 Hz, 2H), 6.95 (d, *J* = 8.1 Hz, 2H). ¹⁹F NMR (376 MHz, CDCl₃) δ -61.44. ¹³C NMR (101 MHz, CDCl₃) δ 143.1, 141.9, 141.0, 137.4, 135.1, 134.0, 132.8 (q, *J* = 32.5 Hz), 132.1 (q, *J* = 5.1 Hz), 126.8, 126.5, 124.7, 124.2, 121.1, 122.1 (q, *J* = 275 Hz), 120.8, 119.4, 116.9, 114.6, 110.3, 110.2.



Chemical structure: C₃₈H₂₈N₂O₄S₂

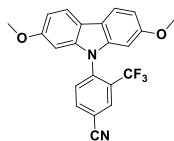
9,9'-Ditosyl-9*H*,9'*H*-3,3'-bicarbazole (BiCzTos). A mixture of *N*-unsubstituted bicarbazole (0.2 g, 0.6 mmol), sodium hydride (NaH) (0.090g, 3.6 mmol) and *p*-toluenesulfonyl chloride (0.30 g, 1.5 mmol) were dissolved in THF under argon atmosphere. The reaction mixture was mixed at room temperature for 20 hours. When the reaction was completed, the crude product was purified by column chromatography (silica, DCM as eluent). The target compound gave colorless powders after crystallization from Hex/DCM. Yield: 0.11 g (29%), melting point 311°C from DSC. IR ($\bar{\nu}$, cm⁻¹): 3064 (arene C–H, 3100–3000 cm⁻¹); 2952, 2923 (aliphatic C–H, 3000–2850 cm⁻¹); 1598, 1470, 1442 (C–C in Ar, 1600–1585, 1500–1400 cm⁻¹); 1369 (C–N in Ar, 1335–1250 cm⁻¹); 1173 (C–O–C, 1250–1050 cm⁻¹); 897, 812 (C–H in Ar, 900–675 cm⁻¹).



Chemical formula: C₂₀H₁₁F₃N₂

4-(9*H*-carbazol-9-yl)-3-(trifluoromethyl)benzonitrile (NCFCz, FW = 336.31 g/mol). A mixture of 9*H*-carbazole (0.50 g, 2.99 mmol), sodium hydride (NaH) (0.22 g, 9.0 mmol) and 4-fluoro-3-(trifluoromethyl)benzonitrile (0.68 g, 3.6 mmol) were dissolved in dry dimethylformamide (DMF) under argon atmosphere. The reaction mixture was mixed at room temperature for 27 hours. When the reaction was completed, it was poured into water. Afterwards, the crude product was filtered and purified by column chromatography

(silica, DCM/Hex=1/1 as eluent). The target compound **NCFMcZ** was obtained as yellowish crystals after recrystallization from acetonitrile. Yield: 0.60 g (58%), m.p.: 123–124 °C. ¹H NMR (400 MHz, CDCl₃) δ 8.29 (d, *J* = 1.4 Hz, 1H), 8.14 (d, *J* = 7.6 Hz, 2H), 8.06 (dd, *J* = 8.1, 1.7 Hz, 1H), 7.53 (d, *J* = 8.1 Hz, 1H), 7.44–7.37 (m, 2H), 7.36–7.28 (m, 2H), 6.92 (d, *J* = 8.1 Hz, 2H); ¹⁹F NMR (376 MHz, CDCl₃) δ -61.53; ¹³C NMR (101 MHz, CDCl₃) δ 142.5, 140.9, 137.3, 134.0, 132.7 (q, *J* = 32.5 Hz), 131.97 (q, *J* = 5.1 Hz), 126.5, 124.0, 121.98 (q, *J* = 274.7 Hz), 120.9, 120.6, 116.9, 114.1, 110.0.

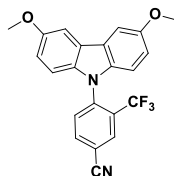


NCFMcZ2

Chemical formula: C₂₂H₁₅F₃N₂O₂

4-(2,7-Dimethoxy-9H-carbazol-9-yl)-3-(trifluoromethyl)benzonitrile (NCFMcZ2, FW = 396.36 g/mol). A mixture of 2,7-dimethoxy-9H-carbazole (0.2 g, 0.88 mmol), sodium hydride (NaH) (0.04 g, 1.76 mmol) and 4-fluoro-3-(trifluoromethyl)benzonitrile (0.13 g, 0.70 mmol) were dissolved in dry DMF under argon atmosphere. The reaction mixture was stirred at room temperature for 23 hours. When the reaction was

completed, the product was poured into water. The crude product was filtered and purified by column chromatography (silica, Hex/EtAc=2/1 as eluent). The target compound **NCFMcZ2** was obtained as white crystals after recrystallization from isopropanol. Yield: 0.14 g (40%), m.p.: 166–168 °C. ¹H NMR (400 MHz, CDCl₃) δ 8.29 (d, *J* = 1.3 Hz, 1H), 8.07 (dd, *J* = 8.1, 1.7 Hz, 1H), 7.88 (d, *J* = 8.5 Hz, 2H), 7.53 (d, *J* = 8.1 Hz, 1H), 6.89 (dd, *J* = 8.5, 2.2 Hz, 2H), 6.31 (d, *J* = 1.9 Hz, 2H); 3.78 (s, 6H). ¹⁹F NMR (375 MHz, CDCl₃) δ -61.48. ¹³C NMR (100 MHz, CDCl₃) δ 158.50, 143.72, 140.70 (q, *J* = 1.4 Hz), 137.30, 133.81, 132.57 (q, *J* = 32.6 Hz), 131.99 (q, *J* = 5.1 Hz), 121.85 (q, *J* = 272.3 Hz), 120.27, 117.65, 116.75, 114.01, 108.71, 94.72, 55.71.



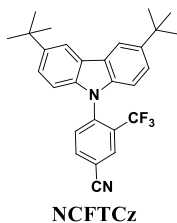
NCFMcZ1

Chemical formula: C₂₂H₁₅F₃N₂O₂

4-(3,6-Dimethoxy-9H-carbazol-9-yl)-3-(trifluoromethyl)benzonitrile (NCFMcZ1, FW = 396.36 g/mol). A mixture of 3,6-dimethoxy-9H-carbazole (0.4 g, 1.76 mmol), sodium hydride (NaH) (0.13 g, 5.28 mmol) and 4-fluoro-3-(trifluoromethyl)benzonitrile (0.40 g, 2.11 mmol) were dissolved in dry DMF under argon atmosphere. The reaction mixture was stirred at room temperature for 26

hours. When the reaction was completed, the product was poured into water. Then, the crude product was purified by column chromatography by using silica, Ac/Hex=1/4 as an eluent. The target compound **NCFMcZ1** was obtained as yellow crystals after recrystallization from isopropanol. Yield: 0.32 g (46%), m.p.: 139–140 °C. ¹H NMR (400 MHz, CDCl₃) δ 8.28 (d, *J* = 1.3 Hz, 1H), 8.04 (dd, *J* = 8.1, 1.6 Hz, 1H), 7.57 (d, *J* = 2.4 Hz, 2H), 7.50 (d, *J* = 8.2 Hz, 1H), 7.03 (dd, *J* = 8.9, 2.5 Hz, 2H), 6.83 (d, *J* = 8.8 Hz, 1H), 3.96 (s, 6H). ¹⁹F NMR (375 MHz, CDCl₃) δ -61.44. ¹³C NMR (100 MHz, CDCl₃) δ 154.62, 141.51 (q, *J* = 1.4 Hz), 138.17, 137.04, 133.77, 132.50

(q, $J = 32.4$ Hz), 131.78 (q, $J = 5.0$ Hz), 124.42, 121.92 (q, $J = 274.7$ Hz), 116.81, 115.41, 113.57, 110.78, 103.22, 56.07.



Chemical formula: $C_{28}H_{27}F_3N_2$

4-(3,6-Di-tert-butyl-9H-carbazol-9-yl)-3-(trifluoromethyl)benzonitrile (NCFTCz, FW = 448.52 g/mol). A mixture of 3,6-di-tert-butyl-9H-carbazole (0.50 g, 1.8 mmol), sodium hydride (NaH) (0.13 g, 5.4 mmol) and 4-fluoro-3-(trifluoromethyl)benzonitrile (0.41 g, 2.15 mmol) was dissolved in dry DMF under argon atmosphere. The

reaction mixture was stirred at room temperature for 26 hours. When the reaction was completed, the product was poured into water and filtered. Afterwards, the crude product was purified by column chromatography (silica, Ac/Hex=1/4 as eluent). The target compound NCFTCz was obtained as yellow crystals after recrystallization from isopropanol. Yield: 0.15 g (19%), m.p.: 200–202°C. 1H NMR (400 MHz, $CDCl_3$) δ 8.27 (d, $J = 1.4$ Hz, 1H), 8.13 (d, $J = 1.6$ Hz, 2H), 8.01 (dd, $J = 8.1, 1.7$ Hz, 1H), 7.47 (d, $J = 8.2$ Hz, 1H), 7.42 (dd, $J = 8.6, 1.8$ Hz, 2H), 6.83 (d, $J = 8.6$ Hz, 2H), 1.46 (s, 18H); ^{19}F NMR (376 MHz, $CDCl_3$) δ -61.33; ^{13}C NMR (101 MHz, $CDCl_3$) δ 143.9, 141.2, 137.1, 133.9, 132.7 (q, $J = 32.4$ Hz), 131.9 (q, $J = 5.1$ Hz), 124.12, 124.10, 122.1 (q, $J = 274.8$ Hz), 117.0, 116.6, 113.7, 109.5, 34.9, 32.1.

4. RESULTS AND DISCUSSION

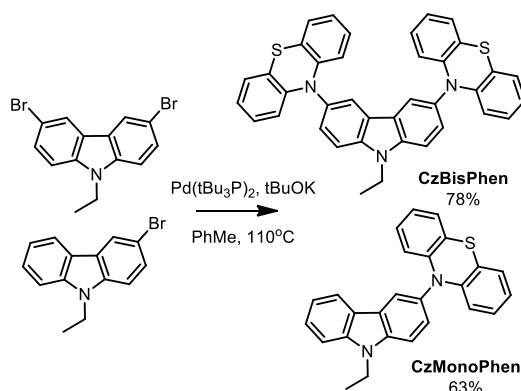
4.1 Derivatives with 9-ethyl-9H-carbazole and 10H-phenothiazine moieties

Phosphorescent organic light-emitting diodes (PhOLEDs) containing transition metal complexes as emitters have attracted much attention because they can achieve high efficiency of light emission through harvesting both singlet and triplet excitons [111]. Generally, PhOLEDs can use both singlet and triplet excitons via intersystem crossing and spin-orbital coupling which is caused by rare transition elements such as Ir and Pt [27]. Particularly, high theoretical internal quantum efficiency of PhOLEDs is suitable to achieve high performance operational modes suited for displays and solid-state lighting.

Herein, two bipolar host materials for green and red PhOLEDs based on carbazole as acceptor and phenothiazine as donor moieties have been reported, i.e., 10,10'-(9-ethyl-9H-carbazole-3,6-diyl)bis(10H-phenothiazine) (**CzBisPhen**) and 10-(9-ethyl-9H-carbazol-3-yl)-10H-phenothiazine (**CzMonoPhen**). The influence of the linking topology on the thermal and photophysical properties of these compounds was investigated with the density functional theory (DFT) and by experimental observations.

4.1.1. Synthesis

Similar compounds containing carbazole and phenothiazine moieties were earlier synthesized by applying the conditions of the conventional Ullmann reaction. The reactions were successfully accomplished by using iodinated carbazole derivatives [112,113]. In our work, we used easily synthesized Br-substituted carbazole compounds. **CzBisPhen** and **CzMonoPhen** were synthesized by palladium-catalyzed Buchwald-Hartwig reactions between a Br-substituted carbazole derivative and phenothiazine. The optimized Buchwald-Hartwig reaction was carried out in refluxing toluene in the presence of bis(tri-*tert*-butylphosphine)palladium(0) ($\text{Pd}(\text{t-Bu}_3\text{P})_2$) as the catalyst and potassium *tert*-butoxide as the strong base; it yielded the desired compounds in relatively high yields (**Scheme 4.1.1**).



Scheme 4.1.1. Synthesis of **CzBisPhen** and **CzMonoPhen**

The starting compounds **1a** and **1b** were prepared by bromination of carbazole with N-bromosuccinimide (NBS) in dimethylformamide (DMF). The target compounds were crystallized to yield pure solid compounds. The chemical structures of the target compounds were confirmed via X-ray crystallography (**Fig. 4.1.1**), also by ^1H and ^{13}C nuclear magnetic resonance (NMR), and Infrared spectroscopy (IR).

4.1.2. Theoretical investigation

To get hints about the hole and electron mobilities of the lowest energy conformers of **CzBisPhen** and **CzMonoPhen** molecules, the electronic molecular orbital distributions were examined through the estimation of frontier orbitals (HOMO and LUMO) energies by DFT. The HOMO dispersion on phenothiazine and the LUMO dispersion on carbazole moieties for both molecules were observed (**Fig. 4.1.1**). The HOMO/LUMO levels of **CzBisPhen** and **CzMonoPhen** (from DFT calculations) were estimated to be $-4.91/-1.28$ eV and $-4.80/-1.00$ eV, respectively. It can be presumed from the molecular orbital diagrams that **CzBisPhen** and **CzMonoPhen** may exhibit a similar electron transport character because of LUMO which is delocalized on the carbazole moiety for both molecules. However, dissimilar hole carrying properties of these compounds were predicted from this study.

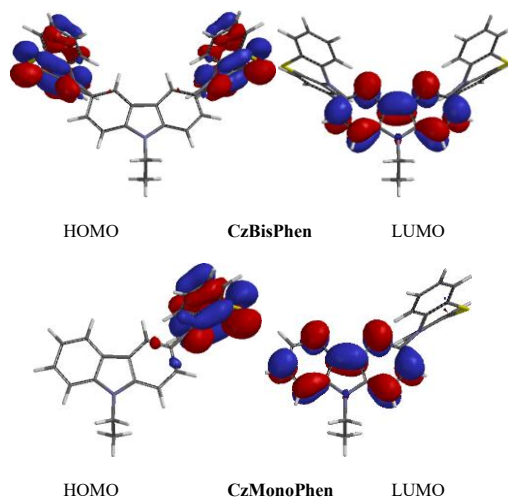


Fig. 4.1.1. Frontier orbitals (HOMO and LUMO) of **CzBisPhen** and **CzMonoPhen**

In addition, the vertical energies of the singlet S_1 and triplet T_1 first excited states of **CzBisPhen** and **CzMonoPhen** were estimated by using the time dependent (TD)-DFT theory and the B3LYP/6-31G(d,p) method in vacuum. The energies of the first excited singlet and triplet states of the molecules were estimated to be 3.00/3.08 eV and 2.65/2.69 eV for **CzBisPhen** and **CzMonoPhen**, respectively.

4.1.3. Thermal properties

The thermal transitions of the compounds were studied by TGA under nitrogen atmosphere. The temperature values of 5% mass loss ($T_{\text{des-5\%}}$) estimated by TGA at a heating rate of $20^\circ\text{C min}^{-1}$ were found to be 419°C and 327°C for **CzBisPhen** and **CzMonoPhen**, respectively. The TGA curve of **CzBisPhen** compound demonstrated evaporation of DMF solvent which is in the crystal lattice at a temperature range from $200\text{--}250^\circ\text{C}$. The presence of DMF in the crystals was proved by X-ray crystallography and NMR analysis. In this case, the decomposition temperature of the **CzBisPhen** compound was calculated from the second decrease of the curve.

4.1.4. Optical and photophysical properties

The experimental photophysical properties (**Fig. 4.1.1**) of **CzBisPhen** and **CzMonoPhen** were examined by UV-vis and photoluminescence (PL) spectrometry analytical techniques. The data is summarized in **Table 4.1.2**. The optical band gaps estimated from the red edge absorption onset by using formula $E = hc/\lambda$ were found to be 3.31 eV and 3.40 eV for **CzBisPhen** and **CzMonoPhen**, respectively. For the better understanding of the electronic properties of carbazole and phenothiazine-based compounds, the excitation energy as the energy of singlet-singlet electronic transition

was estimated by the TD-DFT/B3LYP/6-31G(d,p) method and polarizable continuum model (PCM) of THF ($\epsilon = 7.6$). Importantly, significant similarities between the theoretical and experimental UV-vis spectra were observed (**Fig. 4.1.3** and **Table 4.1.2.**).

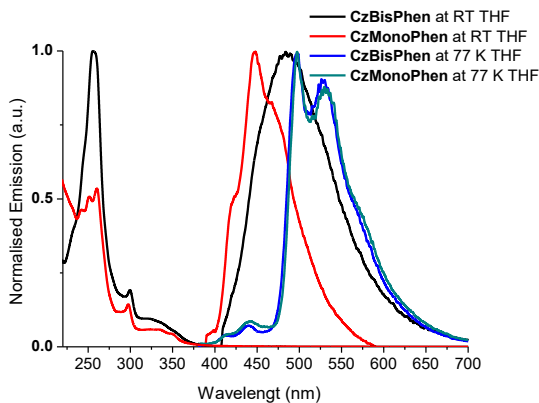


Fig. 4.1.2. Normalized UV-vis and PL emission spectra of dilute solutions of **CzBisPhen** and **CzMonoPhen** in THF at room temperature at 77 °K

The oscillator strengths for $S_0 \rightarrow S_1$ attributed to HOMO \rightarrow LUMO transition for both compounds are very low (*ca.* 0.0001). It leads to the low intensity of the absorption bands. This transition is denoted by the intramolecular charge transfer (CT) character. Moreover, this CT transition is spatially forbidden because HOMO and LUMO are delocalized on the phenothazine and carbazole moieties, respectively. These moieties are perpendicular to each other (*vide supra*). A very small overlap of the frontier orbitals (*vide infra*) indicates the low emission quantum yields of the compounds. However, the small overlap of the frontier molecular orbitals is created on the ambipolar transport of the hole and the electron over the phenothazine and carbazole moieties, respectively. This effect is due to the presence of an indirect band gap for the recombination of carriers [114]. The absorption band of **CzBisPhen** and **CzMonoPhen** at *ca.* 300 nm has the $n \rightarrow \pi^*$ and $\pi \rightarrow \pi^*$ symmetry forbidden characters on the phenothazine and carbazole moieties, respectively, since the orbitals on the carbazole moiety are oriented along the symmetry axis [115]. The highest oscillator strength (i.e., *ca.* $f = 0.72$) of excitations at *ca.* 260 nm is a mixture of the fully allowed $\pi \rightarrow \pi^*$ transitions of both conjugated chromophores (**Table 4.1.2.**).

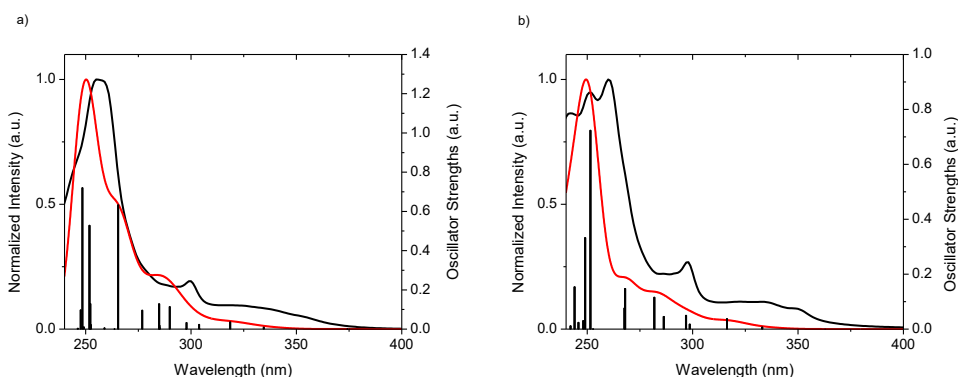


Fig. 4.1.3. Comparison of the experimental (black line) and calculated UV-vis spectra of CzBisPhen and CzMonoPhen (red line) at the B3LYP/6-31G(d,p)/PCM(THF) level ($\sigma = 0.20$ eV); the bars represent the oscillator strength

Table 4.1.1. Data of the TD-DFT calculations of UV-vis spectra

Comp.	Exp. UV λ (nm)	Theor. UV λ (nm)	Electronic transition and character	Oscillator strength (f , au)	MO/character and contributions (%)
CzBisPhen	327	375	$S_0 \rightarrow S_1$ (CT)	0.0001	H \rightarrow L (95)
		318	$S_0 \rightarrow S_5$ ($n \rightarrow \pi^*$)	0.0368	H-2 \rightarrow L (100)
	300	290	$S_0 \rightarrow S_{11}$ ($n \rightarrow \pi^*$)	0.1148	H \rightarrow L+6 (34)
		285	$S_0 \rightarrow S_{14}$ ($\pi \rightarrow \pi^*$)	0.1292	H-3 \rightarrow L (45)
	256	252	$S_0 \rightarrow S_{25}$ ($\pi \rightarrow \pi^*$)	0.5292	H-2 \rightarrow L+3 (41)
CzMonoPhen	330	248	$S_0 \rightarrow S_{27}$ ($\pi \rightarrow \pi^*$)	0.7204	H-3 \rightarrow L+1 (45)
		363	$S_0 \rightarrow S_1$ (CT)	0.0001	H \rightarrow L (91)
	297	316	$S_0 \rightarrow S_3$ ($n \rightarrow \pi^*$)	0.0379	H-1 \rightarrow L (94)
		281	$S_0 \rightarrow S_7$ ($\pi \rightarrow \pi^*$)	0.1157	H-2 \rightarrow L (68)
	260	268	$S_0 \rightarrow S_8$ ($n \rightarrow \pi^*$)	0.1478	H \rightarrow L+1 (82)
	252	$S_0 \rightarrow S_{11}$ ($\pi \rightarrow \pi^*$)	0.7238	H-1 \rightarrow L+3 (59)	

From the onsets of fluorescence spectra (**Fig. 4.1.2**) of the solution of the compounds in tetrahydrofuran (THF), the first excited singlet state (S_1) energies were estimated at room temperature. The energies of S_1 were found to be 3.03 eV and 3.09 eV for **CzBisPhen** and **CzMonoPhen**, respectively. The emission quantum yields of the compounds in THF solution ($c \sim 10^{-5}$ mol/l) and in solid state were found to be lower than 1% (**Table 4.1.1.**). This observation is in good agreement with the results of TD-DFT calculations thus indicating a very small overlap of the frontier orbitals and the low oscillator strengths of the first transitions. The phosphorescence spectra of the solutions of the synthesized compounds in THF were recorded at 77 °K. The first excited triplet state (T_1) energy (E_T) was estimated from the onset of the highest energy peak of phosphorescence spectra. The triplet energies of **CzBisPhen** and **CzMonoPhen** were found to be 2.61 eV and 2.60 eV, respectively. This data offers good consistency with the theoretical results by the emission spectra (*vide supra*).

These values of E_T are sufficiently high for the application of the compounds as host materials for green and red PhOLEDs.

4.1.5. Electrochemical properties and ionization potentials

The electrochemical properties of **CzBisPhen** and **CzMonoPhen** were investigated by cyclic voltammetry (CV). This method was also used for the estimation of the ionization potential (IP) in solution. In addition, the ionization potentials in solid state layers of the compounds were measured by the electron photoemission method in air. The electron photoemission spectra are shown in **Fig. 4.1.4.b**.

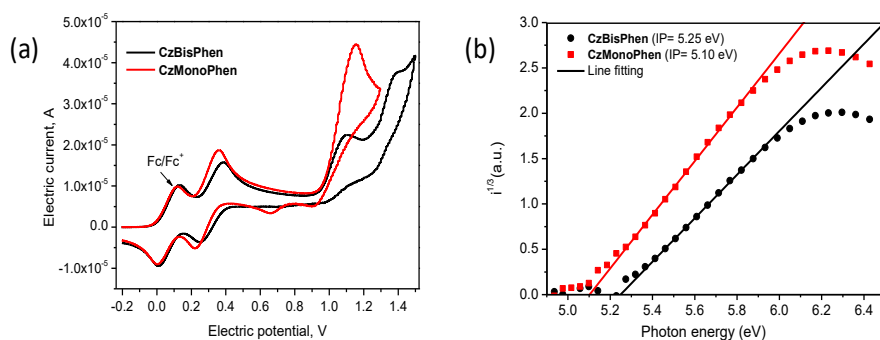


Fig.4.1.4. Cyclic voltammograms (a) and electron photoemission spectra (b) of **CzMonoPhen** and **CzBisPhen**

The IP values (or HOMO values via Koopmans' theorem: $IP = -HOMO$ [116]) for **CzBisPhen** and **CzMonoPhen** estimated from CV curves of the solutions of the compounds in dichloromethane (**Fig. 4.1.4.a**) were found to be 4.86 eV and 4.85 eV, respectively. These values are in good agreement with the results of the theoretical calculations which showed the HOMO values of -4.91 eV and -4.80 eV for **CzBisPhen** and **CzMonoPhen**, respectively (*vide supra*). The ionization potentials of the solid samples of the materials, which correlate with the IP values in solution, were determined from the electron photoemission spectra and found to be 5.25 eV and 5.10 eV for **CzBisPhen** and **CzMonoPhen**, respectively (**Fig. 4.1.4.b**). These observations show that the introduction of a phenothazine moiety increases the HOMO energy levels relative to those of the corresponding carbazole derivatives [117]. The reduction signals up to -2.5 V vs. Fc were not observed in the CV curves of **CzBisPhen** and **CzMonoPhen**. The experimental LUMO energy values were estimated by using the CV technique and the experimental IP values found to be -1.55 eV and -1.45 eV for **CzBisPhen** and **CzMonoPhen**, respectively. The LUMO energy values obtained from the theoretical calculations were -1.28 eV and -1.00 eV for **CzBisPhen** and **CzMonoPhen**, respectively. This mismatch can be explained by the employment of the optical band gap for the estimation of the experimental LUMO

energy. The optical band gap is not identical to the electrochemical band gap. The energy difference between the optical and electrochemical band gaps corresponds to exciton dissociation energy [118]. Yoshida and Yoshizaki showed that more accurate LUMO values of the compounds are received from DFT theoretical calculations [119]. The experimental and theoretical HOMO and LUMO energy levels are summarized in **Table 4.1.1**.

Table 4.1.2. Photophysical characteristics of **CzBisPhen** and **CzMonoPhen**

Comp	$\lambda_{\text{abs}}^{\text{a}}$, nm	$\lambda_{\text{em}}^{\text{a}}$ nm	QY (in THF/solid) %	S ₁ (exp/theo), eV	T ₁ (exp/theo) eV	HOMO (exp ^b /theo), eV	LUMO (exp ^c /theo), eV	IP (solid) ^d , eV
CzBisPhen	327, 300, 256	483	1.03/1.32	3.03/3.00	2.61/2.65	-4.86/ -4.91	-1.55/ 1.28	5.25
CzMonoPhen	330, 297, 260	448	0.07/0.56	3.09/3.08	2.60/2.69	-4.85/ -4.80	-1.45/ 1.00	5.10

^a Absorption and fluorescence spectra of dilute THF solutions (*ca.* 10⁻⁵ M). ^b HOMO energies calculated by formula HOMO = -1.40(qV_{CV}) - 4.60 [120]. ^c LUMO energies calculated by subtracting the band gap energies from HOMO energies via formula LUMO = HOMO + E_g. ^d IP energies evaluated from of the electron photoemission spectra of thin solid films

4.1.6. Charge-transporting properties

To evaluate the charge-transporting properties of **CzMonoPhen** and **CzBisPhen**, the hole (μ_{h}) and electron (μ_{e}) mobilities were measured by employing the Time-of-Flight (ToF) technique. **CzMonoPhen** and **CzBisPhen** showed ambipolar charge transport (**Fig. 4.1.5**). Electron mobility of 1.56×10⁻⁴ cm²/(Vs) at an electric field of 6.73×10⁵ V/cm was observed for the layer of **CzBisPhen**, while the hole mobility was lower by *ca.* one order of magnitude (4×10⁻⁵ cm²/(Vs) at an electric field of 6×10⁵ V/cm) (**Table 4.1.3**). The only slight differences were observed for μ_{h} and μ_{e} of **CzMonoPhen** compared to those of **CzBisPhen** due to the similarity of their molecular structures.

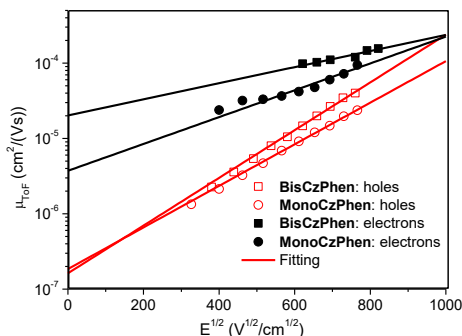


Fig. 4.1.5. Electric field dependences on charge mobilities in the layers of **CzMonoPhen** and

CzBisPhen

Table 4.1.3. Charge transport parameters for **CzMonoPhen** and **CzBisPhen**

Compound	$\mu_0, \text{cm}^2/(\text{V}\times\text{s})$	
	holes	electrons
CzMonoPhen	1.85×10^{-7}	3.72×10^{-6}
CzBisPhen	1.62×10^{-7}	2.02×10^{-5}

4.1.7. Fabrication and characterization of PhOLEDs

To test the synthesized compounds **CzBisPhen** and **CzMonoPhen** as the host materials, phosphorescent light emitting devices were fabricated employing the PVD process. 4,4',4''-Tris[phenyl(m-tolyl)amino]triphenylamine (m-MTDATA) was utilized for the preparation of the hole-transporting layer. 4,7-Diphenyl-1,10-phenanthroline (Bphen) served as the electron-transporting and hole-blocking material. Tris[2-phenylpyridinato- C^2, N]iridium(III) ($\text{Ir}(\text{ppy})_3$) and bis[2-(1-isoquinolinylnyl- N)phenyl- C](2,4-pentanedionato- O^2, O^4)iridium(III) ($\text{Ir}(\text{piq})_2(\text{acac})$) served as the emitting materials. The top calcium layer was deposited at the cathode which was protected by aluminum. The structures of PhOLEDs were the following: ITO/**CzBisPhen**: $\text{Ir}(\text{ppy})_3$ (45 nm)/ Bphen (35 nm)/Ca:Al (Device **IA**); ITO/**CzMonoPhen**: $\text{Ir}(\text{ppy})_3$ (45 nm)/Bphen(35 nm)/Ca:Al (Device **IB**); ITO/m-MTDATA (30 nm)/**CzBisPhen**: $\text{Ir}(\text{ppy})_3$ (20 nm)/Bphen (30 nm)/ Ca:Al (Device **IIA**); ITO/m-MTDATA (30 nm)/**CzMonoPhen**: $\text{Ir}(\text{ppy})_3$ (20 nm)/Bphen(30 nm) /Ca:Al (Device **IIB**); ITO/m-MTDATA(30 nm)/**CzBisPhen**: $\text{Ir}(\text{piq})_2(\text{acac})$ (20 nm)/Bphen(30 nm)/Ca:Al (Device **IIIA**); ITO/m-MTDATA(30 nm)/**CzMonoPhen**: $\text{Ir}(\text{piq})_2(\text{acac})$ (20 nm)/Bphen(30 nm)/Ca:Al (Device **IIIB**). The energy diagrams of the fabricated PhOLEDs are shown in **Fig. 4.1.6**.

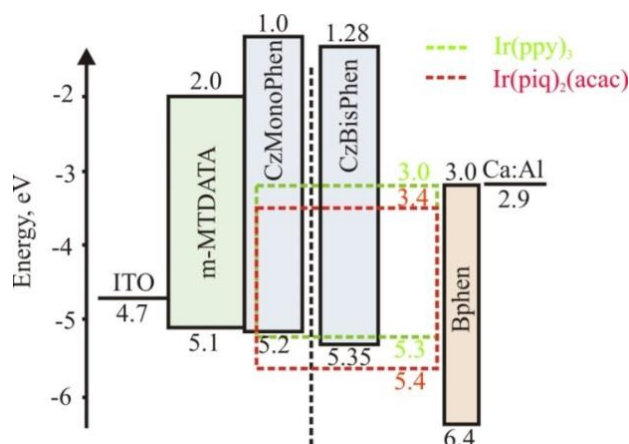


Figure 4.1.6. Energy diagrams of the devices

The electroluminescence (EL) spectra of the fabricated PhOLEDs were characterized by green and red emissions with the *Commission Internationale de l'Éclairage* (CIE) chromaticity coordinates (x, y) of (0.30; 0.63) and (0.68; 0.31) for the green and red devices, respectively. In addition, the EL spectra of the studied PhOLEDs were very similar to the photoluminescence spectra of Ir(ppy)₃ and Ir(piq)₂(acac) dyes [121] thus confirming that the EL originated from the guest materials. The emissions of the hosts **CzBisPhen** and **CzMonoPhen** were characterized by the maximum at 475 nm and 445 nm, respectively. The emission bands of m-MTDATA and Bphen were not observed in the EL spectra of the devices. The energy diagrams (**Fig. 4.1.6**) indicate the efficient injection of holes from the hosts **CzBisPhen** and **CzMonoPhen** to the dopants Ir(ppy)₃ and Ir(piq)₂(acac). The electrons are injected into the Ir(III) dyes, and they are transported through the layers of dyes. The barriers of electron injection from the ETL to Ir(III) dyes are lower than the barriers of injection from the ETL to the host molecules. Therefore, the mechanism of emission generation is the direct recombination of the injected charges (carrier trapping) in the emitting layer.

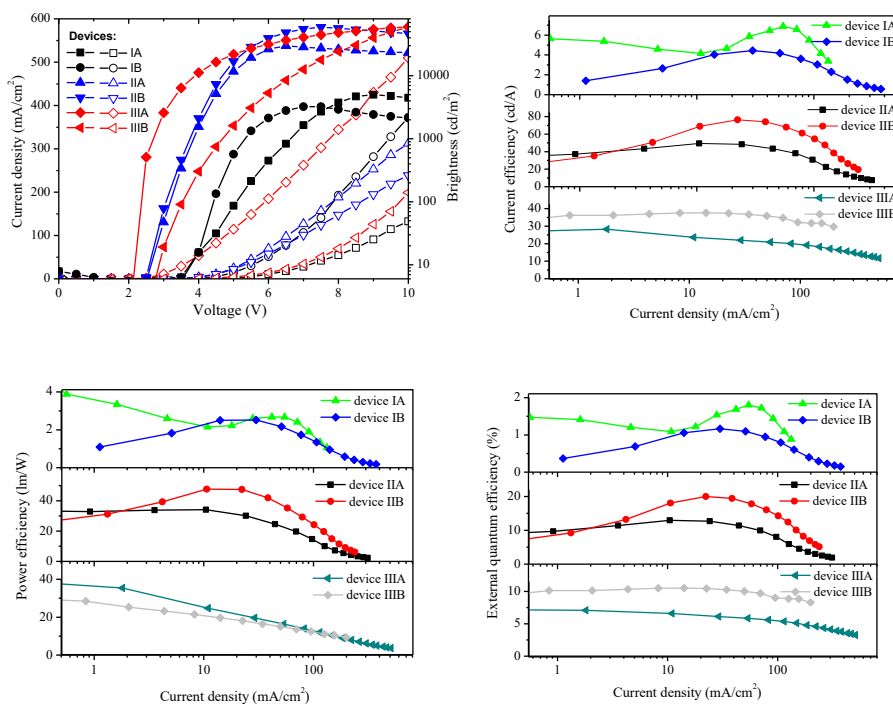


Fig. 4.1.7. Characteristics of PhOLEDs: current density versus voltage and luminance versus voltage (a), current efficiency versus current density (b), power efficiency versus current density (c), external quantum efficiency versus current density (d)

Fig. 4.1.7. demonstrates the current density versus voltage and luminance versus voltage plots of the fabricated devices. The values of 2.5V of the turn-on voltage (V_{on}) for Devices **IIA** and **IIB** were observed, while V_{on} of 3.8V were recorded for m-MTDATA-layer-free devices for Devices **IA** and **IB** (V_{on} were taken at 10 cd/m²). This result confirms the improvement of the charge balance after the introduction of the additional hole-transporting m-MTDATA layer which reduced the potential barrier for holes in Devices **IIA** and **IIB**.

Table 4.1.4. Parameters of PhOLEDs

Device	V_{on}/V at 10 cd/m ²	Maximum brightness/cd/m ²	Maximum current efficiency/ cd/A	Maximum power efficiency/ lm/W	Maximum EQE/ %
IA	3.5	4995 (9.0V)	6.89	5.4	1.8
IB	3.5	3235 (7.5V)	4.45	2.5	1.16
IIA	2.5	29913 (6.5V)	49.4	34.1	12.9
IIB	2.5	58974 (7.5V)	74.1	47.5	20.0
IIIA	2.5	59558 (10.0V)	28.2	40.6	7.2
IIIB	3.0	59110 (10.0V)	37.4	29.6	10.5

The use of the additional m-MTDATA layer as a hole-transporting layer also leads to the improvement of other characteristics of the devices. The brightness maxima of 27262 cd/m² and 58974 cd/m² (at 7.5V) were recorded for Devices **IIA** and **IIB** respectively, while the maximum brightness of 2698 cd/m² and 3235 cd/m² was observed for Devices **IA** and **IB**, respectively, at the same voltage (**Fig. 4.1.7**). The V_{on} of 2.5V and the maximum brightness of 59558 cd/m² and 59110 cd/m² were observed for Devices **IIIA** and **IIIB**, respectively (**Fig. 4.1.7**). The maximum current efficiency of 74.1 cd/A and the maximum power efficiency of 47.5 lm/W were established for Device **IIB** (**Fig. 4.1.7.b,c, Table 4.1.4.**). The maximum brightness observed for the devices fabricated in this work is comparable with that of the recently developed PhOLEDs with a similar architecture [122].

To conclude, two low molar mass compounds based on phenothiazine as the donor and carbazole as the acceptor moieties were synthesized and investigated. The computational studies were well supported by the experimental findings. The compounds exhibited appropriate ionization potentials of 5.10 eV and 5.25 eV and good ambipolar charge transporting properties. The time-of-flight hole and electron drift mobilities in its layers approached 10⁻⁵ cm²/(V s) and 10⁻⁴ cm²/(V s) at high electric fields, respectively. The maximum power and external quantum efficiencies up to 47.5/40.6 lm/W and 20.0/10.5% of green and red PhOLEDs, respectively, were observed.

4.2. Triphenylsilane and sulfonyl-4-methylbenzene-substituted bicarbazolyl derivatives

Carbazole derivatives are among superior host materials which demonstrate promising performances in phosphorescent OLEDs. Many carbazole derivatives have adequate high triplet energy to be able to host red [123,124], green [125] or even blue [126,127] triplet emitters. These examples demonstrate that carbazole derivatives can be operated as the host material for both small-molecule and polymer OLEDs.

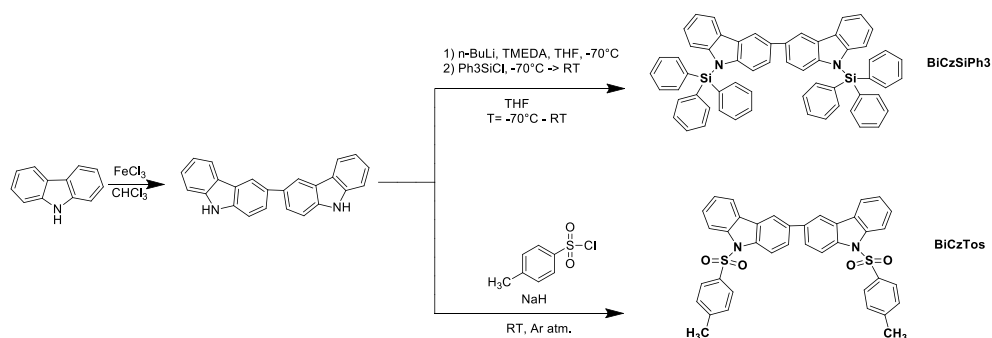
Hence, 3,3'-bicarbazole has not only a high E_T , but also a small ΔE_{ST} of 0.48 eV. In 2011, Kim and co-workers predicted by DFT calculations that a carbazole-based oligomer linked with the 3,3'-position can have a higher E_T than a common blue phosphorescent emitter, iridium(III) bis[(4,6-difluorophenyl)-pyridinate-*N,C* 2']picolinate (FIrpic) [128]. Concerning the sterically twisted structure, bicarbazole derivatives can considerably diminish the host-host aggregation and form an excimer. Meanwhile, dimerization of carbazole can improve the thermal and morphological stability of a thin film. Furthermore, the electronic properties of bicarbazole derivatives can be combined by chemical modification on the 9,9'-positions. These desirable properties exhibit great opportunities as a host material in blue PhOLEDs. However, bicarbazole derivatives have never been used either for blue PhOLEDs or in green PhOLEDs [129,130]. Consequently, a new series of functionalized 3,3'-bicarbazole derivatives was prepared and studied; these derivatives were modified with triphenylsilane (**BiCzSiPh₃**) and with 1-hydrosulfonyl-4-methylbenzene (**BiCzTos**) moieties on the 9,9'-positions.

4.2.1. Synthesis

The synthetic route of compounds **BiCzSiPh₃** and **BiCzTos** is shown in **Scheme 4.2.1**. First of all, by Friedel-Crafts reaction, while using $FeCl_3$ as the Lewis acid catalyst, 9*H*,9'*H*-3,3'-bicarbazole was synthesized. Afterwards, two symmetric bipolar materials were designed and synthesized with the 3,3'-bicarbazole core.

Compound **BiCzSiPh₃** was synthesized when 3,3'-bicarbazole was treated with tetramethylethylenediamine (TMEDA) and with 1.7 M *n*-BuLi at -40 °C to yield a lithiated intermediate which was subsequently quenched with chlorotriphenylsilane at -70 °C. The target compound of **BiCzSiPh₃** gave a colorless amorphous powder after washing with methanol.

Meanwhile, **BiCzTos** was synthesized when *N*-unsubstituted bicarbazole, sodium hydride (NaH) and *p*-toluenesulfonyl chloride were dissolved in THF under argon atmosphere. The target compound gave colorless powders after crystallization.



Scheme 4.2.1. Synthetic routes and chemical structures of **BiCzSiPh₃** and **BiCzTos**

4.2.2. Thermal properties

All the target compounds exhibited excellent thermal stability (**Table 4.2.1**). The thermal decomposition temperatures (T_d , corresponding to 5% weight loss) were measured as 372 °C and 349 °C for **BiCzSiPh₃** and **BiCzTos**, respectively, while for the parent molecule BCzPh [131], it is estimated to be 340 °C. The clear glass transition temperatures (T_g) of functionalized bicarbazole derivatives **BiCzSiPh₃** and **BiCzTos** were observed under heating at 149 °C and 126 °C, respectively, which are 49 °C and 26 °C higher than that of phenyl-substituted BCzPh (T_g of BCzPh is 100 °C). Compared with T_g 100°C for BCzPh, the glass-transition temperatures significantly increased because of the molecular polarity; also, molecular masses increased in comparison with BCzPh. The melting points were evaluated from DSC and are 40–406 °C and 311 °C for **BiCzSiPh₃** and **BiCzTos**, respectively. Also, only **BiCzSiPh₃** demonstrates a temperature of crystallisation, which is 253 °C. Ultimately, these results obviously highlight the excellent thermal stability of a thin solid film by using these bicarbazole derivatives. In this case, all these new compounds could create morphologically stable and steady amorphous films by vacuum deposition for OLED fabrication.

Table 4.2.1. Thermal characteristics of **BiCzSiPh₃** and **BiCzTos**

Compound	T_g^a , °C	T_m^a , °C	T_{cr}^a , °C	$T_{d-5\%}^b$, °C
BiCzSiPh₃	149	406; 404	253	372
BiCzTos	126	311	-	349
BCzPh	100	-	-	340

^a Determined by DSC; ^b Determined by TGA

4.2.3. Optical and photophysical properties

UV/Vis and PL spectra of **BiCzSiPh₃** and **BiCzTos** are shown in **Fig. 4.2.1** and summarized in **Table 4.2.2**. The optical band gaps were estimated to be 3.49 eV and 3.70 eV from the red edge absorption onset by using formula $E_g = hc/\lambda$ for **BiCzSiPh₃** and **BiCzTos**, respectively. The emission quantum yields of the compounds in THF solution ($c \sim 10^{-5}$ mol/l) were found to be 41.2 and 11.5% for **BiCzSiPh₃** and **BiCzTos**,

respectively. The emission quantum yields of the compounds in the solid state were found to be 1.44 and <1% for **BiCzSiPh₃** and **BiCzTos**, respectively.

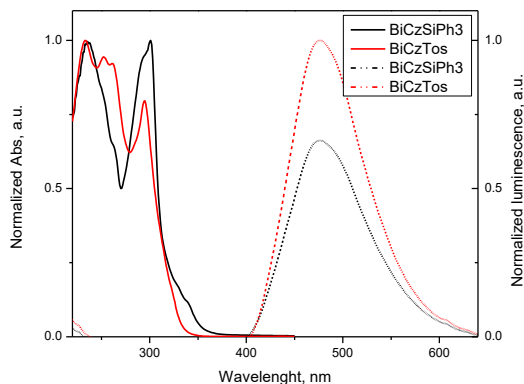


Figure 4.2.1. Normalized UV-vis and PL emission spectra of dilute solutions of **BiCzSiPh₃** and **BiCzTos** in THF at room temperature and at 77 °K

Table 4.2.2. Photophysical properties of bicarbazolyl derivatives

Comp.	λ_{em}^a , nm	QY (in THF/solid), %	S ₁ (exp), eV	T ₁ (exp), eV	HOMO (exp ^b), eV	LUMO (exp ^c), eV	IP (solid), eV ^d
BiCzSiPh₃	390	41.2/1.44	3.29	2.84	-5.43	-1.94	5.45
BiCzTos	350	11.5/<1	3.30	2.82	-6.08	-2.38	5.73

^a Absorption and fluorescence spectra of dilute THF solutions (ca. 10⁻⁵ M); ^b HOMO energies calculated by the formula HOMO = -1.40·(qV_{CV}) - 4.60 [120]; ^c LUMO energies calculated by subtracting the band gap energies from HOMO energies via formula LUMO=HOMO+E_g; ^d IP energies evaluated from of the electron photoemission spectra of thin solid films

The phosphorescence spectra of the solutions of the synthesized compounds in THF were recorded at 77 °K. The first excited triplet state (T₁) energy (E_T) was estimated from the onset of the highest energy peak of phosphorescence spectra. From the onsets of fluorescence spectra recorded at 77 °K (**Fig. 4.2.2**) of the solution of the compounds in tetrahydrofuran (THF), the first excited singlet state (S₁) energies were estimated at room temperature. The energies of S₁ were estimated to be 3.29 eV and 3.30 eV for the **BiCzSiPh₃** and **BiCzTos**, respectively. The triplet energies of **BiCzSiPh₃** and **BiCzTos** were found to be 2.84 eV and 2.82 eV, respectively. These values of E_T are sufficiently high for the application of the compounds as host materials for blue PhOLEDs.

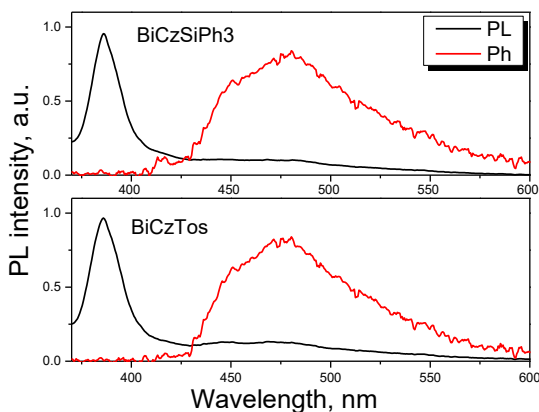


Figure 4.2.2. Photoluminescence (PL) and phosphorescence (Ph) spectra of dilute THF solutions of **BiCzSiPh₃** and **BiCzTos** at 77 °K. Ph spectra were recorded with delay of 50 ms after excitation at 300 nm

4.2.4. Electrochemical and photoelectrical properties

The bipolar electrochemical properties of **BiCzSiPh₃** and **BiCzTos** were probed by cyclic voltammetry (CV) and are shown in **Fig. 4.2.3.a**. The measurements were performed in DCM for oxidation and reduction scans, with ferrocene as the internal reference. The HOMO levels of **BiCzSiPh₃** and **BiCzTos** were estimated to be -5.43 eV and -6.08 eV, respectively. The HOMO level of **BiCzTos** is lower than for FIrpic (-5.60 eV) thus specifying that both host materials can enhance hole charge trapping in the FIrpic and lead to direct charge recombination in the dopant [132]. The LUMO levels were determined as -1.94 eV for **BiCzSiPh₃** and -2.38 eV for **BiCzTos**, according to equation $E_{\text{LUMO}} = E_{\text{HOMO}} + E_{\text{g}}$. (E_{g} , band gap was estimated from the UV-vis experiment). Compared with BCzPh (LUMO of 2.30 eV), these values are superficial. That is the mean that electron injection to emitting layers should be upgraded in the device [133].

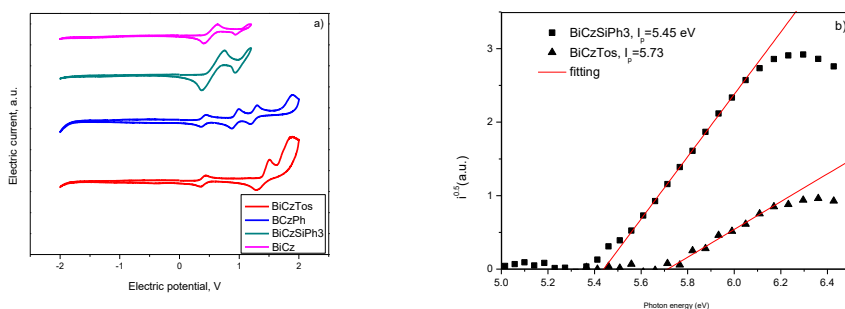


Figure 4.2.3. Cyclic voltammograms of BiCz, BCzPh, **BiCzSiPh₃** and **BiCzTos** (a); Electron photoemission spectra of the layers of **BiCzSiPh₃** and **BiCzTos** (b)

Since the energy levels for solid-state samples are required for device designing, the ionization potentials of the solid-state layers of the compounds were measured by the electron photoemission method in air. The values of 5.45 eV and 5.73 eV were obtained, respectively (**Fig. 4.2.3.b**). This observation lies in agreement with the data established by cyclic voltammetry. Considering that I_p of BCzPh was detected at -5.67 eV, this is the property of a 3,3'-bicarbazole skeleton. The electron affinity (E_a) for solid-state samples was calculated by subtraction of the optical energy gap (E_g) from the I_p ($E_a = E_g - I_p$) and was calculated to be 1.96 eV and 2.03 eV for **BiCzSiPh₃** and **BiCzTos**, respectively.

4.2.5. Charge-transporting properties

The charge carrier mobilities of the vacuum-deposited layers for compounds **BiCzSiPh₃** and **BiCzTos** were tested by employing the TOF technique. To find the electron and hole mobilities in the layers of compounds **BiCzSiPh₃** and **BiCzTos**, photocurrent transients were recorded for the tested samples at different applied external voltages (**Fig. 4.2.4.a,b**). In contrast to the transients for holes in the **BiCzSiPh₃**-based layer, the transients for electrons were highly dispersive, which is typically observed for donor-acceptor compounds with twisted chemical structures. The charge transit times for holes and electrons were obtained at different electric fields for compound **BiCzSiPh₃** analyzing these photocurrent transients (**Fig. 4.2.4.a,b**). This finding indicates bipolar charge-transporting properties of **BiCzSiPh₃**-based layers. In contrast to compound **BiCzSiPh₃**, charge transit times for neither holes nor electrons were indicated for compound **BiCzTos**. This observation says that the hole and electron mobility of compound **BiCzTos** is out of mobility values which can be detected by the TOF method. Most probably, the mobilities of triphenylsilane-substituted bicarbazolyl derivative **BiCzTos** are much lower than these of the 1-hydrosulfonyl-4-methylbenzene-substituted bicarbazolyl derivative **BiCzSiPh₃**.

The Poole-Frenkel type dependencies ($\mu = \mu_0 \cdot \exp(\alpha \cdot E^{1/2})$) of hole and electron mobilities measured at room temperature for the samples of **BiCzSiPh₃** in different applied positive electric fields (E) are plotted in **Fig. 4.2.4.c**. The hole and electron mobilities in the **BiCzSiPh₃**-based samples were found on the orders of 10^{-5} – 10^{-4} $\text{cm}^2\text{V}^{-1}\text{s}^{-1}$. The electron mobilities were a few times higher than the hole mobilities, at the same electric fields achieving 1.4×10^{-4} $\text{cm}^2\text{V}^{-1}\text{s}^{-1}$ and 5.4×10^{-4} $\text{cm}^2\text{V}^{-1}\text{s}^{-1}$ for holes and electrons at an electric field of 5.3×10^5 Vcm^{-1} , respectively. Such mobilities are good enough for the applications of compound **BiCzSiPh₃** as an organic semiconductor in solid-state devices.

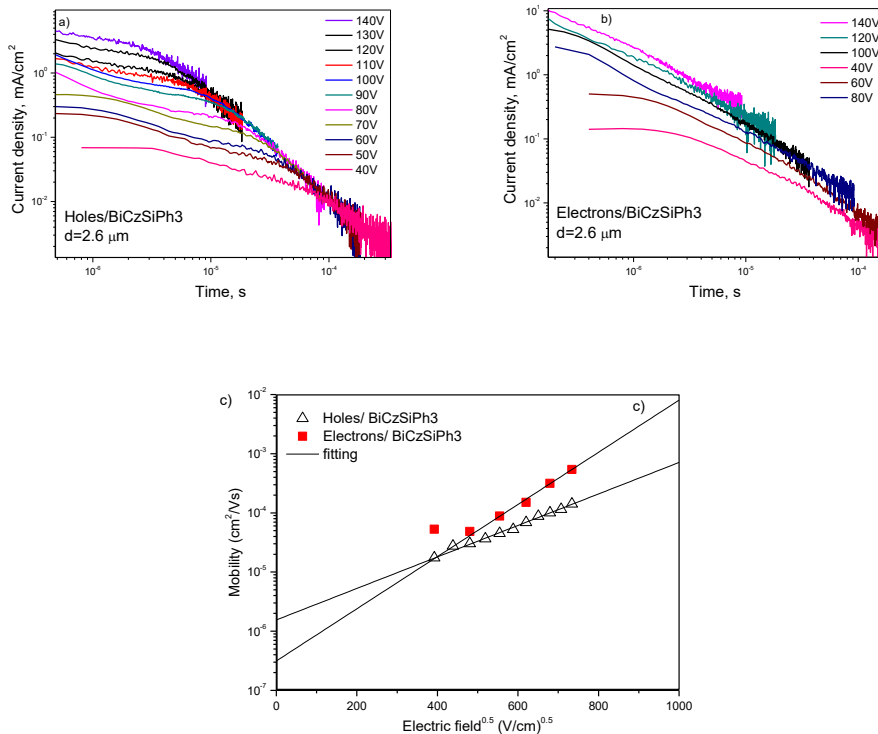


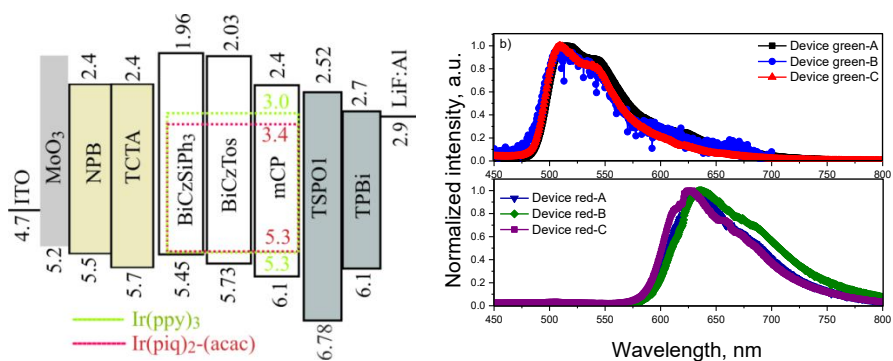
Figure 4.2.4. Hole and electron current ToF transient pulses for the layers of **BiCzSiPh₃** at different electric fields at room temperature (a, b); Electric field dependencies of charge drift mobilities for the layers of **BiCzSiPh₃** at room temperature (c)

4.2.6. Fabrication and characterization of PhOLEDs

The electroluminescence (EL) performances of **BiCzSiPh₃** and **BiCzTos** as hosts in PhOLEDs were tested by employing the device structures of indium tin oxide (ITO)/ molybdenum trioxide (MoO₃, 1 nm), *N,N'*-bis(naphthalen-1-yl)-*N,N'*-bis(phenyl)benzidine (NPB, 40 nm)/tris(4-(9H-carbazol-9-yl)phenyl)amine (TCTA, 25 nm)/light emitting layer (30 nm, 7% of emitter)/ diphenyl-4-triphenylsilylphenylphosphineoxide (TSPO1, 4 nm)/ 2,2',2''-(1,3,5-benzinetriyl)-tris(1-phenyl-1*H*-benzimidazole) (TPBi, 40 nm) /LiF (0.5 nm)/Al (60 nm). Depending on the selected green or red phosphorescent emitter (Tris[2-phenylpyridinato-*C*²,*N*]iridium(III) [Ir(ppy)₃] and bis[2-(1-isoquinolinyl)N]phenyl-C(2,4-pentanedionato-*O*²,*O*⁴)iridium(III) [Ir(piq)₂-(*acac*)] and on the tested host (**BiCzSiPh₃**, **BiCzTos**, or 1,3-Bis(*N*-carbazolyl)benzene (mCP)), six **green-A**, **green-B**, **green-C**, **red-A**, **red-B**, **red-C** devices were fabricated, respectively. Their equilibrium energy diagram is shown in **Fig. 4.2.5.a**, while their performances are listed in **Table 4.2.3**. The mCP-based devices were fabricated as reference devices. Green and red phosphorescent

emitters Ir(ppy)₃ and Ir(piq)₂-(acac)] were chosen due to the HOMO, LUMO and triplet energy levels of the tested hosts **BiCzSiPh₃** and **BiCzTos**. Hole-injecting and hole-transporting functional layers MoO₃ and NPB, TCTA as well as electron-injecting and electron-transporting functional layers LiF, and TSPO1, TPBi were used for getting minimal injecting-energy barriers of charges to the light-emitting layers of the studied devices (**Fig. 4.2.5.a**). As a result, EL spectra related only to the used emitters were obtained due to the charge recombinations and exciton generations within the light-emitting layers of these devices (**Fig. 4.2.5.b**). No emission related to the used hosts was detected thus indicating good host-guest energy transfer.

When analyzing the output performances of the studied devices (**Fig. 4.2.5.b-f**, **Table 4.2.3**), it is well-recognized that the performances of **BiCzTos**-based devices are much lower than these of **BiCzSiPh₃**- and mCP-based devices. Since TOF-transients for **BiCzTos**-based layers were not obtained, the achievements for **BiCzTos**-based devices can be mainly related to the charge-transporting properties of the **BiCzTos** compound. The performances of **BiCzSiPh₃**- and mCP-based devices are well comparable as they display satisfactory host-properties of the **BiCzSiPh₃** compound for green and red PhOLEDs. Looking more attentively to the performances of **BiCzSiPh₃**- and mCP-based devices, lower turn-on voltages, higher maximum EQE of green-A device, and higher roll-off efficiency of the red-A device were obtained for **BiCzSiPh₃**-based devices in comparison to that of the relative mCP-based devices (**Fig. 4.2.5.c**, **Table 4.2.3**). These observations can be explained by the better hole-injecting properties and bipolar charge-transporting properties of compound **BiCzSiPh₃** in comparison to these of the mCP host.



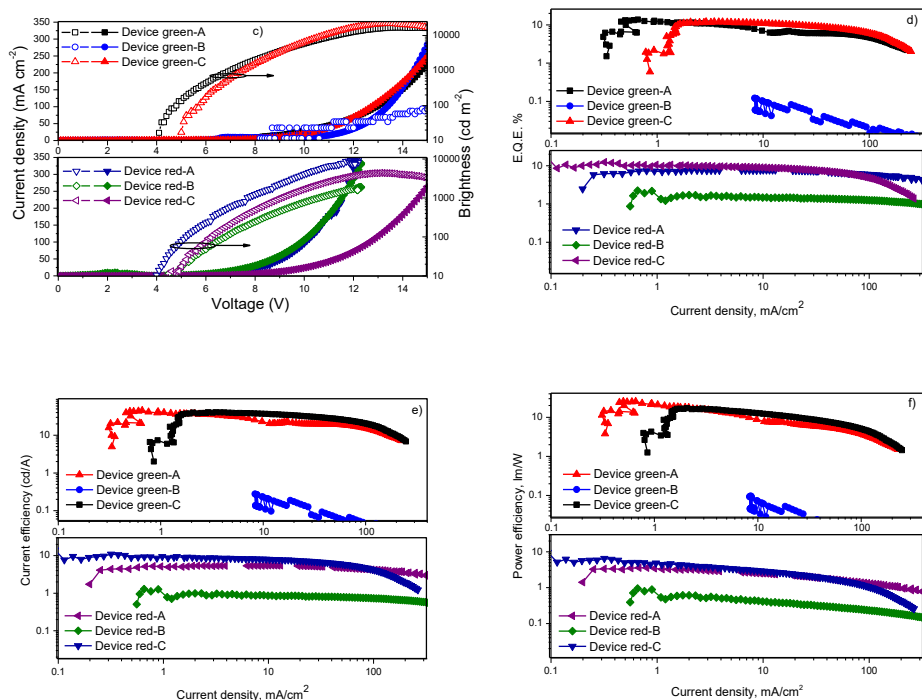


Figure 4.2.5. Equilibrium energy diagram for the fabricated devices (a); EL spectra of the studied devices recorded at 8 V (b); current density and brightness as functions of voltage (c); external quantum efficiency (EQE) (d), current (e), and power (f) efficiencies as functions of current density for all devices. The equilibrium energy diagram was developed by using results of photoelectron spectroscopy measurements for the layers of **BiCzSiPh₃**

Table 4.2.3. Selected device data

Device	Structure	V _{on} , V	Max. brightness, cd/m ²	Max. η _c , cd/A	Max. η _p , lm/W	Max. EQE, %
green-A	ITO/MoO ₃ /NPB/TCTA/mCP/ BiCzSiPh₃ : Ir(ppy) ₃ /TSPO1/TPBi/LiF/Al	4.0	16200	45	25	13.8
green-B	ITO/MoO ₃ /NPB/TCTA/mCP/ BiCzTos : Ir(ppy) ₃ /TSPO1/TPBi/LiF/Al	8.2	80	0.27	0.1	0.1
green-C	ITO/MoO ₃ /NPB/TCTA/mCP/mCP:Ir(ppy) ₃ /TSPO1/TPBi/LiF/Al	5.0	22000	40	17	12.1
red-A	ITO/MoO ₃ /NPB/TCTA/mCP/ BiCzSiPh₃ : Ir(piq) ₂ (acac)/TSPO1/TPBi/LiF/Al	4.0	10000	5.4	3.5	7.7
red-B	ITO/MoO ₃ /NPB/TCTA/mCP/ BiCzTos : Ir(piq) ₂ (acac)/TSPO1/TPBi/LiF/Al	4.5	1600	1.3	0.9	2.2
red-C	ITO/MoO ₃ /NPB/TCTA/mCP/mCP: Ir(piq) ₂ (acac)/TSPO1/TPBi/LiF/Al	4.3	4300	10.1	5.8	12.3

To conclude, two new 3,3'-bicarbazole derivatives modified with triphenylsilane (**BiCzSiPh₃**) and with 1-sulfonyl-4-methylbenzene (**BiCzTos**) moieties on the 9,9'-positions were synthesized, and their thermal, optical, photophysical, electrochemical and charge-transporting properties were studied. The cyclic voltammetry revealed the solid state ionization potential for the derivative of bicarbazoyl derivatives of 5.43 eV and 6.08 eV for **BiCzSiPh₃** and **BiCzTos**, respectively. Electron mobility of 5.6×10^{-4} cm²/(Vs) at an electric field of 5.4×10^5 V/cm was observed for the layer of **BiCzSiPh₃**, while hole mobility was recorded to be 1.4×10^{-4} cm²/(Vs) at an electric field of 5.4×10^5 V/cm. The best green device demonstrated high brightness of 16200 cd/m² (at 4 V), current efficiency of 45 cd/A, and power efficiency of 25 lm/W, while the external quantum efficiency reached 13.8%. The best red device demonstrated high brightness of 10000 cd/m² (at 4 V), current efficiency of 5.4 cd/A and power efficiency of 3.5 lm/W, while the external quantum efficiency reached 7.7%. The fabricated devices demonstrated high emission characteristics even for the standard test at 4300 cd/m² (current efficiency of 10.1 cd/A, power efficiency of 5.8 lm/W, EQE of 12.3%).

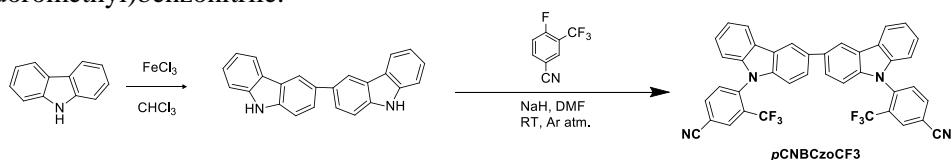
4.3. Bicarbazole-based derivative with (trifluoromethyl)benzotrile moiety as effective delayed fluorescence emitter

Recently, a new family of bicarbazole-based TADF materials was synthesized via a simple one-step catalyst-free C–N coupling reaction by using 9H,9'H-3,3'-bicarbazole and alkyl substituted fluorocyanobenzene as starting reagents [134]. These compounds were used as host materials for another type of TADF green dopant 2,3,5,6-tetra(9H-carbazol-9-yl)-4-cyano-pyridine (4CzCNPY) materials. All the devices described in reference [134] exhibit only green electroluminescence (EL) of 4CzCNPY, while no emission from the host bicarbazole-based materials was observed. In the present work, we take this idea a step further by using the material not only as the host matrix but also by involving it in the emission process. We thereby take account of the fact that carbazole derivatives are able to form exciplexes at organic-organic interfaces with star-shaped molecules [135], a feature which, as we show here, can be used for the broadening of the EL spectrum of OLEDs.

In the present work, we studied the behavior in OLED of bicarbazole-based TADF material 4,4'-(9H,9'H-[3,3'-bicarbazole]-9,9'-diyl)bis(3-(trifluoromethyl)benzotrile), named as **pCNBCzoCF₃**, whose synthesis was reported recently [168]. In contrast to the previous work, we presently propose to use **pCNBCzoCF₃** as both the emissive and the exciplex-forming material for the fabrication of white OLED (WOLED). By combining the TADF emission of **pCNBCzoCF₃** with the exciplex emission from the organic-organic interface between **pCNBCzoCF₃** and the layers of star-shaped 4''-tris[phenyl(m-tolyl)amino]triphenylamine (m-MTDATA), we thus fabricate highly efficient WOLEDs with a warm-white emission color.

4.3.1. Synthesis

The synthetic route of compound $p\text{CNBCzoCF}_3$ is shown in **Scheme 4.3.1**. First of all, by Friedel-Crafts reaction, by using FeCl_3 as the Lewis acid catalyst, 9*H*,9'*H*-3,3'-bicarbazole was synthesized. Afterwards one symmetric bipolar material was designed and synthesized with the 3,3'-bicarbazole core. Compound $p\text{CNBCzoCF}_3$ was synthesized at room temperature in argon atmosphere via the nucleophilic substitution reaction with sodium hydride and 4-fluoro-3-(trifluoromethyl)benzonitrile.



Scheme 4.3.1. Synthetic route and chemical structure of the target compound ($p\text{CNBCzoCF}_3$)

A mixture of the *N*-unsubstituted bicarbazole, sodium hydride (NaH) and 4-fluoro-3-(trifluoromethyl)benzonitrile was dissolved in dimethylformamide (DMF) under argon atmosphere. The reaction mixture was mixed at room temperature for 20 hours. Target compound $p\text{CNBCzoCF}_3$ was obtained as a yellowish powder after recrystallization from hot methanol.

4.3.2. Thermal properties

The target compound exhibited excellent thermal stability. The thermal decomposition temperatures ($T_{d-5\%}$, corresponding to 5% weight loss) were measured as 100.7 °C, while, for BCzPh, it is estimated to be 399 °C. The clear glass transition temperatures (T_g) of the functionalized bicarbazole derivative were observed under heating at 162 °C, which is 57 °C higher than that of phenyl-substituted BCzPh. Compared with T_g 105 °C for BCzPh, the glass-transition temperature was significantly increased because of the expanded molecular polarity of BCzPh. These results obviously promise excellent thermal stability of the thin solid film by using a bicarbazole derivative. The melting points were evaluated and are in the range between 305–314 °C. From DSC traces for $p\text{CNBCzoCF}_3$, two melting point peaks were observed because this compound can be found in two crystalline strains.

4.3.3. Spectroscopic characterization

The experimental absorption spectrum of the solution of $p\text{CNBCzoCF}_3$ in THF recorded at ambient conditions is presented in **Fig. 4.3.1** (orange line). For comparison, the theoretical spectrum simulated by the TD DFT method accounting for the PCM model is shown in **Fig. 4.3.1** (blue line). The first singlet electronic transition in the spectrum of $p\text{CNBCzoCF}_3$ takes place at 447.6 nm (**Table 4.3.1**.) but appears only weakly in the experimental and theoretically simulated spectra. By taking into account the fact that $p\text{CNBCzoCF}_3$ is a σ -bond coupled dimer of 4-(9*H*-carbazol-9-yl)-3-(trifluoromethyl)benzonitrile, the first singlet and triplet excited

states are almost doubly degenerated. Due to the absence of strict symmetry constraints, the S_1 and S_2 states are split by 0.2 nm in our calculations, and the T_1 and T_2 states are split by 0.3 nm (Table 4.3.1). As it can be seen from Fig. 4.3.2, both S_1 and S_2 states of $p\text{CNBCzoCF}_3$ are of the charge transfer (CT) type, and these transitions correspond to electron density moving from the 3-(trifluoromethyl)benzointrile moieties to the carbazole fragments. It is a general rule that CT transitions are characterized by very weak intensity and also are sensitive to the influence of a solvent [136]. Indeed, the energy of S_1 and S_2 states increases significantly in the THF solvent environment (2.77 eV) comparing with the vacuum approximation (2.64 eV).

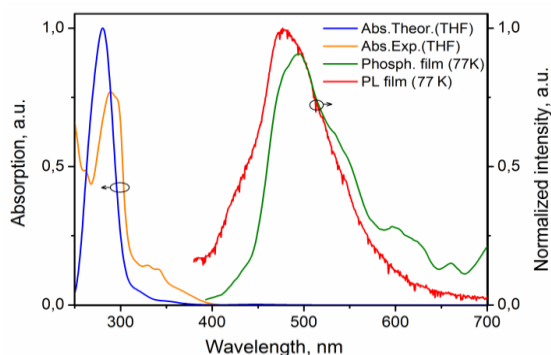


Figure 4.3.1. Absorption and emission spectra of $p\text{CNBCzoCF}_3$

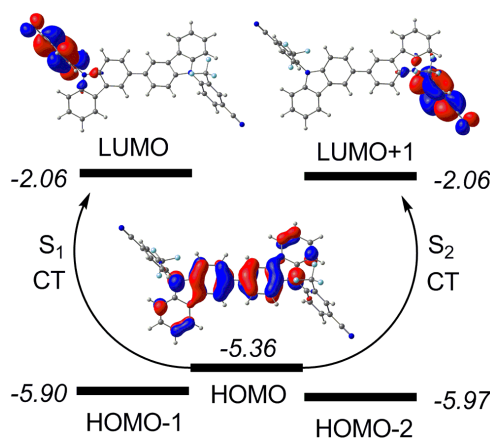


Figure 4.3.2. MOs levels diagram for $p\text{CNBCzoCF}_3$ (italic numbers are MOs energies in eV)

Due to the weak intensity of the $S_0 \rightarrow S_1$ transition, the photoluminescence quantum yield of $p\text{CNBCzoCF}_3$ was measured as 19.3% and 20% for the THF

solution and the solid film state, respectively, thus indicating the dominant role of non-radiative quenching processes in the deactivation of the first excited singlet state.

The long wavelength shoulder in the absorption spectrum of *p*CN BCzoCF_3 solution (310–370 nm) can be assigned to the manifold of weak singlet-singlet electronic transitions $S_0 \rightarrow S_{3-14}$. Among them, the electronic transitions into the S_5 and S_{12} states are the most intense (**Table 4.3.1**). The high-intensity absorption band at *ca.* 290 nm corresponds to two electronic transitions $S_0 \rightarrow S_{15}$ and $S_0 \rightarrow S_{20}$ from the frontier-occupied MOs into the high-lying unoccupied orbitals.

Table 4.3.1. Assignment of absorption spectrum of *p*CN BCzoCF_3 together with estimations of the S_1 and T_1 states energies

State	$\lambda_{\text{theor.}}^{\text{abs.}}$, nm	$\lambda_{\text{exp.}}^{\text{abs.}}$, nm	$E_{\text{exp.}}/E_{\text{theor.}}$, eV	f	Assignment
T_1	449.4	-	2.64 ^a /2.586 ^c / 2.757 ^e / /2.447 ^f	0	HOMO \rightarrow LUMO (78%)
T_2	449.1	-	-	0	HOMO \rightarrow LUMO+1 (78%)
S_1	447.6	-	2.83 ^b /2.597 ^d / 2.768 ^e / /2.455 ^f	0.0024	HOMO \rightarrow LUMO (91%)
S_2	447.4	-	-	0.0011	HOMO \rightarrow LUMO+1 (91%)
S_5	349	342	-	0.020	HOMO \rightarrow LUMO+2 (91%)
S_{12}	318	330	-	0.067	HOMO \rightarrow LUMO+5 (88%)
S_{15}	289	289	-	0.525	HOMO \rightarrow LUMO+6 (79%)
S_{20}	281	-	-	1.103	HOMO-1 \rightarrow LUMO+4 (67%)

^a Estimated from the phosphorescence spectrum (at 77 °K) in ref. [134]; ^b Estimated from the fluorescence spectrum (at 77 °K) in ref. [134]; ^c Estimated from the phosphorescence spectrum of solid film (at 77 °K) in this work. ^d Estimated from the photoluminescence spectrum of solid film (at 77 °K) in this work; ^e Calculated by the TDDFT B3LYP/6-31G(d) method with PCM model (THF); ^f Calculated by the TDDFT B3LYP/6-31G(d) method with PCM model (THF) in adiabatic approximation

The most intriguing property of *p*CN BCzoCF_3 is the extremely small ΔE_{ST} . As one can see from **Fig.4.3.1**, both PL and phosphorescence spectra of the solid film of *p*CN BCzoCF_3 are characterized by almost the same peak positions. The PL maximum appears at 477.0 nm (red curve), while the highest energy vibronic sub-band in the phosphorescence spectrum (the left-hand shoulder at the green curve) appears at 479.0 nm. These values correspond to the ΔE_{ST} value of only 0.011 eV, which is favorable for efficient TADF emission. Such a small ΔE_{ST} value is in complete agreement with our vertical TD DFT calculations (2.768 eV for S_1 and 2.757 eV for T_1) thereby proving the equivalent ΔE_{ST} value (0.011 eV). We additionally performed computations for the ΔE_{ST} value in adiabatic approximation by direct optimization of S_1 and T_1 excited states within the TDDFT/B3LYP/6-31G(d) method. The calculated adiabatic difference between S_1 (2.455 eV) and T_1 (2.447 eV) states was found to be only 0.008 eV in complete agreement with the ‘vertical’

approximation and the experimental value. Moreover, the calculated 0-0 energies for S_1 and T_1 states are in even better agreement with the experimental values than the 'vertical' energies (Table 4.3.1.).

4.3.4. PL decay measurements

The TADF nature of *p*CNBCzoCF₃ emission was confirmed by PL decay measurements for the neat film of *p*CNBCzoCF₃ (Fig. 4.3.3). The double exponential law for the PL decay curve of the solid sample of *p*CNBCzoCF₃ was required for fitting ($\chi^2=1.157$) of the decay curve according to the formula $A+B_1\exp(-t/\tau_1)+B_2\exp(-t/\tau_2)$. The corresponding PL lifetimes $\tau_1=17.36$ ns (83%) and $\tau_2=503$ ns (17%) were obtained. The second component (τ_2) is much shorter than that of 8.12 μ s recorded earlier for solution *p*CNBCzoCF₃ in toluene [134]. The longer-lived component of the decay can be determined by two effects: one being due to the triplet-triplet annihilation [135], the other being due to the TADF effect [171]. However, with a linear dependence of PL intensity on the laser flux with the slope of *ca.* 1 for the solid layer of *p*CNBCzoCF₃ (Fig. 4.3.3), this longer-lived component must be attributed to the reverse intersystem crossing process (RISC), hence proving the TADF nature of the PL emission of *p*CNBCzoCF₃.

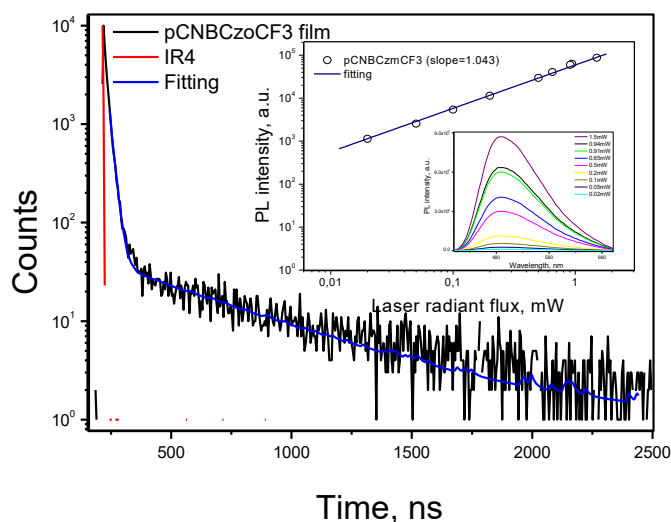


Figure 4.3.3. Photoluminescence decay curves of the vacuum-deposited layer of *p*CNBCzoCF₃ in nanosecond time ranges; (insert) the dependence of PL intensity of the layer of *p*CNBCzoCF₃ on laser flux (insert: PL spectra for various excitation power)

4.3.5. Ionization potential and charge-transporting properties

The solid-state ionization potential (IP) of 5.84 eV was recorded by the electron photoemission method before the fabrication of OLEDs (as solid-state layers of

*p*CNBCzoCF₃ were utilized) (Fig. 4.3.4.a). This IP value observed for the vacuum deposited layer of *p*CNBCzoCF₃ was found to be higher than that obtained from the electrochemical measurements (HOMO(CV) of -5.41 eV) [134]. Such disagreement in the IP which was used for the design of OLEDs is apparently due to the intermolecular interactions of the *p*CNBCzoCF₃ molecules that can take place in the solid-state layers. Having the solid-state IP energy levels of 5.84 eV and the solid-state optical band-gap energy (E_g) of ca. 2.92 eV [134], the electron affinity (E_A) can be calculated as $E_A = IP - E_g = 2.92$ eV. Therefore, the HOMO and LUMO values of -5.84 eV and -2.92 eV were used to design our OLEDs as they are related to the IP and E_A of the observed energy levels, respectively.

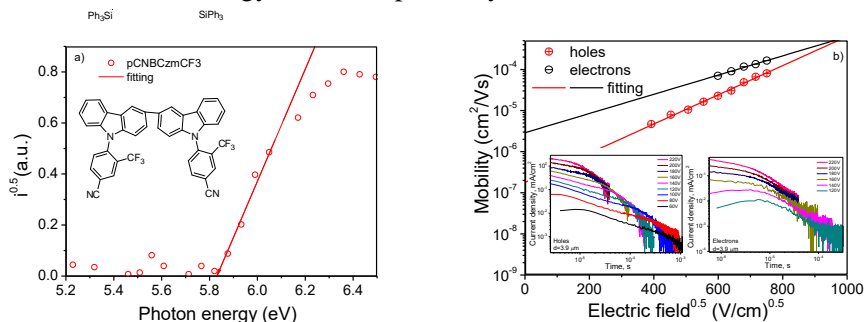


Figure 4.3.4. Electron photoemission spectrum of the vacuum deposited layer of *p*CNBCzoCF₃ (a); electric field dependencies of hole and electron mobilities and the hole and electron TOF transient curves for *p*CNBCzoCF₃ in log-log scales (inserts) (b)

The charge-transporting properties of *p*CNBCzoCF₃ were studied by the time-of-flight (TOF) method. Fig. 4.3.4.b shows electric field dependencies of the hole and electron mobilities of the vacuum deposited layer of *p*CNBCzoCF₃. The bipolar nature of *p*CNBCzmCF was proved by observing the transit times for both holes and electrons on the TOF transient curves (Fig. 4.3.4.b, inserts). The twice higher electron mobility of $1.6 \times 10^{-4} \text{ cm}^2/(\text{V} \times \text{s})$ comparing to the hole mobility of $8 \times 10^{-5} \text{ cm}^2/(\text{V} \times \text{s})$ was found at the electric field of ca. $5.6 \times 10^5 \text{ V/cm}$. This finding can be explained by the introduction of the strong electron-withdrawing meta-positioned CF₃ moieties to the molecules of *p*CNBCzoCF₃ [134]. The charge mobilities observed for *p*CNBCzoCF₃ are comparable to the best known values reported for TADF materials [135].

4.3.6. OLEDs characteristics

Three light-emitting devices A–C were fabricated. The principal schemes of these devices are presented in Fig. 4.3.5.

- Sky-blue non-doped OLEDs based on *p*CNBCzoCF₃ emission

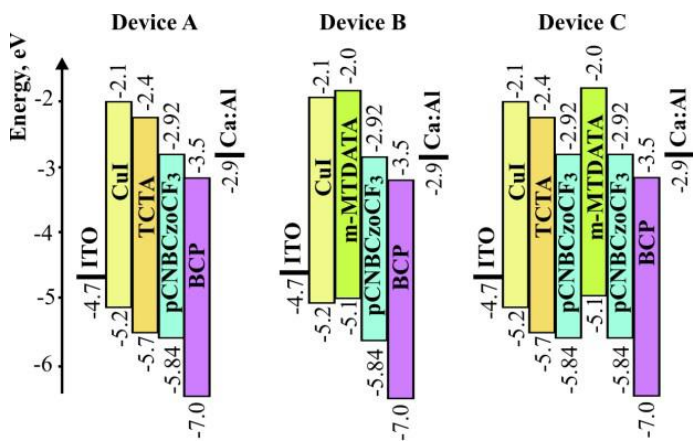


Figure 4.3.5. Energy diagrams for devices A–C

The EL spectrum of device **A** is almost the same as the photoluminescence spectrum of the vacuum deposited film of *pCNBCzoCF₃* recorded at ambient conditions (**Fig. 4.3.6**). This observation indicates the absence of exciplex-type emission from interfaces TCTA/*pCNBCzoCF₃* and *pCNBCzoCF₃*/BCP. Device **A** is characterized by a relatively low turn on voltage of only 3.4 V. The maximum external quantum efficiency, power efficiency and current efficiency of 6.2%, 7.75 lm W⁻¹ and 15.3 cd A⁻¹ respectively, were observed for Device **A**. The maximal brightness reached 29300 cd m⁻² at 15 V (**Table 4.3.2**). Such lighting parameters characterize the emissive properties of pure *pCNBCzoCF₃* which can be regarded as a promising electroluminescent material for sky-blue OLEDs (**Table 4.3.2**, **Fig. 4.3.7**).

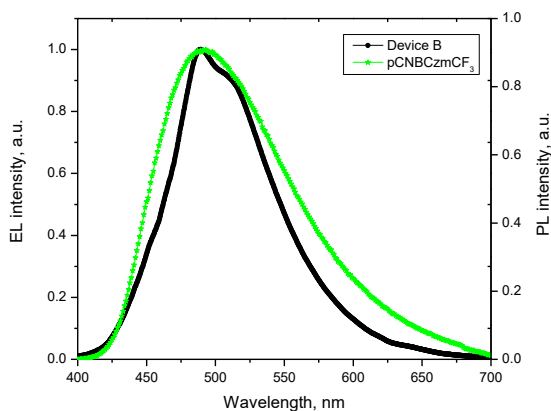


Figure 4.3.6. Normalized electroluminescence spectrum of Device **B** vs. photoluminescence spectrum of the solid film of *pCNBCzoCF₃* at room temperature

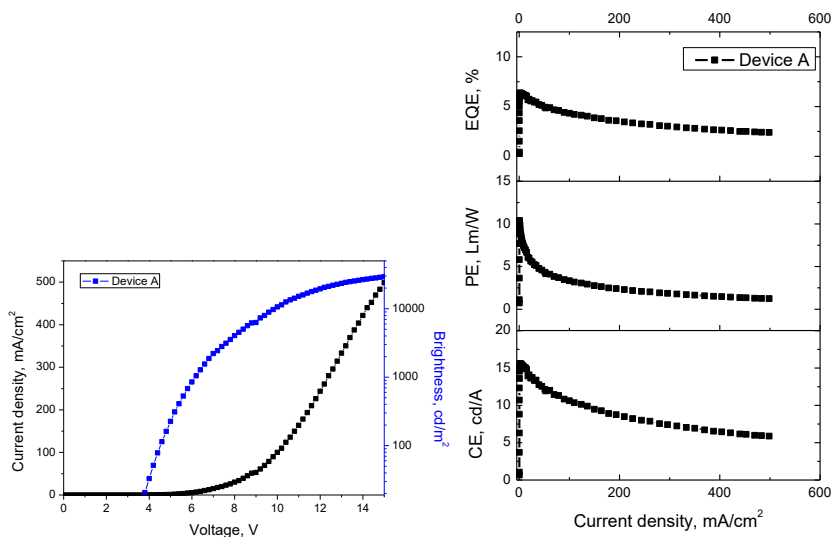


Figure 4.3.7. Current density vs. voltage, luminance vs. voltage characteristics (a); Current efficiency vs. current density characteristics and current density vs. power and quantum efficiency characteristics of fabricated Device A (b)

- **Orange device exhibiting *m*-MTDATA:*p*CNBCzoCF₃ interface exciplex emission**

The EL spectrum of Device **B** coincides with the PL spectrum of the molecular blend *m*-MTDATA: *p*CNBCzoCF₃. At the same time, both spectra are significantly red-shifted with respect of the PL spectrum of *p*CNBCzoCF₃ and the EL spectrum of Device **A** (Fig. 4.3.8). This observation indicates the exciplex formation at the *m*-MTDATA/*p*CNBCzoCF₃ interface which was not observed at interface TCTA/*p*CNBCzoCF₃.

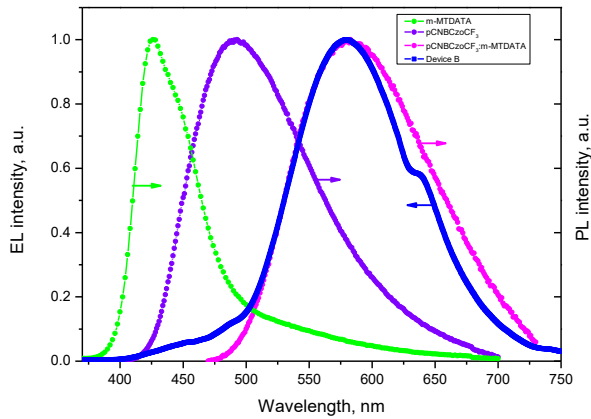


Figure 4.3.8. Normalized electroluminescence spectrum of Device **B** vs. photoluminescence spectra of the solid films of *m*-MTDATA, *p*CNBCzoCF₃ and *m*-MTDATA:*p*CNBCzoCF₃ recorded at room temperature

The TADF emission of the layer of *p*CNBCzoCF₃ remains visible as a structureless shoulder in the higher-energy region of 400–500 nm (**Fig. 4.3.8**). The lighting characteristics of device **B** are slightly better than those of Device **A** (**Fig. 4.3.9**). The chromaticity coordinates of Device **B** lie in the ‘warm-white’ region in contrast with the green emission of Device **A**.

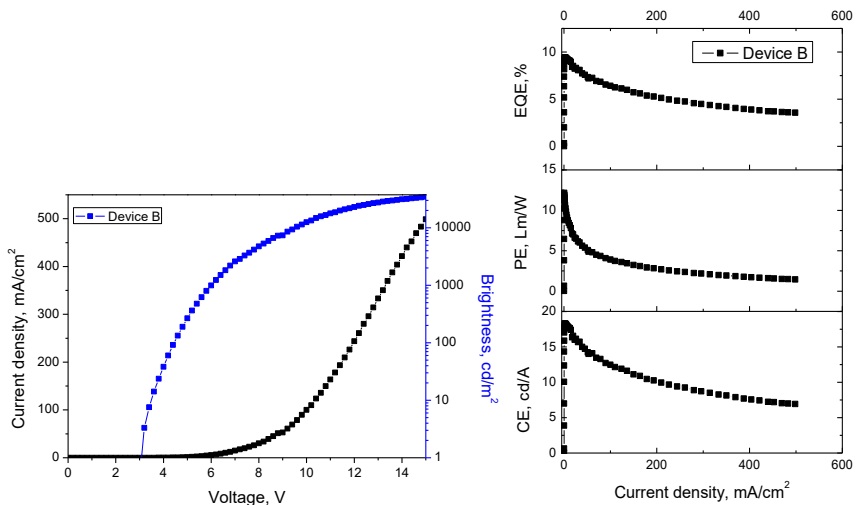


Figure 4.3.9. Current density vs. voltage, luminance vs. voltage characteristics (a) and current efficiency vs. current density characteristics and current density vs. power and quantum efficiency characteristics (b) of fabricated Device **B**

- ‘Warm-white device’ based on both $p\text{CNBCzoCF}_3$ TADF emission and on m-MTDATA: $p\text{CNBCzoCF}_3$ interface exciplex emission

By combining devices A and B within one OLED, we fabricated the highly-efficient device C with a warm-white emission color. The EL spectrum of Device C represents the superposition of the EL spectra of Devices A and B. The additional $p\text{CNBCzoCF}_3$ layer (adjacent to that of TCTA) provides enhancement of the short-wavelength emission which originates from the TADF emission of $p\text{CNBCzoCF}_3$. As a result, the EL spectrum of Device C covers the region from 450 nm to 750 nm (Fig. 4.3.10).

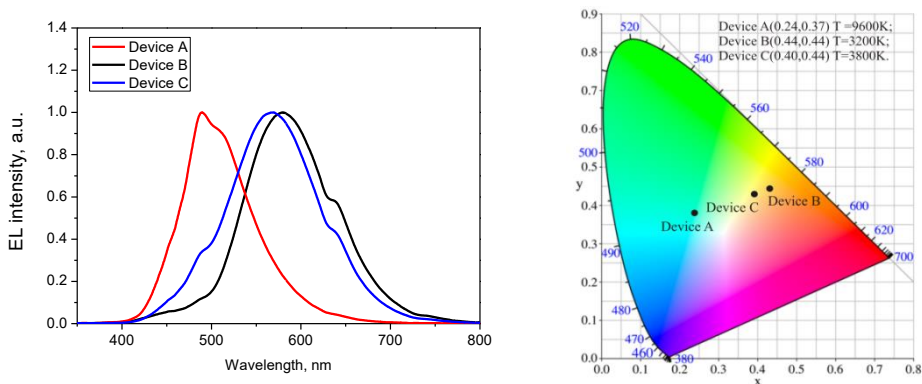


Figure 4.3.10. Normalized EL spectra of Devices A–C (a) and their CIE1976 chromaticity coordinates with the corresponding values of color temperature (b)

Table 4.3.2. Lighting characteristics of Devices A–C

Device	V_{on} (V)	Max. brightness at 15 V (cd/m ²)	Max. current efficiency (cd/A)	Max. power efficiency (Lm/W)	Max. external quantum efficiency (%)	At 1000 cd/m ²			Color coordinate (CIE 1976)
						Current efficiency (cd/A)	Power efficiency (%)	External quantum efficiency (%)	
A	3.4	29300	15.5	10.3	6.3	15.3	7.75	6.2	(0.24, 0.37)
B	2.8	34500	18.2	12.1	9.4	18.0	9.46	9.3	(0.44, 0.44)
C	6.8	40900	53.8	19.3	18.8	46.2	10.6	17.0	(0.40, 0.44)

The lighting characteristics of Devices A–C are presented in Table 4.3.2. Device C demonstrates outstanding lighting characteristics comparing with those of Devices A and B. These characteristics were achieved by the rational combination of the green-blue TADF emission of the $p\text{CNBCzoCF}_3$ layer with the orange exciplex

emission of the *m*-MTDATA/*p*CNBCzoCF₃ interface within the single OLED. The special feature of Device C (as well as that of Device B) is the absence of a high-energy emission component in its EL spectrum. Therefore, the EL of fabricated devices B and C is harmless to the human eye. Particularly, the color temperatures of Devices B and C were estimated as 3200 °K and 3800 °K, respectively, that are close to the common standards (2700–3500 °K) for the warm-white compact fluorescent and LED lamps [136].

In addition, Devices B and C exhibiting warm white electroluminescence were characterized by 60 of color rendering index (CRI) which is a satisfactory value of white light sources for lighting applications. It should be noted that the efficiencies of Devices B and C are comparable (**Fig. 4.3.11**) (or even higher) to those of iridium-based warm-white phosphorescent OLEDs [156].

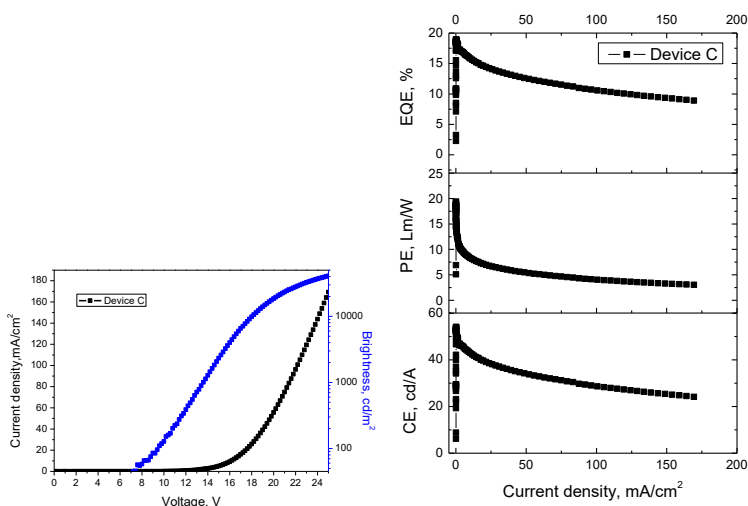


Figure 4.3.11. Current density-voltage, luminance-voltage (a) and current efficiency vs. power efficiency vs. external quantum efficiency-current density characteristics (b) for Device C

In conclusion, 4,4'-(9H,9'H-[3,3'-bicarbazole]-9,9'-diyl)bis(3-(trifluoromethyl)benzotrile) (*p*CNBCzoCF₃) was studied; it demonstrated clear thermally-activated delayed fluorescence (TADF) depending on the temperature factor. This material is characterized by the singlet-triplet energy splitting of only 0.011 eV as estimated both by experimental measurements and TDDFT calculations. *p*CNBCzoCF₃ was used as a green-blue emitter and also as an exciplex-forming material for OLED fabrication. In order to improve the efficiency of the device and to extend its EL spectrum over the whole visible range, the green-blue TADF-type electroluminescence of *p*CNBCzoCF₃ was combined with the exciplex-type emission from the *m*-MTDATA/*p*CNBCzoCF₃ interface. The obtained device is characterized by warm-white emission and by outstanding lighting characteristics: brightness of

40900 cd/m² (at 15 V), current efficiency of 53.8 cd/A, and power efficiency of 19.3 lm/W, as well as external quantum efficiency of 18.8%.

4.4. Carbazole and benzonitrile-based compounds

Carbazole is a widely employed electron-donating building block for the developing efficient electroactive materials including TADF emitters owing to its high triplet energy (3.02 eV), excellent hole-transporting abilities, good thermal stability, etc. [137,138]. Three active positions (i.e., C-3, C-6, and N-9) are readily available for tuning its electronic properties [137]. Carbazole derivatives found a wide range of applications in (opto)electronic devices not only in OLEDs but also in organic thin-film transistors and organic solar cells [139,140,141]. A substantial number of investigations has been reported on 3,6-substituted carbazole derivatives, including small molecules, oligomers, and polymers that were studied as hole-transporting and ambipolar materials.

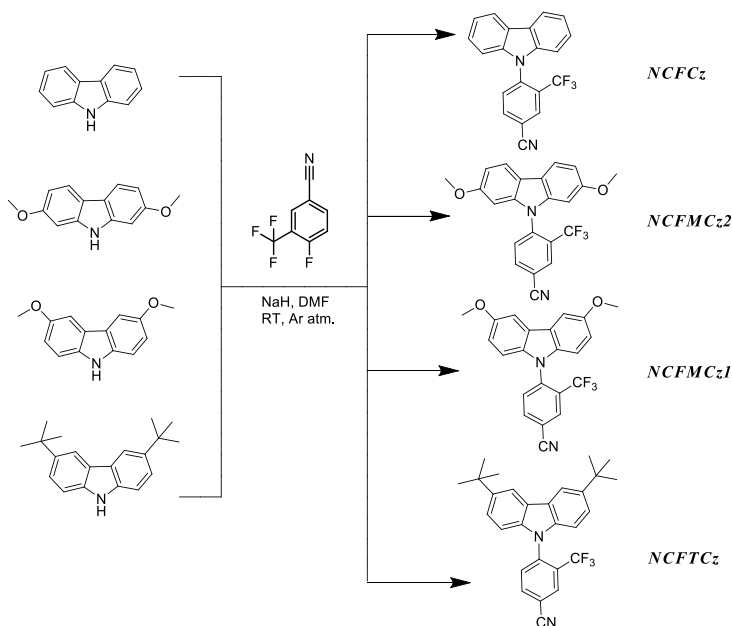
Cyano group is a strong electron-withdrawing moiety. It is useful for the design of highly polar D-A type TADF materials with a reduced singlet-triplet energy gap [190]. The use of the electron-accepting cyano group linked to a suitable electron-donating system is a universal and convenient strategy to develop high-performance TADF emitters [142].

In this work, as we aimed to design carbazole and benzonitrile derivatives with both TADF and AIEE properties, new derivatives of trifluoromethyl-substituted benzonitrile and carbazole having different substituents 2,7-, 3,6-positions were designed and synthesized. By applying various theoretical and experimental methods, both TADF and AIEE effects were proved for the synthesized derivatives. In addition, the influence of methoxy- and *tert*-butyl substituents attached to a carbazole moiety on TADF and AIEE behavior was studied. Two compounds were found to be promising emitters for non-doped OLEDs. The electroluminescence properties of the compounds were studied in both non-doped and doped OLEDs. The efficiencies of the simple non-doped OLEDs even exceeded those of more complex doped devices.

4.4.1. Synthesis

The starting materials 2,7-dimethoxy-9*H*-carbazole, 3,6-dimethoxy-9*H*-carbazole, 3,6-di-*tert*-butyl-9*H*-carbazole were prepared according to the literature methods [143,144,145]. 2,7-Dimethoxycarbazole was obtained by Ullmann-coupling and the Cadogan cyclization reaction BY using triphenylphosphine, and 3,6-dimethoxy-9*H*-carbazole was synthesized starting from 3,6-dimethoxycarbazole which was prepared by bromination of carbazole with N-bromosuccinimide (NBS) in dimethylformamide (DMF), followed by the direct methoxide displacement of bromine [146,147]. 3,6-Di-*tert*-butyl-9*H*-carbazole was obtained from carbazole which was dissolved in CH₂Cl₂, then cooled to 0 °C, and the solution of 2-chloro-2-

methylpropane and AlCl_3 was added afterwards. The synthetic route to the target compounds **NCFCz**, **NCFMCz2**, **NCFMCz1**, **NCFTCz** is shown in **Scheme 4.4.1**. All the target compounds were synthesized via the aromatic nucleophilic substitution ($\text{S}_{\text{N}}\text{Ar}$) reaction of 4-fluoro-3-(trifluoromethyl)benzonitrile with the derivatives of carbazole. The chemical structures of the target compound were confirmed by using NMR. The final compounds **NCFCz**, **NCFMCz2**, **NCFMCz1** and **NCFTCz** were found to be soluble in common organic solvents, such as tetrahydrofuran, toluene and chloroform.



Scheme 4.4.1. Synthesis of **NCFCz**, **NCFMCz2**, **NCFMCz1** and **NCFTCz**

4.4.2. Theoretical investigation

To get insight into the effect of the substituents on the properties of the designed compounds, DFT calculations were performed at B3LYP/6-31G** level in the gas phase. The theoretical geometries of isolated molecules of **NCFCz**, **NCFMCz2**, **NCFMCz1** and **NCFTCz** are similar (**Fig. 4.4.1**). In these compounds, the benzene ring is perpendicular to the carbazolyl moiety (dihedral angle of *ca.* -80°) because of steric hindrance caused by the trifluoromethyl group. Due to the multiple relative orientations of the methoxy groups, three different conformer geometries of compounds **NCFMCz2** and **NCFMCz1** were identified (**Fig. 4.4.2**). The theoretical results revealed that only **NCFMCz2** can adopt different conformers with energy differences of less than 0.5 kcal/mol between them. The conformers of **NCFMCz2** and **NCFMCz1** with the lowest energy were selected for the further investigation. The twisted structure of the compounds separates the electron density between

HOMO and LUMO. Therefore, methoxy and tert-butyl groups attached to the carbazole moiety impact more importantly the HOMO energies as compared to the LUMO ones. According to the DFT calculations, the HOMO of **NFCz** is localized on the carbazolyl group with less contribution from the benzene unit. In the case of **NCFMCz1** and **NCFMCz2**, π -conjugation of HOMO is extended due to the presence of methoxy and tert-butyl groups attached to the C-3 and C-6 positions of the carbazole moiety. While the HOMO of **NCFMCz2** is completely localized on the carbazole unit and the methoxy groups attached to the C-2 and C-7 positions, no electron density is observed on the nitrogen atom. For all the studied compounds, LUMO was found to be distributed over the 3-(trifluoromethyl)benzonitrile moiety.

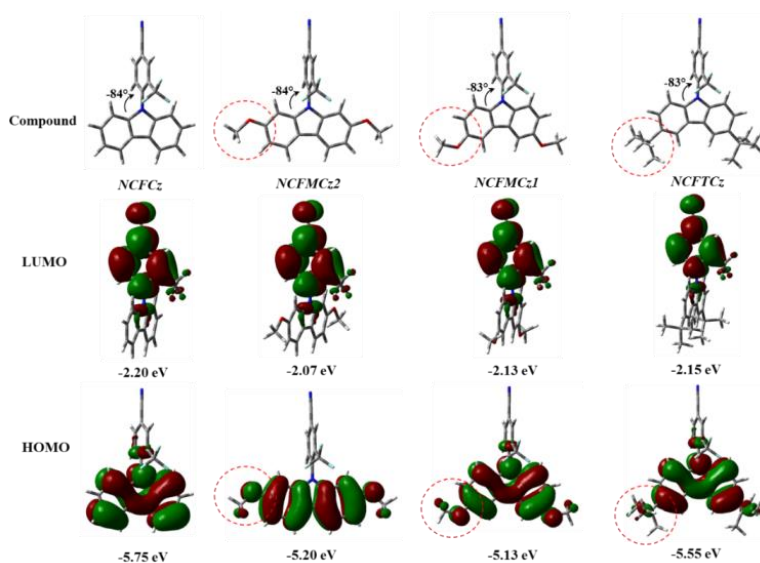


Figure 4.4.1. Theoretical geometries and frontier orbitals of the compounds obtained at the B3LYP/6-31G** level

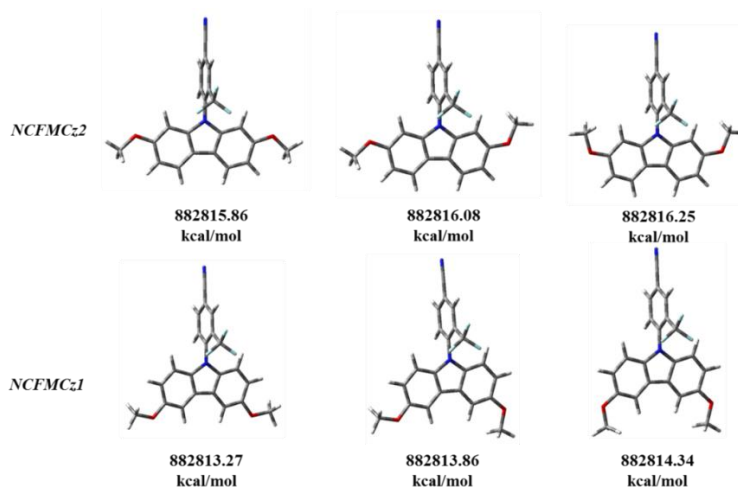


Figure 4.4.2. Various conformers of compounds *NCFMCz2* and *NCFMCz1* obtained at the B3LYP/6-31G** level

4.3.3. Thermal properties

The determined thermal characteristics are listed in **Table 4.4.1**. In the TGA measurements, the compounds exhibited 5% mass loss temperature ($T_{d-5\%}$) in the range of 231–254 °C. The shape of the TGA curves and the very low quantity of residue at the end of the experiment allows assuming that, during heating, carbazole and benzonitrile derivatives were sublimated. All the compounds were isolated after the synthesis as crystalline substances and their first DSC heating scans exposed endothermic melting signals (T_m). It is noticeable that T_m of compound **NCFTCz** (228 °C) is considerably higher than those of **NCFCz**, **NCFMCz2** and **NCFMCz1** (**Table 4.4.1**). During the cooling and the second heating scans, glass transitions were observed at 33, 53, 55 and 88 °C for **NCFCz**, **NCFMCz2**, **NCFMCz1** and **NCFTCz**, respectively. Thus **NCFTCz** showed both the highest melting point and the highest glass transition temperature. These observations can, apparently, be explained by the higher molecular weight of **NCFTCz** resulting in stronger intermolecular interaction. The linking topology of methoxy groups in case of **NCFMCz2** and **NCFMCz1** has no effect on their glass transition temperatures. In the case of **NCFMCz2** and **NCFTCz**, further heating revealed crystallization and melting signals. Compound **NCFTCz** showed different crystal structures after crystallization from the solution and from the melt. After recrystallization from isopropanol in the first DSC heating scan, it showed T_m of 228 °C while, after cooling from the melt in the second heating, it showed a lower T_m of 216 °C.

Table 4.4.1. Thermal characteristics of carbazoly-benzonitrile derivatives

Compound	$T_{d-5\%}^a$, °C	T_m^b , °C	T_g^b , °C	T_{cr}^b , °C
NCFCz	231	142	33	-
NCFMCz2	248	181	53	121

NCFMCz1	254	152	55	-
NCFTCz	242	228, 216 ^c	88	171

^a 5% weight loss determined by TGA, heating rate 10 °C/min, N₂ atmosphere; ^b Determined by DSC, scan rate 10 °C/min, N₂ atmosphere; ^c Established from DSC second heating scan

4.4.4. Photophysical properties

Calculations of the optimized geometries of the molecules at excited states while using TD-DFT at B3LYP/6-31G** level were performed. The trifluoromethyl group suppresses the geometrical changes of the molecules, therefore, compounds maintain their orthogonal structure at excited singlet (S₁) and triplet (T₁) states with separate HOMO and LUMO (**Fig. 4.4.3**). Such a geometrical structure of **NCFCz**, **NCFMCz2**, **NCFMCz1** and **NCFTCz** at excited states determines the photophysical properties of the compounds.

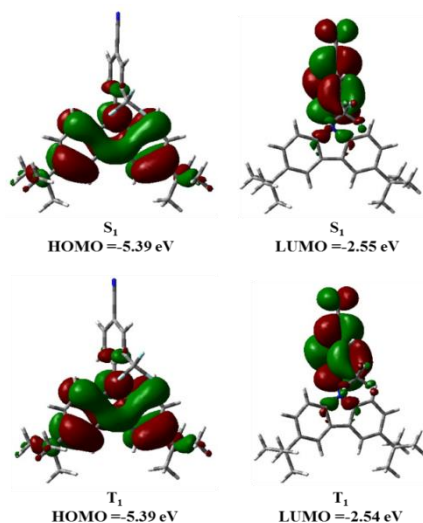


Figure 4.4.3. Molecular orbitals and vertical transition energies of **NCFTCz** at S₁ and T₁ excited states obtained using TD-DFT at B3LYP/6-31G** level

The PL spectra of the solutions of **NCFCz**, **NCFMCz2**, **NCFMCz1** and **NCFTCz** in toluene showed emission maxima at 433, 529, 510 and 448 nm, respectively (**Fig. 4.4.4** and **Table 4.4.2**).

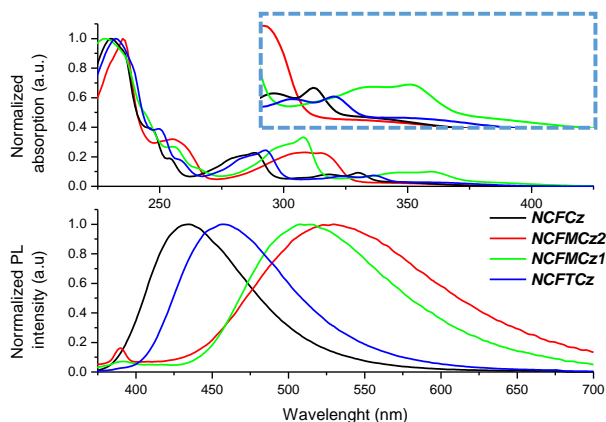


Figure 4.4.4. UV-vis and PL spectra of dilute toluene solutions (10^{-5} M) of **NCFCz**, **NCFMCz2**, **NCFMCz1** and **NCFTCz**

Table 4.4.2. Photophysical characteristics of carbazole and benzonitrile derivatives

Compound	λ_{em} ,	PLQY,	Stokes shift ^a ,	Dipole moment ^b , D	S_1 ,	T_1 ,	ΔE_{S1T1} ,
	nm						
toluene/THF/solid							
NCFCz	433/458/430	15.36/5.48/29.48	102	2.5	3.26	3.05	0.21
NCFMCz2	529/563/513	3.73/~0/16.95	212	4.3	2.91	2.91	0.05
NCFMCz1	510/545/513	19.9/2.62/52.17	152	2.2	3.01	2.90	0.11
NCFTCz	458/483/459	22.02/12.01/52.5 3	120	2.8	3.05	3.01	0.04

^a Difference between the positions of the lowest energy absorption band and the PL maximum in toluene; ^b Dipole moment at the excited singlet state calculated at TDDFT B3LYP/6-31G** level

Due to the charge transfer character at the excited state, the solvatochromic effect in the PL spectra of the solutions in THF of the compounds was detected with the increase of solvent polarity ($\epsilon^{THF}=7.5$ and $\epsilon^{toluene}=2.38$). PL maxima of the

solutions in THF of **NCFCz**, **NCFMCz2**, **NCFMCz1** and **NCFTCz** was detected at 458, 563, 545 and 483 nm, respectively (**Table 4.4.2.**). The wavelengths of PL maxima of the solid samples of the compounds were found to be very close to those of the solutions in toluene; they range from 430 nm to 513 nm (**Fig. 4.4.4** and **Fig. 4.4.5**).

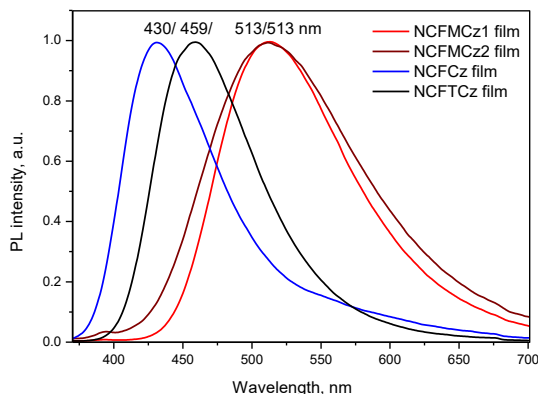


Fig. 4.4.5. PL spectra for non-doped films based on compounds **NCFCz**, **NCFMCz2**, **NCFMCz1** and **NCFTCz**

Upon cooling, the PL spectra of the solutions of **NCFCz**, **NCFMCz2**, **NCFMCz1** and **NCFTCz** in THF shifted towards the blue region by 10, 77, 67 and 17 nm, respectively (**Fig. 4.4.6** and **Table 4.4.2.**). At 77 °K, THF becomes solid, and the geometric relaxation of the solvent is no longer possible, therefore, the PL spectra of the compounds were blue-shifted compared to the PL spectra recorded at room temperature [148].

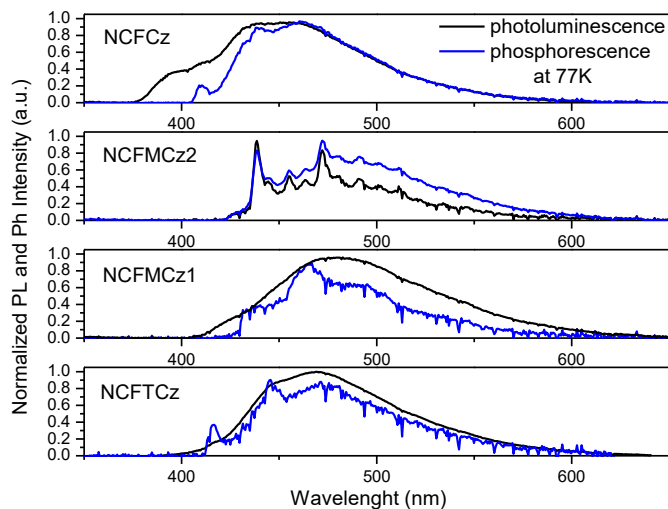


Figure 4.4.6. Photoluminescence and phosphorescence spectra of dilute THF solutions (10^{-5} M) of **NCFCz**, **NCFMCz2**, **NCFMCz1** and **NCFTCz** in THF solutions (10^{-5} M) recorded at 77 °K. Phosphorescence spectra were recorded with 50 ms delay after excitation

Large Stokes shifts observed for **NCFCz**, **NCFMCz2**, **NCFMCz1** and **NCFTCz** ranging from 102 nm to 212 nm can apparently be explained by the intramolecular charge transfer (ICT) which causes large geometry relaxation of molecules upon photoexcitation. ICT from carbazole to 3-(trifluoromethyl)benzoyl moieties in **NCFCz** determines a Stokes shift of 102 nm. The expansion of π -conjugated systems in compounds **NCFTCz** and **NCFMCz1** leads to an increase of the relaxation time and results in higher Stokes shifts of 120 nm and 152 nm, respectively. In case of **NCFMCz2**, methoxy groups attached at C-2, C-7 positions of the carbazole moiety not only expand the conjugation of the π -electron system but also increase the dipole moment of the molecule (from 2.5 D to 4.3 D). The combination of these two effects causes a large Stokes shift of 9833 cm^{-1} for **NCFMCz2**. Additionally, Stokes shifts of the solutions of **NCFCz**, **NCFMCz2**, **NCFMCz1** and **NCFTCz** in various solvents were analyzed by Lippert-Mataga equation. The dependences of Stokes shifts ($\nu_{\text{abs}} - \nu_{\text{em}}$) versus the orientation polarizability of solvents (Δf) were fitted by linear fitting. The slopes of 11400, 12172, 13607, and 12810 cm^{-1} obtained for **NCFCz**, **NCFMCz1**, **NCFMCz2** and **NCFTCz**, respectively, indicate differences in the dipole moment of the emissive excited state of these compounds. The highest slope was obtained for compound **NCFMCz2** relating to its highest dipole moment in comparison to the other studied compounds. This dependence is in good agreement with the calculated dipole moments of the molecules (**Table 4.4.2**).

The PLQY of the solutions of **NCFCz**, **NCFMCz1**, **NCFMCz2** and **NCFTCz** in toluene, THF and of solid films of the compounds were measured (**Table 4.4.2**). Dilute solutions of the compounds in toluene showed low PLQY ranging from 4% to 22%, while, for the solutions in more polar THF, these values were considerably lower. Apparently, the molecules with ICT characteristics interact with the polar solvent, which enhances the nonradiative decay rate and results in lower PLQY. It was found that the PLQY of the solid films of the compounds is influenced by the aggregation-induced emission enhancement (AIEE) effect. The PLQY of the solid sample of **NCFCz** was found to be two times higher than that of the dilute solution in toluene. The expansion of the π -conjugated system and the AIEE effect in **NCFMCz1** and **NCFTCz** determines the PLQY of the solid samples of these compounds exceeding 50%. The low value of PLQY of the solid film of **NCFMCz2** (17%) can apparently be explained by the large dipole moment of the compound. It is almost two times larger than those of the other compounds (**Table 4.4.2**). To study the AIEE effect, the solutions and dispersions of **NCFCz**, **NCFMCz2**, **NCFMCz1**, and **NCFTCz** in water/THF mixtures were studied. A considerable increase of PL intensities of the dispersions of all the studied compounds was observed at a certain water fraction (fw) in comparison to those of dilute THF solutions.

The energies of S_1 state were estimated from the onsets of PL spectra of the solutions of the compounds in THF at 77 °K and were found to be 3.26, 2.91, 3.01 and 3.05 eV for **NCFCz**, **NCFMCz2**, **NCFMCz1** and **NCFTCz**, respectively. The energies of T_1 ranging from 2.90 eV to 3.05 eV were determined from the onsets of the Ph spectra of the solutions of the compounds in THF at 77 °K. The separated HOMO and LUMO at S_1 and T_1 states determined low values of ΔE_{ST} which were in the range of 0.04–0.21 eV [149].

4.4.5. Electrochemical properties and ionization potentials

The electrochemical characteristics are summarized in **Table 4.4.3**. The CV curves of **NCFCz** and **NCFTCz** are shown in **Fig. 4.4.7**. The ionization potential (I_p^{CV}) values of the compounds were estimated from the onset potentials of the first oxidation event after calibration of the measurements against ferrocene. I_p^{CV} for **NCFCz**, **NCFMCz2**, **NCFMCz1** and **NCFTCz** were found to be 5.91, 5.47, 5.45 and 5.75 eV, respectively.

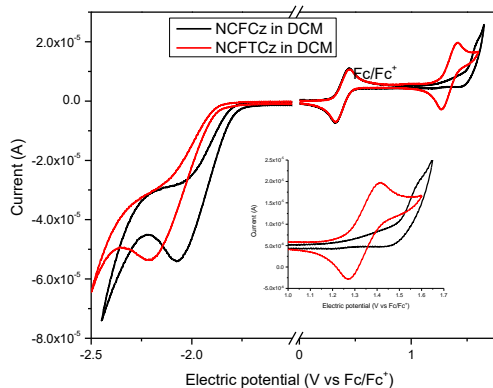


Figure 4.4.7. Cyclic voltammograms of dilute solutions (10^{-3} M) of *NCFCz* and *NCFTCz* in DCM

Solid state ionization potentials (I_p^{PE}) for vacuum deposited layers of carbazoyl-benzonitrile derivatives were taken from the photoelectron emission spectra (**Fig.4.4.8**). I_{PE} for *NCFCz* was not obtained as its value was higher than 6.2 eV (photoelectron emission spectrometry performed in air limitation due to oxygen absorption). For comparison, the theoretical adiabatic ionization potential values (I_p^{theor}) were calculated at the B3LYP/6-31G** level in the gas phase. I_p^{CV} , I_p^{PE} and I_p^{theor} demonstrate similar trends, and the ionization potentials arrange in the order *NCFCz* > *NCFTCz* > *NCFMCz2* > *NCFMCz1*. This trend can be explained by the σ and π donor effect of *tert*-butyl and methoxy groups, respectively. Considering the HOMO pictograms of the compounds, one can see that the electron donating groups expand the π -conjugation system in *NCFTCz*, *NCFMCz2* and *NCFMCz1* thus increasing the HOMO energies. The more effective conjugation of π -electrons in *NCFMCz1* compared to that inherent to *NCFMCz2* is apparently due to the negligible electron density on the nitrogen atom in the 2,7-methoxy substituted carbazole moiety.

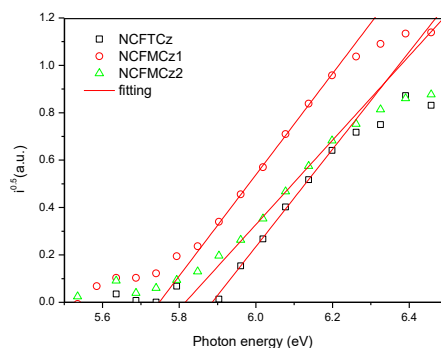


Figure 4.4.8. Electron photoemission spectra for the layers of carbazole and benzonitrile derivatives

The electron affinities (E_A^{CV}) of the compounds were estimated from the onset potentials of the first reduction event after calibration of the measurements against ferrocene. E_A of **NCFCz**, **NCFMCz2**, **NCFMCz1** and **NCFTCz** was estimated to be 2.57, 2.58, 2.59 and 2.35 eV, respectively.

Electron affinities (E_A^{PE}) for materials in the solid state were calculated as $E_A = IP^{PE} - E_g$ by using the optical band-gap energies taken from the absorption spectra of the **NCFMCz2**, **NCFMCz1** and **NCFTCz** layers. E_A for **NCFMCz2**, **NCFMCz1** and **NCFTCz** were estimated to be 2.66, 2.79 and 2.77 eV, respectively.

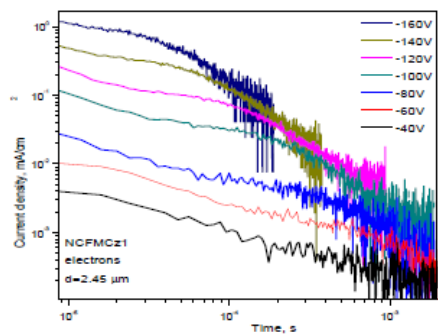
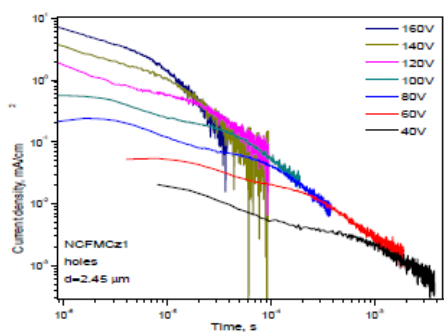
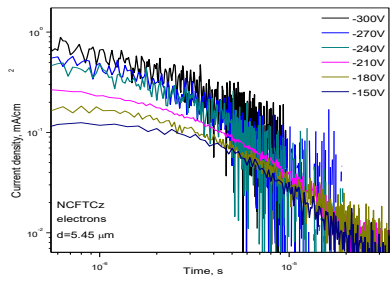
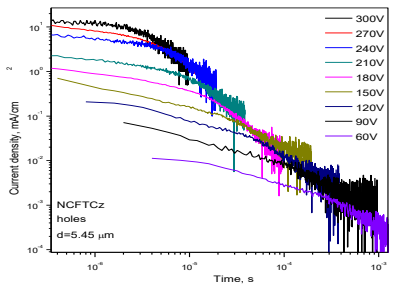
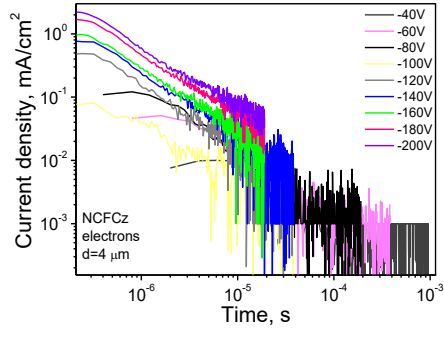
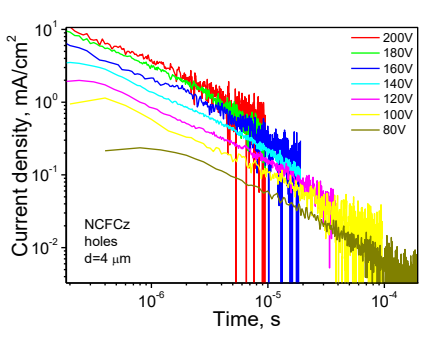
Table 4.4.3. Electronic and charge-transporting parameters of carbazole and benzonitrile derivatives

Compound	$I_p^{cv}/I_p^{PE}/I_p^{theor}$ ^a eV	E_A/E_A^{PE} , eV	μ_h ,	μ_e ,
			cm ² /Vs at 5.6×10^5 V/cm	
NCFCz	5.91 / - / 7.20	2.57/-	6.6×10^{-4}	-
NCFMCz2	5.47 / 5.82 / 6.47	2.58/2.66	-	-
NCFMCz1	5.45 / 5.75 / 6.40	2.59/2.79	3.6×10^{-5}	6×10^{-6}
NCFTCz	5.75 / 5.89 / 6.82	2.35/2.77	4.4×10^{-4}	3.2×10^{-4}

^a Adiabatic ionization potentials calculated at B3LYP/6-31G** level

4.4.6. Charge-transporting properties

The charge-transporting properties of carbazole and benzonitrile derivatives were studied by employing the time-of-flight (ToF) technique. ToF current transients with well-recognized transit times (t_{tr}) were recorded for vacuum-deposited films of **NCFMCz1** and **NCFTCz** by applying both positive and negative electric fields (**Fig. 4.4.9**). This observation shows that **NCFMCz1** and **NCFTCz** are capable to transport both holes and electrons. Only t_{tr} for holes was observed for the **NCFCz** layer (**Fig. 4.4.9**). Since the relaxation time (τ_σ) of the photogenerated charges was lower than the ToF transit time, it was not possible to measure the charge drift mobilities for **NCFMCz1** by the ToF method (**Fig. 4.4.9**). Despite the same core of the molecules, the hole (μ_h) and electron (μ_e) mobilities for the layers of **NCFMCz1** and **NCFTCz** were found to be different depending on the nature of the substituents attached to the carbazole moiety (**Fig. 4.4.10.b**).



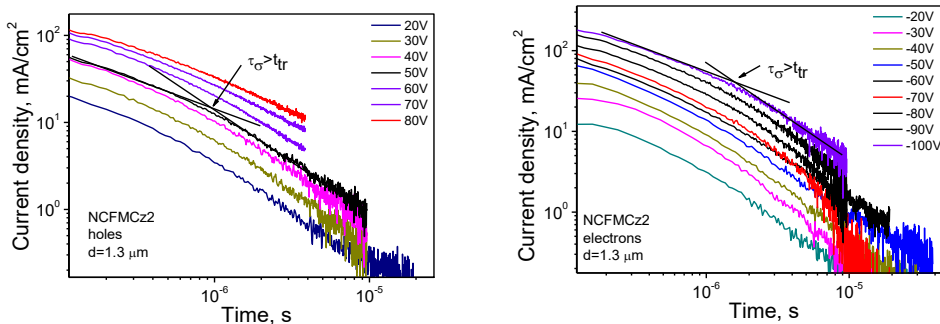


Figure 4.4.9. Holes and electrons ToF pulses for the layers of NCFMCz, NCFTCz, NCFMCz1 and NCFMCz2

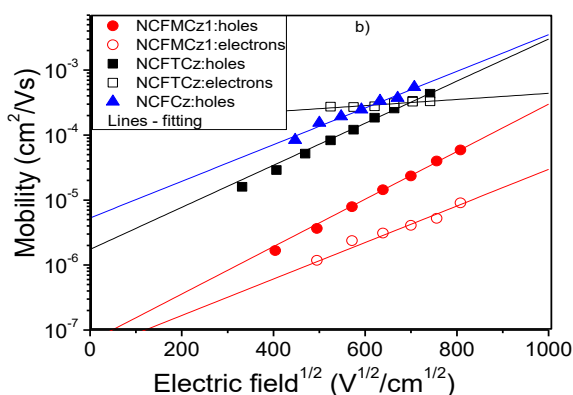


Figure 4.4.10. Electric field dependences of charge mobilities for the layers of carbazole and benzonitrile derivatives

This observation can apparently be explained by variation in the geometrical randomness component which mainly stems from the additional C–H \cdots π , O, N hydrogen bonds induced by methoxy groups as it was previously shown for triphenylamine derivatives [150]. The differences in the charge mobility parameters of the studied derivatives were apparently also determined by the differences in the energetic disorder parameters for electrons and holes in these carbazole and benzonitrile derivatives differently substituted by methoxy and *tert*-butyl groups. In addition, the differences in the charge mobility parameters of the studied derivatives can be related to the different carrier hopping distance in the solid-state layers [151]. The electron mobility of NCFMCz1 was found to be considerably lower relative to its hole mobility. This observation can be explained by the different HOMO-HOMO and LUMO-LUMO overlapping of the neighboring molecules in the solid state layers. Compounds NCFMCz1 and NCFTCz exhibiting bipolar charge transport with balanced mobilities exceeding 10^{-4} cm²/(V \times s) at electric fields higher than *ca.* 3×10^5

V/cm can be considered as promising candidates for the application in the light-emitting layers of electroluminescent devices.

4.4.7. TADF behaviour

Because of the small values of ΔE_{ST} for the studied compound (**Table 4.4.2.**), the TADF effect can be expected. The PL spectra and PL decay curves of the solutions of carbazole and benzonitrile derivatives in toluene recorded before and after degassing are shown in **Fig. 4.4.11.a,b**. Similar PL spectra of both air-equilibrated and degassed solutions of the studied compounds were observed; they showed that the emission originated from the same excited singlet state. PL decay curves of air equilibrated toluene solutions were observed mainly in the *ns* range. In contrast, the emission of degassed solutions was observed up to the μs range. The short-lived and long-lived components of PL decays for oxygen-free solutions belong to the prompt fluorescence (PF) and delayed fluorescence (DF), respectively. The ratio of PL intensities of degassed and non-degassed toluene solutions of the studied carbazole and benzonitrile compounds (I_d/I_{n-d}) ranged from 1.42 to 4.19 thus confirming the contribution of triplet excited states into PL. The contribution of TADF emission (\bar{n}) (which is related to the ratio of prompt and delayed fluorescence DF/PF by formula $\bar{n}=I_d/I_{n-d}-130$) for the solutions of compounds *NCFCz*, *NCFMCz2*, *NCFMCz1* and *NCFTCz* was found to be 0.42, 2.56, 3.19 and 1.38, respectively. These results show that the efficiency of DF of carbazole and benzonitrile compounds can be increased just by attachment of methoxy or *tert*-butyl substituents to the carbazole units.

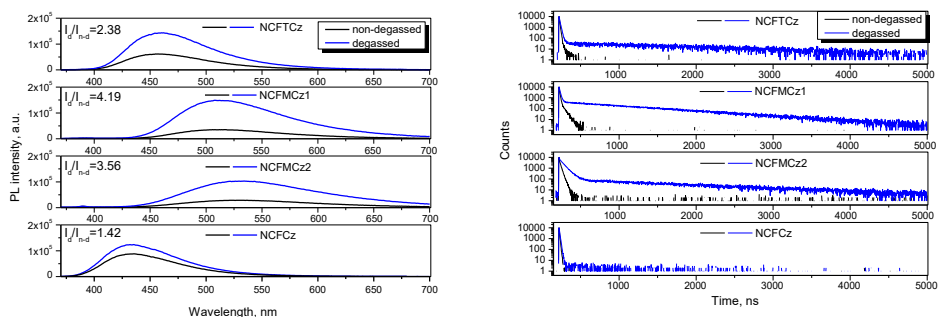


Figure 4.4.11. PL spectra (a) and PL decay curves (b) of air equilibrated and deoxygenated solutions of carbazole and benzonitrile derivatives in toluene

Since DF can be activated by temperature [152], the PL spectra and PL decay curves of solid films of the studied compound were recorded at different temperatures ranging from 77 °K to 300 °K (**Fig. 4.4.12.a,b**). Taking into account the shapes of the PL decay curves recorded at various temperatures, it can be concluded that the DF of the films of the studied compound was caused by the TADF effect. Very similar PL spectra of the films of *NCFMCz2*, *NCFMCz1* and *NCFTCz* were observed at various temperatures. This observation indicates the similarity of phosphorescence

(Ph), prompt and delay fluorescence spectra of the compounds. Indeed, the Ph spectrum of the solid sample of **NCFMCz1** was observed at the spectral region almost coinciding with that of its PL spectrum. Consequently, a small ΔE_{ST} of 0.07 eV was recorded for this compound (**Fig. 4.4.12.b**).

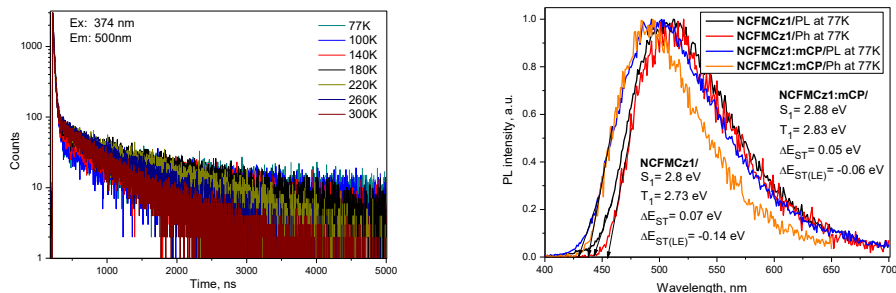


Figure 4.4.12. PL decay curves of non-doped layer of **NCFMCz1** at different temperatures (a) PL and Ph spectra **NCFMCz1** doped in mCP and of neat **NCFMCz1** layer recorded at 77 °K

The ΔE_{ST} values of **NCFMCz2**, **NCFMCz1** and **NCFTCz** were small enough for getting effective TADF. A solid sample of **NCFCz** having no substituents at the carbazole moiety exhibited a slightly higher ΔE_{ST} value of 0.19 eV which determined the lower TADF efficiency of **NCFCz** than the efficiency of other studied compounds (**Fig. 4.4.11.b**). Usually, the PLQY values of host:guest systems based on TADF emitters as guests are higher than those of non-doped layers of the guests [153]. Taking this into account, we looked for appropriate hosts for the studied carbazole and benzonitrile derivatives. Unexpectedly low PLQY values of 4.85, 7.78, 8.12, and 10.54% were observed for mCP:**NCFCz**, mCP:**NCFMCz2**, mCP:**NCFMCz1**, and mCP:**NCFTCz** systems containing 7 wt.% of guests. These values were lower than the PLQY of the non-doped layers of **NCFCz**, **NCFMCz2**, **NCFMCz1** and **NCFTCz** which were 29.48, 16.95, 52.17, and 52.53%, respectively (**Table 4.4.2.**). When TCz1 and DPEPO were used as hosts for **NCFTCz**, also lower PLQY values of 18.67% for TCz1:**NCFTCz** (7 wt.%) and 8.85% for DPEPO:**NCFTCz** (7 wt.%) as compared to the PLQY of the non-doped **NCFTCz** layer (52.53%) were detected. These results cannot be explained by an increase of ΔE_{ST} since smaller ΔE_{ST} values of 0.05 eV and 0.035 eV were observed for mCP:**NCFMCz1** and mCP:**NCFTCz** host:guest systems relative to 0.07 eV and 0.049 eV recorded for non-doped **NCFMCz1** and **NCFTCz** layers, respectively (**Fig. 4.4.12.b**, **Fig. 4.4.13**). The lower values of PLQY for the doped layers in comparison to those observed for non-doped ones can apparently be explained by the restriction of AIEE in the layers of molecular mixtures containing only 7 wt.%.

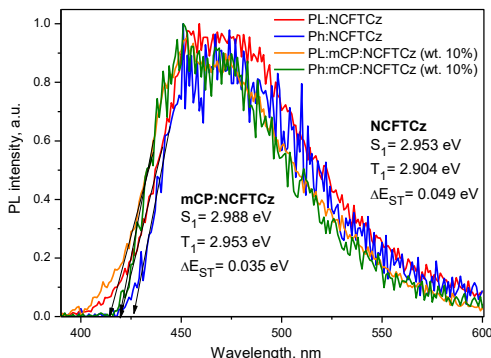


Figure 4.4.13. PL and Ph spectra for doped in mCP and non-doped *NCFTCz* layers recorded at 77 °K

4.4.8. TADF OLEDs performance

- **TADF OLED based on non-doped blue *NCFTCz* and green *NCFMCz1* emitters**

NCFTCz and *NCFMCz1* showing bipolar charge transport and PLQY higher than 50% in the solid-state layers were used for the fabrication of electroluminescent Devices I and II of the following structure: ITO/MoO₃(2nm)/TCTA(40nm)/mCP(8nm)/ tested TADF emitter (32nm) /TSPO1(8nm) /TPBi(40nm)/Ca/Al. Molybdenum trioxide (MoO₃) was used for the preparation of the hole injection layer. Tris(4-carbazoyl-9-ylphenyl)amine (TCTA) and 2,2',2''-(1,3,5-benzinetriyl)-tris(1-phenyl-1-H-benzimidazole) (TPBi) were utilized as hole- and electron-transporting materials. 3-Bis(9-carbazoyl)benzene (mCP) and diphenyl-4-triphenylsilylphenyl-phosphineoxide (TSPO1) with high triplet energies of 2.9 eV for mCP and 3.36 eV for TSPO1 were used as exciton blocking materials. The HOMO and LUMO values of the fabricated devices are displayed in the equilibrium energy diagram (**Fig. 4.4.14**).

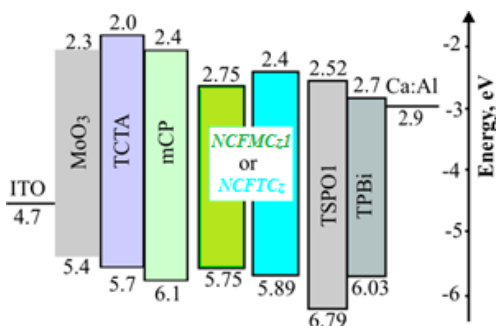


Figure 4.4.14. Equilibrium energy diagram for Devices I and II

Blue and green TADF OLEDs fabricated by using **NCFTCz** and **NCFMCz1** for non-doped light-emitting layers showed very stable electroluminescence (EL) spectra at various electric fields (**Fig. 4.4.15.a**). The shape of the EL spectra with the maxima at 466 nm and 503 nm of Devices I and II were similar to the solid-state PL spectra of **NCFTCz** and **NCFMCz1**, respectively (**Fig. 4.4.15.a**). Thus the EL of Devices I and II can be attributed to the emission of **NCFTCz** and **NCFMCz1**. Slight differences between the EL spectra of the devices and PL spectra of **NCFTCz** and **NCFMCz1** can be explained by the enhancement of delayed fluorescence by electrical excitation [154]. The different energy values of HOMO and LUMO of **NCFTCz** and **NCFMCz1** affect the injection from charge-transporting to light-emitting layers, which results in the different turn-on voltages of *ca.* 4.4 V and 3.9 V observed for Devices I and II (**Fig. 4.4.14**, **Fig. 4.4.15.b**). Considerably different brightness of 3100 cd/m² and 15000 cd/m² at 9V was recorded for EL in the blue and green regions, in which the human eye's sensitivity is different. The maximum current of *ca.* 5.4 cd/A and 20.3 cd/A and the external quantum efficiencies of 3.2% and 7.2% were recorded for Devices I and II, respectively (**Fig. 4.4.15.c**). Notably, the external quantum efficiencies of 2.54% and 6.7% were observed for Devices I and II yielding low values of roll-off efficiencies of *ca.* 21% and 7%. While having similar values of PLQY for **NCFTCz** and **NCFMCz1**, the differences in external quantum efficiencies of the devices can be explained by the difference in charge balance which is better for Device II than for Device I according to the results of ToF measurements for the films of **NCFTCz** and **NCFMCz1**. The maximum external quantum efficiencies (η_{ext}) of blue and green OLEDs were found to be lower than the corresponding theoretical values of 10.5% and 10.4% obtained according to formula $\eta_{\text{ext}} = \gamma \times \Phi_{\text{PL}} \times \chi \times \eta_{\text{out}}$ [155]. To calculate the values of the theoretical maximum efficiency η_{ext} , the charge-balance factor $\gamma=1$, the photoluminescence quantum efficiency $\Phi_{\text{PL}}=0.5257\%$ or 0.5217% , the efficiency of exciton production $\chi=1$, and the outcoupling efficiency $\eta_{\text{out}}=0.2$ were taken. Since the experimental values of η_{ext} were lower than the theoretical ones, γ apparently is not equal to 1. The optimization of the OLED structure can apparently enable an increase in γ . Both γ and Φ_{PL} can be increased by the usage of appropriate hosts for the preparation of the light-emitting layer of TADF OLEDs [156]. The charge-balance factor γ for an **NCFTCz**-based device may also be increased by replacing the charge-transporting layers and by changing their thicknesses.

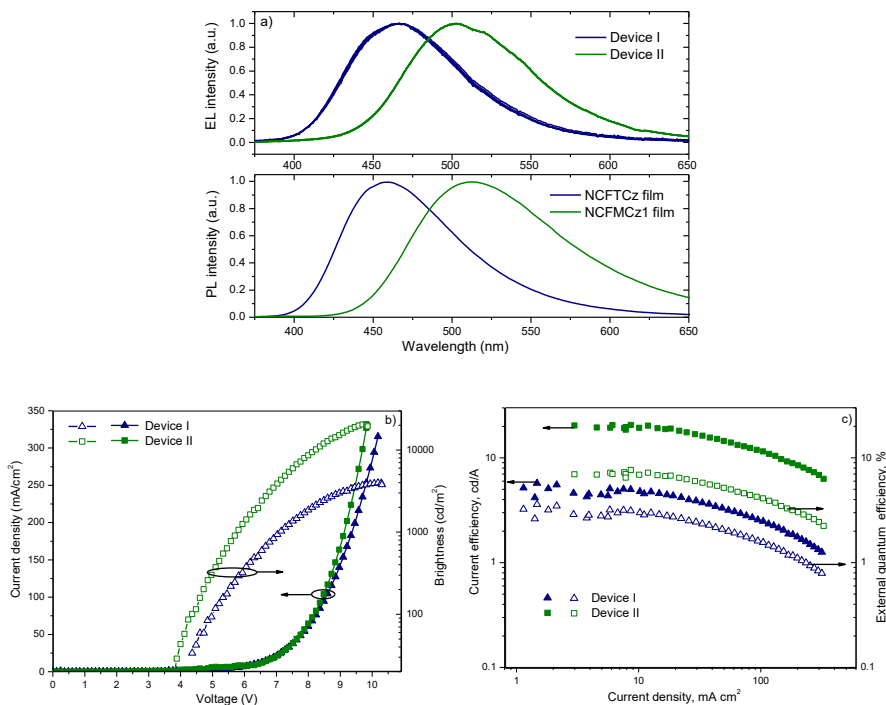


Figure 4.4.15. EL spectra of Devices I and II recorded at the voltages ranging from 5 V to 10 V (a); current density and brightness versus voltage (b); current and external quantum efficiencies versus current density for Devices I and II (c)

It should be acknowledged that the performances of the non-doped green device are average among those of the recently reported devices based on AIEE/TADF emitters (**Table 4.4.4**). Moreover, the results described in this article allow to believe that the performances of the earlier reported AIEE/TADF emitters may be improved by introduction of methoxy or tert-butyl substituents.

Table 4.4.4. Summary of PL and EL performances for AIEE/TADF emitters in non-doped films and non-doped devices

Emitter	PL _{max} , nm	PLQY, %	EL _{max} , nm	EQE _{max} , %	Ref.
	non-doped film		non-doped device		
Blue devices (EL _{max} <500 nm)					
<i>NCFTCz</i>	460	52.53	466	3.2	This work
<i>4-CzPyCl₄</i>	435	16	-	-	[157]
m-DTPACO	477	75	480	2.4	[158]
Green to yellow devices (500 nm<EL _{max} <580 nm)					
<i>NCFMCzI</i>	513	52.17	503	7.2	This work
<i>DBT-BZ-DMAC</i>	505	82.2	516	14.2	[159]
<i>TXO-PhCz</i>	~550	93	-	-	[160]
PCZ-CB-TRZ	557	97	586	11	[161]
2PCZ-CB	571	55	590	10.3	[161]
tCzDSO2	553	92	-	-	[162]
3tCzDSO2	595	19	-	-	[162]
p-DTPACO	522	39	517	1.8	[158]
Cz-AQ	601	28	572	5.8	[163]
DBT-BZ-PXZ	549	38.1	~560	9.2	[164]
DBT-BZ-PTZ	547	40.3	~560	9.7	[164]
Red devices (EL _{max} >580 nm)					
<i>TXO-TPA</i>	~630	36	-	-	[160]
<i>TPA-CB-TRZ</i>	624	94	631	10.1	[161]
<i>TPA-AQ</i>	622	52	612	7.5	[163]
Cz-AQ	541/604	-	600/680	0.75/1.15	[165]

- **Host-guest type blue TADF OLED based on NCFTCz**

Both γ and Φ PL can be increased by usage of the appropriate hosts for the preparation of the light-emitting layer of TADF OLEDs. Charge-balance factor γ for an **NCFTCz**-based device may also be increased by replacing the charge-transporting layers and by changing their thicknesses. Therefore, electroluminescent Devices Ia, Ib and Ic of the structures ITO/MoO₃(2 nm)/NPB(45 nm)/ TCz1:**NCFTCz** (ca. 10 wt%) (30 nm)/TPBi(45 nm)/Ca/Al (Device Ia); ITO/MoO₃(2 nm)/NPB(45 nm)/TCTA(8 nm)/mCP(4 nm)/ mCP:**NCFTCz** (ca. 10 wt%) (30 nm)/DPEPO(4 nm)/TPBi(30 nm)/Ca/Al (Device Ib); and ITO/MoO₃(2 nm)/NPB(40 nm)/TCTA(8 nm)/mCP(4 nm)/ DPEPO:**NCFTCz** (ca. 10 wt%) (30 nm)/TSPO1(4 nm)/TPBi(30 nm)/Ca/Al (Device Ic) were fabricated by using a blue TADF emitter **NCFTCz** dispersed in different hosts. 9'-(2-Ethylhexyl)-9'H-9,3':6',9''-tercarbazole (TCz1), bis[2-(diphenylphosphino)phenyl] ether oxide (DPEPO), and mCP were used as bipolar accepting and donating hosts. To form a lower energy barrier for holes than it was in Device I, N,N'-di(1-naphthyl)-N,N'-diphenyl-(1,1'-biphenyl)-4,4'-diamine (NPB) was utilized as the hole-transporting material.

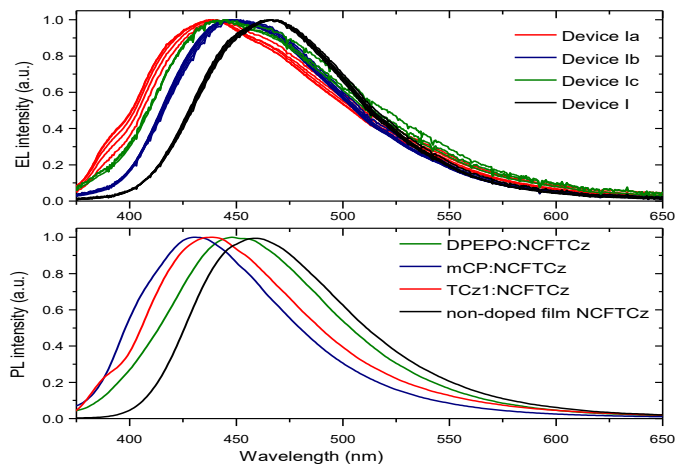


Figure 4.4.16. EL spectra for Devices I, Ia, Ib and Ic recorded at different voltages (above) and PL spectra of doped and non-doped light-emitting layers of the devices (below)

The EL spectra of Devices Ia, Ib and Ic were attributed to **NCFTCz** emission (**Fig.4.4.16**). The spectra were stable at various applied voltages. The slight differences between the EL spectra recorded at different voltages can be recognized in case of Device Ia. The differences are apparently related to the additional emission of the TCz1 host [166]. In comparison to the EL spectrum of Device I, the shifts of EL spectra of the devices with doped light-emitting layers to the high-energy region were observed. These shifts can be explained by dipole interactions between the host and guest molecules [167]. The EL spectra of Devices I, Ia, Ib and Ic were found to be similar to the PL spectra of the system host:**NCFTCz**. However, the wavelengths of maxima (λ_{max}) of the EL and PL spectra were in slight disagreement due to the application of different excitations (electrical and optical).

The lower values of the turn-on voltage (V_{on}) observed for Devices Ia and Ib (2.4 V and 2.9 V respectively) than that recorded for Device I (4.4 V) can be explained by the improved charge-balance (γ) in Devices Ia and Ib. The brightness of 2958, 2100, 1118 cd m^{-2} was recorded for Devices Ia, Ib, Ic; meanwhile, the maximum current and external quantum efficiencies of 4.8, 3.1, 2.8 cd/m^2 and 3.1, 2.05, 1.75 % respectively were recorded (**Fig.4.4.17**). Despite the improved charge-balance in Devices Ia and Ib, they showed worse performance in comparison with Device I. Lower PLQY values of 18.67, 10.54, and 8.85% observed for TCz1:**NCFTCz**, mCP:**NCFTCz**, and DPEPO:**NCFTCz** with 7 wt.% concentration of the guest were obtained as compared to the PLQY of the non-doped **NCFTCz** layer (52.17 %). PLQY in the range from 15% to 26% was recorded for the TCz1:**NCFTCz** system varying the **NCFTCz** guest concentration from 5 to 80 wt.%. The lower values of the PLQY for doped **NCFTCz** layers in comparison to those observed for a non-doped emitter can be explained by restrictions of the AIEE effect for **NCFTCz** molecularly

dispersed in hosts which led to the decrease of the output characteristics of doped Devices Ia, Ib, Ic.

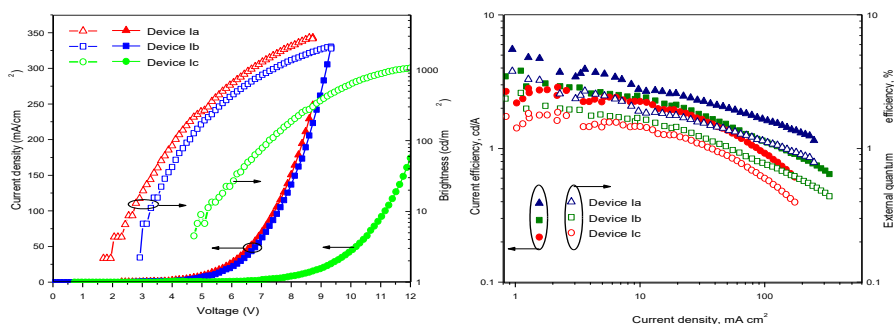


Figure 4.4.17. Current density and brightness versus voltage; and current and external quantum efficiencies versus current density for Devices Ia, Ib, Ic

In conclusion, we designed, synthesized and characterized derivatives of 9-phenyl-9*H*-carbazole exhibiting both thermally activated delayed fluorescence and aggregation induced emission enhancement. The combination of various experimental and theoretical tools including fluorescence steady-state and time-resolved spectrometry, photoelectron emission spectrometry, time of flight technique and density functional theory calculations was used to study the properties of the materials. Two compounds exhibited bipolar charge transport with balanced charge mobilities exceeding 10^{-4} $\text{cm}^2/(\text{V}\times\text{s})$ at electric fields higher than *ca.* 3×10^5 V/cm . Low values of excited singlet-triplet energy differences were obtained (0.04–0.21 eV) resulting in efficient delayed fluorescence. Effects of methoxy and *tert*-butyl-substituents attached to the carbazole moiety on the photophysical properties were studied. It was established that the attachment of these substituents allows to increase the efficiency of delayed fluorescence. Depending on the substitution, emission of compounds was observed in the color range from deep-blue to green. The highest solid-state photoluminescence quantum yields were observed for compounds substituted at C-3, C-6 positions of the carbazole moiety due to the expansion of the π -conjugated system and aggregation-induced emission enhancement. A combination of thermally activated delayed fluorescence and aggregation induced emission enhancement effects allowed to achieve PLQY values exceeding 50% for non-doped solid films. The compounds were used to fabricate highly efficient non-doped OLEDs with maximum external quantum efficiency and brightness values of 7.2% and 15000 cd/m^2 , respectively.

5. CONCLUSIONS

1. Two low molar mass compounds based on phenothiazine as the donor and carbazole as the acceptor moieties were synthesized, and their properties were studied. The compounds exhibited high thermal stability with 5% weight loss temperatures exceeding 327 °C. Moderately high ionization potential values (5.10–5.25 eV) of the amorphous layers of the synthesized compounds were deduced. Carbazole derivatives containing 10*H*-phenothiazine fragments showed ambipolar charge transport in air with the hole mobilities reaching 10^{-5} cm²/(V s) and 10^{-4} cm²/(V s) at high electric fields. Due to the effective charge transporting properties, 10,10'-(9-ethyl-9*H*-carbazole-3,6-diyl)bis(10*H*-phenothiazine) and 10-(9-ethyl-9*H*-carbazol-3-yl)-10*H*-phenothiazine compounds were employed as host materials in the phosphorescent organic light emitting devices which exhibited the maximum power and external quantum efficiencies up to 47.5/40.6 lm W⁻¹ and 20.0/10.5% of green and red PhOLEDs, respectively.

2. Two new 3,3'-bicarbazole derivatives containing triphenylsilane and 1-hydrosulfonyl-4-methylbenzene moieties at 9,9'-positions of the bicarbazole moiety were synthesized, and their properties were studied. The bicarbazolyl group proved to be a stronger donor than a single carbazole fragment by providing a lower ionization potential and superior thermal and electrochemical stability. The derivatives exhibited ability to form molecular glasses with glass transition temperatures that are in the range of 126–149 °C, and they demonstrated high thermal stability with 5% weight loss temperatures exceeding 372 °C. Compound 9,9'-bis(triphenylsilyl)-9*H*,9'*H*-3,3'-bicarbazole displayed ambipolar charge transport behavior with balanced hole and electron mobility with the best results determined for 3,3'-bicarbazole derivative which was modified with triphenylsilane (1.4×10^{-4} cm²V⁻¹s⁻¹ for holes and 5.4×10^{-4} cm²V⁻¹s⁻¹ for electrons at an electric field of 5.3×10^5 Vcm⁻¹). The synthesized compounds were found to be efficient red or green-emitting fluorophores. They were used for the preparation of emissive layers of the effective organic light emitting diodes with the brightness value exceeding 16200 cd/m² (at 4 V), and external quantum efficiency reaching 7.7%.

3. A bicarbazole derivative containing a trifluoromethyl benzonitrile moiety was synthesized, characterized and investigated as TADF emitters. The bicarbazole group proved to be a stronger donor than the single carbazole fragment by providing a lower ionization potential and superior thermal and electrochemical stability. The studied derivative showed strong intramolecular charge transfer and small singlet-triplet energy splitting of 0.011 eV, which was favorable for efficient TADF emission. The compound exhibited bipolar charge-transporting properties with the highest charge mobilities characteristic of 4,4'-(9*H*,9'*H*-[3,3'-bicarbazole]-9,9'-diyl)bis(3-(trifluoromethyl)benzonitrile) (8×10^{-5} cm²V⁻¹s⁻¹ for holes and 1.6×10^{-4} cm²V⁻¹s⁻¹ for electrons at the electric field of *ca.* 5.6×10^5 Vcm⁻¹). The compound was able to form exciplex-type excited states at the interface with star-shaped electron donor m-MTDATA. By combining the TADF emission of the compound with the exciplex emission from the interface, a number of highly efficient 'warm-white' OLEDs were fabricated, whose electroluminescence was close to candle emission. The best device

demonstrated very high brightness of 40900 cd/m² (at 15 V), current efficiency of 53.8 cd/A and power efficiency of 19.3 lm/W, while the external quantum efficiency reached 18.8%.

4. A series of new 9-phenyl-9*H*-carbazole-based derivatives containing various donating units were synthesized, and their properties were studied. The ionization potential values of the amorphous layers of the synthesized compounds depend on the nature of the donor. Only two compounds exhibited balanced bipolar charge transport with charge mobilities exceeding 10⁻⁴ cm²V⁻¹s⁻¹ at electric fields higher than *ca.* 3×10⁵ Vcm⁻¹, and PLQY higher than 50% in solid state layers. The attachment of methoxy and *tert*-butyl-substituents allowed to increase the efficiency of delayed fluorescence. The green non-doped OLED exploiting the effect of thermally activated delayed fluorescence exhibited maximum brightness of 15000 cd/m² and maximum external quantum efficiency of 7.2%.

6. REFERENCES

1. IM, Y. et al. Molecular Design Strategy of Organic Thermally Activated Delayed Fluorescence Emitters. In: *Chemistry of Materials* [interaktyvus]. 2017. Vol. 29, no. 5, p. 1946–1963. Internet access: <<http://pubs.acs.org/doi/10.1021/acs.chemmater.6b05324>>.
2. UOYAMA, H. et al. Highly efficient organic light-emitting diodes from delayed fluorescence. In: *Nature* [interaktyvus]. 2012. Vol. 492, no. 7428, p. 234–238. Internet access: <<http://www.ncbi.nlm.nih.gov/pubmed/23235877>>.
3. FORREST, S.R. The path to ubiquitous and low-cost organic electronic appliances on plastic. In: *Nature* [interaktyvus]. 2004. Vol. 428, no. 6986, p. 911–918. Prieiga per internetą: <<http://www.nature.com/doi/10.1038/nature02498>>.
4. KAMTEKAR, K.T. et al. Recent Advances in White Organic Light-Emitting Materials and Devices (WOLEDs). In: *Advanced Materials* [interaktyvus]. 2010. Vol. 22, no. 5, p. 572–582. Prieiga per internetą: <<http://doi.wiley.com/10.1002/adma.200902148>>.
5. ADACHI, C. Third-generation organic electroluminescence materials. In: *Japanese Journal of Applied Physics* [interaktyvus]. 2014. Vol. 53, no. 6, p. 060101. Prieiga per internetą: <<http://stacks.iop.org/1347-4065/53/i=6/a=060101?key=crossref.9149d8bcbde56db368491506fcb8830a>>.
6. GIOVANELLA, U. et al. Organic Light-Emitting Diodes (OLEDs): Working Principles and Device Technology. In: [interaktyvus]. 2016. p. 145–196. Prieiga per internetą: <http://link.springer.com/10.1007/978-3-319-31671-0_3>.
7. BURROUGHERS, J.H. et al. Light-emitting diodes based on conjugated polymers. In: *Nature* [interaktyvus]. 1990. Vol. 347, no. 6293, p. 539–541. Prieiga per internetą: <<http://www.nature.com/articles/347539a0>>.
8. SINGH, V. et al. Indium Tin Oxide (ITO) films on flexible substrates for organic light emitting diodes. In: *Asid* . 2006. p. 388–391. .
9. GASPAR, D.J. - POLIKARPOV, E. *OLED fundamentals : materials, devices, and processing of organic light-emitting diodes* [interaktyvus]. . ISBN 1466515198.
10. HUNG, L.S. et al. Enhanced electron injection in organic electroluminescence devices using an Al/LiF electrode. In: *Applied Physics Letters* [interaktyvus]. 1998. Vol. 70, no. 2, p. 152. Prieiga per internetą: <<https://aip.scitation.org/doi/abs/10.1063/1.118344>>.
11. BRÜTTING, W. et al. *Physics of organic semiconductors* [interaktyvus]. . [s.l.]: Wiley-VCH, 2012. 634 p. ISBN 3527654968.
12. BRÜTTING, W. et al. Device efficiency of organic light-emitting diodes: Progress by improved light outcoupling. In: *physica status solidi (a)* [interaktyvus]. 2013. Vol. 210, no. 1, p. 44–65. Prieiga per internetą: <<http://doi.wiley.com/10.1002/pssa.201228320>>.
13. BRÜTTING, W. et al. Device efficiency of organic light-emitting diodes: Progress by improved light outcoupling. In: *Physica Status Solidi (A) Applications and Materials Science* . 2013. Vol. 210, no. 1, p. 44–65. .
14. COTTAAR, J. et al. Modeling of charge transport across disordered organic heterojunctions. In: *Organic Electronics* [interaktyvus]. 2012. Vol. 13, no. 4, p. 667–672. Prieiga per internetą: <<http://linkinghub.elsevier.com/retrieve/pii/S1566119912000365>>.
15. PFEIFFER, M., Et al. Electrophosphorescent p-i-n organic light-emitting devices for very-high-efficiency flat-panel displays — The University of Michigan. In: *Advanced Materials* [interaktyvus]. 2002. Vol. 14, no. 22, p. 1633–1636. Prieiga per internetą: <<https://experts.umich.edu/en/publications/electrophosphorescent-p-i-n-organic-light-emitting-devices-for-ve>>.
16. IM, Y. et al. Molecular Design Strategy of Organic Thermally Activated Delayed

- Fluorescence Emitters. In: *Chemistry of Materials* [interaktyvus]. 2017. Vol. 29, no. 5, p. 1946–1963. Prieiga per internetą: <<http://pubs.acs.org/doi/10.1021/acs.chemmater.6b05324>>.
17. PARKER, C.A. Phosphorescence and Delayed Fluorescence from Solutions. In: [interaktyvus]. [s.l.]: Wiley-Blackwell, 2007. p. 305–383. Prieiga per internetą: <<http://doi.wiley.com/10.1002/9780470133323.ch8>>.
18. SCHORE, N.E. Modern molecular photochemistry (Turro, Nicholas J.). In: *Journal of Chemical Education* [interaktyvus]. 1981. Vol. 58, no. 10, p. A312. Prieiga per internetą: <<http://pubs.acs.org/doi/abs/10.1021/ed058pA312.1>>.
19. BOHNE, C. et al. Characterization of the triplet-triplet annihilation process of pyrene and several derivatives under laser excitation. In: *Journal of the American Chemical Society* [interaktyvus]. 1990. Vol. 112, no. 11, p. 4226–4231. Prieiga per internetą: <<http://pubs.acs.org/doi/abs/10.1021/ja00167a018>>.
20. ENDO, A. et al. Efficient up-conversion of triplet excitons into a singlet state and its application for organic light emitting diodes. In: *Applied Physics Letters* [interaktyvus]. 2011. Vol. 98, no. 8, p. 083302. Prieiga per internetą: <<http://aip.scitation.org/doi/10.1063/1.3558906>>.
21. GIBSON, J. et al. The Importance of Vibronic Coupling for Efficient Reverse Intersystem Crossing in Thermally Activated Delayed Fluorescence Molecules. In: *ChemPhysChem* [interaktyvus]. 2016. Vol. 17, no. 19, p. 2956–2961. Prieiga per internetą: <<http://doi.wiley.com/10.1002/cphc.201600662>>.
22. FRÖBEL, M. et al. Get it white: color-tunable AC/DC OLEDs. In: *Light: Science & Applications* [interaktyvus]. 2015. Vol. 4, no. 2, p. e247–e247. Prieiga per internetą: <<http://www.nature.com/articles/lsa201520>>.
23. BUI, T.T. et al. [interaktyvus]. [s.l.]: Beilstein-Institut, 2018. Prieiga per internetą: <<https://www.beilstein-journals.org/bjoc/articles/14/18>>.
24. DIAS, F.B. et al. Photophysics of thermally activated delayed fluorescence molecules. In: *Methods Appl. Fluoresc* [interaktyvus]. 2017. Vol. 5. Prieiga per internetą: <<https://doi.org/10.1088/2050-6120/aa537e>>.
25. MILIÁN-MEDINA, B. - GIERSCHNER, J. Computational design of low singlet–triplet gap all-organic molecules for OLED application. In: *Organic Electronics* [interaktyvus]. 2012. Vol. 13, no. 6, p. 985–991. Prieiga per internetą: <<https://www.sciencedirect.com/science/article/pii/S156611991200081X>>.
26. BALDO, M.A. et al. Excitonic singlet-triplet ratio in a semiconducting organic thin film. In: *Physical Review B* [interaktyvus]. 1999. Vol. 60, no. 20, p. 14422–14428. Prieiga per internetą: <<https://link.aps.org/doi/10.1103/PhysRevB.60.14422>>.
27. BALDO, M.A. et al. Highly efficient phosphorescent emission from organic electroluminescent devices. In: *Nature* [interaktyvus]. 1998. Vol. 395, no. 6698, p. 151–154. Prieiga per internetą: <<http://www.nature.com/articles/25954>>.
28. FRÉ, N.A. et al. Iridium (III) complexes as promising emitters for solid-state Light-Emitting Electrochemical Cells (LECs). In: *International Journal of Nanotechnology* [interaktyvus]. 2012. Vol. 9, no. 3/4/5/6/7, p. 377. Prieiga per internetą: <<http://www.inderscience.com/link.php?id=45343>>.
29. DUMUR, F. Recent advances in organic light-emitting devices comprising copper complexes: A realistic approach for low-cost and highly emissive devices? In: *Organic Electronics* [interaktyvus]. 2015. Vol. 21, p. 27–39. Prieiga per internetą: <<http://linkinghub.elsevier.com/retrieve/pii/S1566119915000890>>.
30. DUMUR, F. Zinc complexes in OLEDs: An overview. In: *Synthetic Metals* [interaktyvus]. 2014. Vol. 195, p. 241–251. Prieiga per internetą:

<<http://linkinghub.elsevier.com/retrieve/pii/S0379677914002239>>.

31. TAO, Y. et al. Organic host materials for phosphorescent organic light-emitting diodes. In: *Chemical Society Reviews* [interaktyvus]. 2011. Vol. 40, no. 5, p. 2943. Prieiga per internetą: <<http://xlink.rsc.org/?DOI=c0cs00160k>>.
32. HIRATA, S. et al. Highly efficient blue electroluminescence based on thermally activated delayed fluorescence. In: *Nature Materials* [interaktyvus]. 2015. Vol. 14, no. 3, p. 330–336. Prieiga per internetą: <<http://www.ncbi.nlm.nih.gov/pubmed/25485987>>.
33. ZHANG, Q. et al. Efficient blue organic light-emitting diodes employing thermally activated delayed fluorescence. In: *Nature Photonics* [interaktyvus]. 2014. Vol. 8, no. 4, p. 326–332. Prieiga per internetą: <<http://www.nature.com/articles/nphoton.2014.12>>.
34. BERBERAN-SANTOS, M.N. - GARCIA, J.M.M. Unusually Strong Delayed Fluorescence of C₇₀. In: *Journal of the American Chemical Society* [interaktyvus]. 1996. Vol. 118, no. 39, p. 9391–9394. Prieiga per internetą: <<http://pubs.acs.org/doi/abs/10.1021/ja961782s>>.
35. ENDO, A. et al. Efficient up-conversion of triplet excitons into a singlet state and its application for organic light emitting diodes. In: *Applied Physics Letters* [interaktyvus]. 2011. Vol. 98, no. 8, p. 083302. Prieiga per internetą: <<http://aip.scitation.org/doi/10.1063/1.3558906>>.
36. SAMANTA, P.K. et al. Up-Conversion Intersystem Crossing Rates in Organic Emitters for Thermally Activated Delayed Fluorescence: Impact of the Nature of Singlet vs Triplet Excited States. In: *Journal of the American Chemical Society* [interaktyvus]. 2017. Vol. 139, no. 11, p. 4042–4051. Prieiga per internetą: <<http://pubs.acs.org/doi/10.1021/jacs.6b12124>>.
37. ETHERINGTON, M.K. et al. Regio- and conformational isomerization critical to design of efficient thermally-activated delayed fluorescence emitters. In: *Nature Communications* [interaktyvus]. 2017. Vol. 8, p. 14987. Prieiga per internetą: <<http://www.nature.com/doi/10.1038/ncomms14987>>.
38. TAO, Y. et al. A Simple Carbazole/Oxadiazole Hybrid Molecule: An Excellent Bipolar Host for Green and Red Phosphorescent OLEDs. In: *Angewandte Chemie International Edition* [interaktyvus]. 2008. Vol. 47, no. 42, p. 8104–8107. Prieiga per internetą: <<http://www.ncbi.nlm.nih.gov/pubmed/18798180>>.
39. JEON, S.-O. et al. 100% internal quantum efficiency and stable efficiency roll-off in phosphorescent light-emitting diodes using a high triplet energy hole transport material. In: *Applied Physics Letters* [interaktyvus]. 2008. Vol. 93, no. 6, p. 063306. Prieiga per internetą: <<http://aip.scitation.org/doi/10.1063/1.2969786>>.
40. LI, B. et al. Dicarbazolyldicyanobenzenes as Thermally Activated Delayed Fluorescence Emitters: Effect of Substitution Position on Photoluminescent and Electroluminescent Properties. In: *Chemistry Letters* [interaktyvus]. 2014. Vol. 43, no. 3, p. 319–321. Prieiga per internetą: <<http://www.journal.csj.jp/doi/10.1246/cl.130907>>.
41. CAO, X. et al. Alkyl effects on the optoelectronic properties of bicarbazole/cyanobenzene hybrid host materials: Double delayed fluorescent host/dopant systems in solution-processed OLEDs. In: *Dyes and Pigments* [interaktyvus]. 2017. Vol. 136, p. 543–552. Prieiga per internetą: <<http://linkinghub.elsevier.com/retrieve/pii/S0143720816306441>>.
42. CHANG, C.-H. et al. A dicarbazole–triazine hybrid bipolar host material for highly efficient green phosphorescent OLEDs. In: *Journal of Materials Chemistry* [interaktyvus]. 2012. Vol. 22, no. 9, p. 3832. Prieiga per internetą: <<http://xlink.rsc.org/?DOI=c2jm14686j>>.
43. KIM, M. - LEE, J.Y. Engineering of Interconnect Position of Bicarbazole for High External Quantum Efficiency in Green and Blue Phosphorescent Organic Light-Emitting Diodes. In: *ACS Applied Materials & Interfaces* [interaktyvus]. 2014. Vol. 6, no. 17,

- p. 14874–14880. Prieiga per internetą: <<http://pubs.acs.org/doi/10.1021/am502848c>>.
44. KIM, M. et al. Correlation of Molecular Structure with Photophysical Properties and Device Performances of Thermally Activated Delayed Fluorescent Emitters. In: *The Journal of Physical Chemistry C* [interaktyvus]. 2016. Vol. 120, no. 5, p. 2485–2493. Prieiga per internetą: <<http://pubs.acs.org/doi/10.1021/acs.jpcc.5b09114>>.
45. LEE, S.Y. et al. X-shaped benzoylbenzophenone derivatives with crossed donors and acceptors for highly efficient thermally activated delayed fluorescence. In: *Dalton Transactions* [interaktyvus]. 2015. Vol. 44, no. 18, p. 8356–8359. Prieiga per internetą: <<http://xlink.rsc.org/?DOI=C4DT03608E>>.
46. LEE, J. et al. Oxadiazole- and triazole-based highly-efficient thermally activated delayed fluorescence emitters for organic light-emitting diodes. In: *Journal of Materials Chemistry C* [interaktyvus]. 2013. Vol. 1, no. 30, p. 4599. Prieiga per internetą: <<http://xlink.rsc.org/?DOI=c3tc30699b>>.
47. CAO, X. et al. Systematically tuning of optoelectronic properties from electron donating to accepting substituents on bicarbazole/cyanobenzene hybrids: Host to dopant materials for phosphorescent and delayed fluorescence OLEDs. In: *Organic Electronics* [interaktyvus]. 2018. Vol. 52, p. 22–31. Prieiga per internetą: <<https://www.sciencedirect.com/science/article/pii/S1566119917304792?via%3Dihub>>.
48. KIM, H.M. et al. Blue thermally activated delayed fluorescent emitters having a bicarbazole donor moiety. In: *RSC Advances* [interaktyvus]. 2016. Vol. 6, no. 68, p. 64133–64139. Prieiga per internetą: <<http://xlink.rsc.org/?DOI=C6RA13240E>>.
49. TANAKA, H. et al. Efficient green thermally activated delayed fluorescence (TADF) from a phenoxazine–triphenyltriazine (PXZ–TRZ) derivative. In: *Chemical Communications* [interaktyvus]. 2012. Vol. 48, no. 93, p. 11392. Prieiga per internetą: <<http://xlink.rsc.org/?DOI=c2cc36237f>>.
50. LEE, S.Y. et al. Luminous Butterflies: Efficient Exciton Harvesting by Benzophenone Derivatives for Full-Color Delayed Fluorescence OLEDs. In: *Angewandte Chemie International Edition* [interaktyvus]. 2014. Vol. 53, no. 25, p. 6402–6406. Prieiga per internetą: <<http://www.ncbi.nlm.nih.gov/pubmed/24839234>>.
51. SEREVIČIUS, T. et al. Enhanced electroluminescence based on thermally activated delayed fluorescence from a carbazole–triazine derivative. In: *Physical Chemistry Chemical Physics* [interaktyvus]. 2013. Vol. 15, no. 38, p. 15850. Prieiga per internetą: <<http://xlink.rsc.org/?DOI=c3cp52255e>>.
52. KIM, M. et al. Highly efficient and color tunable thermally activated delayed fluorescent emitters using a “twin emitter” molecular design. In: *Chemical communications (Cambridge, England)* [interaktyvus]. 2016. Vol. 52, no. 2, p. 339–42. Prieiga per internetą: <<http://www.ncbi.nlm.nih.gov/pubmed/26515454>>.
53. SHIZU, K. et al. Highly Efficient Blue Electroluminescence Using Delayed-Fluorescence Emitters with Large Overlap Density between Luminescent and Ground States. In: *The Journal of Physical Chemistry C* [interaktyvus]. 2015. Vol. 119, no. 47, p. 26283–26289. Prieiga per internetą: <<http://pubs.acs.org/doi/10.1021/acs.jpcc.5b07798>>.
54. LEE, D.R. et al. Design Strategy for 25% External Quantum Efficiency in Green and Blue Thermally Activated Delayed Fluorescent Devices. In: *Advanced Materials* [interaktyvus]. 2015. Vol. 27, no. 39, p. 5861–5867. Prieiga per internetą: <<http://www.ncbi.nlm.nih.gov/pubmed/26308481>>.
55. TANAKA, H. et al. Dual Intramolecular Charge-Transfer Fluorescence Derived from a Phenothiazine-Triphenyltriazine Derivative. In: *The Journal of Physical Chemistry C* [interaktyvus]. 2014. Vol. 118, no. 29, p. 15985–15994. Prieiga per internetą: <<http://pubs.acs.org/doi/10.1021/jp501017f>>.

56. SUN, J.W. et al. A Fluorescent Organic Light-Emitting Diode with 30% External Quantum Efficiency. In: *Advanced Materials* [interaktyvus]. 2014. Vol. 26, no. 32, p. 5684–5688. Prieiga per internetą: <<http://www.ncbi.nlm.nih.gov/pubmed/24890507>>.
57. ZHANG, X. et al. Theoretical investigation of dihydroacridine and diphenylsulphone derivatives as thermally activated delayed fluorescence emitters for organic light-emitting diodes. In: *RSC Advances* [interaktyvus]. 2015. Vol. 5, no. 64, p. 51586–51591. Prieiga per internetą: <<http://xlink.rsc.org/?DOI=C5RA04929F>>.
58. KIM, M. et al. Stable Blue Thermally Activated Delayed Fluorescent Organic Light-Emitting Diodes with Three Times Longer Lifetime than Phosphorescent Organic Light-Emitting Diodes. In: *Advanced Materials* [interaktyvus]. 2015. Vol. 27, no. 15, p. 2515–2520. Prieiga per internetą: <<http://www.ncbi.nlm.nih.gov/pubmed/25757226>>.
59. YANG, Z. et al. Recent advances in organic thermally activated delayed fluorescence materials. In: *Chemical Society Reviews* [interaktyvus]. 2017. Vol. 46, no. 3, p. 915–1016. Prieiga per internetą: <<http://xlink.rsc.org/?DOI=C6CS00368K>>.
60. YOO, S.G. et al. Molecular engineering of donor moiety of donor–acceptor structure for management of photophysical properties and device performances. In: *Dyes and Pigments* [interaktyvus]. 2016. Vol. 128, no. 128, p. 201–208. Prieiga per internetą: <<http://linkinghub.elsevier.com/retrieve/pii/S0143720816000322>>.
61. LEE, I.H. et al. High efficiency blue fluorescent organic light-emitting diodes using a conventional blue fluorescent emitter. In: *Journal of Materials Chemistry C* [interaktyvus]. 2015. Vol. 3, no. 34, p. 8834–8838. Prieiga per internetą: <<http://xlink.rsc.org/?DOI=C5TC01626F>>.
62. LIN, T.-A. et al. Sky-Blue Organic Light Emitting Diode with 37% External Quantum Efficiency Using Thermally Activated Delayed Fluorescence from Spiroacridine-Triazine Hybrid. In: *Advanced Materials* [interaktyvus]. 2016. Vol. 28, no. 32, p. 6976–6983. Prieiga per internetą: <<http://www.ncbi.nlm.nih.gov/pubmed/27271917>>.
63. KAJI, H. et al. Purely organic electroluminescent material realizing 100% conversion from electricity to light. In: *Nature Communications* [interaktyvus]. 2015. Vol. 6, no. 1, p. 8476. Prieiga per internetą: <<http://www.nature.com/articles/ncomms9476>>.
64. KIM, B.S. - LEE, J.Y. Engineering of Mixed Host for High External Quantum Efficiency above 25% in Green Thermally Activated Delayed Fluorescence Device. In: *Advanced Functional Materials* [interaktyvus]. 2014. Vol. 24, no. 25, p. 3970–3977. Prieiga per internetą: <<http://doi.wiley.com/10.1002/adfm.201303730>>.
65. TSAI, W.-L. et al. A versatile thermally activated delayed fluorescence emitter for both highly efficient doped and non-doped organic light emitting devices. In: *Chemical Communications* [interaktyvus]. 2015. Vol. 51, no. 71, p. 13662–13665. Prieiga per internetą: <<http://xlink.rsc.org/?DOI=C5CC05022G>>.
66. GANESAN, P. et al. Functional Pyrimidine-Based Thermally Activated Delay Fluorescence Emitters: Photophysics, Mechanochromism, and Fabrication of Organic Light-Emitting Diodes. In: *Chemistry - A European Journal* [interaktyvus]. 2017. Vol. 23, no. 12, p. 2858–2866. Prieiga per internetą: <<http://www.ncbi.nlm.nih.gov/pubmed/28028848>>.
67. PARK, I.S. et al. Pyrimidine-based twisted donor–acceptor delayed fluorescence molecules: a new universal platform for highly efficient blue electroluminescence. In: *Chemical Science* [interaktyvus]. 2017. Vol. 8, no. 2, p. 953–960. Prieiga per internetą: <<http://xlink.rsc.org/?DOI=C6SC03793C>>.
68. NAKAO, K. et al. OLEDs: Significant Enhancement of Blue OLED Performances through Molecular Engineering of Pyrimidine-Based Emitter (Advanced Optical Materials 6/2017). In: *Advanced Optical Materials* [interaktyvus]. 2017. Vol. 5, no. 6. Prieiga per internetą: <<http://doi.wiley.com/10.1002/adom.201770036>>.

69. IM, J.B. et al. Thermally Activated Delayed Fluorescence Behavior Investigation in the Different Polarity Acceptor and Donor Molecules. In: *The Journal of Physical Chemistry C* [interaktyvus]. 2017. Vol. 121, no. 2, p. 1305–1314. Prieiga per internetą: <<http://pubs.acs.org/doi/10.1021/acs.jpcc.6b10854>>.
70. SASABE, H. et al. High Power Efficiency Blue-to-Green Organic Light-Emitting Diodes Using Isonicotinonitrile-Based Fluorescent Emitters. In: *Chemistry - An Asian Journal* [interaktyvus]. 2017. Vol. 12, no. 6, p. 648–654. Prieiga per internetą: <<http://www.ncbi.nlm.nih.gov/pubmed/28029223>>.
71. TAKAHASHI, T. et al. Donor–acceptor-structured 1,4-diazatriphenylene derivatives exhibiting thermally activated delayed fluorescence: design and synthesis, photophysical properties and OLED characteristics. In: *Science and Technology of Advanced Materials* [interaktyvus]. 2014. Vol. 15, no. 3, p. 034202. Prieiga per internetą: <<http://www.ncbi.nlm.nih.gov/pubmed/27877670>>.
72. KITAMOTO, Y. et al. Light blue and green thermally activated delayed fluorescence from 10H-phenoxaborin-derivatives and their application to organic light-emitting diodes. In: *Journal of Materials Chemistry C* [interaktyvus]. 2015. Vol. 3, no. 35, p. 9122–9130. Prieiga per internetą: <<http://xlink.rsc.org/?DOI=C5TC01380A>>.
73. PARK, I.S. et al. Full-Color Delayed Fluorescence Materials Based on Wedge-Shaped Phthalonitriles and Dicyanopyrazines: Systematic Design, Tunable Photophysical Properties, and OLED Performance. In: *Advanced Functional Materials* [interaktyvus]. 2016. Vol. 26, no. 11, p. 1813–1821. Prieiga per internetą: <<http://doi.wiley.com/10.1002/adfm.201505106>>.
74. KOMATSU, R. et al. Light-blue thermally activated delayed fluorescent emitters realizing a high external quantum efficiency of 25% and unprecedented low drive voltages in OLEDs. In: *Journal of Materials Chemistry C* [interaktyvus]. 2016. Vol. 4, no. 12, p. 2274–2278. Prieiga per internetą: <<http://xlink.rsc.org/?DOI=C5TC04057D>>.
75. LEE, I. - LEE, J.Y. Molecular design of deep blue fluorescent emitters with 20% external quantum efficiency and narrow emission spectrum. In: *Organic Electronics* [interaktyvus]. 2016. Vol. 29, p. 160–164. Prieiga per internetą: <<https://www.sciencedirect.com/science/article/pii/S1566119915302251>>.
76. NUMATA, M. et al. High efficiency pure blue thermally activated delayed fluorescence molecules having 10H-phenoxaborin and acridan units. In: *Chemical Communications* [interaktyvus]. 2015. Vol. 51, no. 46, p. 9443–9446. Prieiga per internetą: <<http://xlink.rsc.org/?DOI=C5CC00307E>>.
77. KOBAYASHI, J. et al. Synthesis of Dibenzochalcogenaborins and Systematic Comparisons of Their Optical Properties by Changing a Bridging Chalcogen Atom. In: *Chemistry - An Asian Journal* [interaktyvus]. 2009. Vol. 4, no. 1, p. 42–49. Prieiga per internetą: <<http://www.ncbi.nlm.nih.gov/pubmed/19021190>>.
78. NODA, T. - SHIROTA, Y. 5,5'-Bis(dimesitylboryl)-2,2'-bithiophene and 5,5''-Bis(dimesitylboryl)-2,2':5',2''-terthiophene as a Novel Family of Electron-Transporting Amorphous Molecular Materials. In: [interaktyvus]. 1998. Prieiga per internetą: <<https://pubs.acs.org/doi/abs/10.1021/ja9817343>>.
79. WU, S. et al. High-efficiency deep-blue organic light-emitting diodes based on a thermally activated delayed fluorescence emitter. In: *J. Mater. Chem. C* [interaktyvus]. 2014. Vol. 2, no. 3, p. 421–424. Prieiga per internetą: <<http://xlink.rsc.org/?DOI=C3TC31936A>>.
80. OHKUMA, H. et al. Thermally Activated Delayed Fluorescence from a Spiro-diazafluorene Derivative. In: *Chemistry Letters* [interaktyvus]. 2014. Vol. 43, no. 7, p. 1017–1019. Prieiga per internetą: <<http://www.journal.csj.jp/doi/10.1246/cl.140360>>.
81. LEE, S.Y. et al. High-Efficiency Blue Organic Light-Emitting Diodes Based on

- Thermally Activated Delayed Fluorescence from Phenoxaphosphine and Phenoxathiin Derivatives. In: *Advanced Materials* [interaktyvus]. 2016. Vol. 28, no. 23, p. 4626–4631. Prieiga per internetą: <<http://www.ncbi.nlm.nih.gov/pubmed/27059783>>.
82. LUO, J. et al. Multi-carbazole encapsulation as a simple strategy for the construction of solution-processed, non-doped thermally activated delayed fluorescence emitters. In: *Journal of Materials Chemistry C* [interaktyvus]. 2016. Vol. 4, no. 13, p. 2442–2446. Prieiga per internetą: <<http://xlink.rsc.org/?DOI=C6TC00418K>>.
83. CAO, X. et al. Simple phenyl bridge between cyano and pyridine units to weaken the electron-withdrawing property for blue-shifted emission in efficient blue TADF OLEDs. In: *Organic Electronics* [interaktyvus]. 2018. Vol. 57, p. 247–254. Prieiga per internetą: <<http://linkinghub.elsevier.com/retrieve/pii/S1566119918301332>>.
84. UOYAMA, H. et al. Highly efficient organic light-emitting diodes from delayed fluorescence. In: *Nature* [interaktyvus]. 2012. Vol. 492, no. 7428, p. 234–238. Prieiga per internetą: <<http://www.nature.com/doi/10.1038/nature11687>>.
85. GOUSHI, K. et al. Organic light-emitting diodes employing efficient reverse intersystem crossing for triplet-to-singlet state conversion. In: *Nature Photonics* [interaktyvus]. 2012. Vol. 6, no. 4, p. 253–258. Prieiga per internetą: <<http://www.nature.com/articles/nphoton.2012.31>>.
86. MAYR, C. et al. Efficiency Enhancement of Organic Light-Emitting Diodes Incorporating a Highly Oriented Thermally Activated Delayed Fluorescence Emitter. In: *Advanced Functional Materials* [interaktyvus]. 2014. Vol. 24, no. 33, p. 5232–5239. Prieiga per internetą: <<http://doi.wiley.com/10.1002/adfm.201400495>>.
87. LIU, Y. et al. Boosting reverse intersystem crossing by increasing donors in triarylboron/phenoxazine hybrids: TADF emitters for high-performance solution-processed OLEDs. In: *Journal of Materials Chemistry C* [interaktyvus]. 2016. Vol. 4, no. 20, p. 4402–4407. Prieiga per internetą: <<http://xlink.rsc.org/?DOI=C6TC01353H>>.
88. SAGARA, Y. et al. Highly Efficient Thermally Activated Delayed Fluorescence Emitters with a Small Singlet–Triplet Energy Gap and Large Oscillator Strength. In: *Chemistry Letters* [interaktyvus]. 2015. Vol. 44, no. 3, p. 360–362. Prieiga per internetą: <<http://www.journal.csj.jp/doi/10.1246/cl.141054>>.
89. CHEN, D.-Y. et al. Isomeric Thermally Activated Delayed Fluorescence Emitters for Color Purity-Improved Emission in Organic Light-Emitting Devices. In: *ACS Applied Materials & Interfaces* [interaktyvus]. 2016. Vol. 8, no. 26, p. 16791–16798. Prieiga per internetą: <<http://pubs.acs.org/doi/10.1021/acsami.6b03954>>.
90. CHEN, J. - TANG, B.Z. Restricted Intramolecular Rotations: a Mechanism for Aggregation-Induced Emission. In: *Aggregation-Induced Emission: Fundamentals* [interaktyvus]. Chichester, United Kingdom: John Wiley and Sons Ltd, 2013. p. 307–322. Prieiga per internetą: <<http://doi.wiley.com/10.1002/9781118735183.ch14>>.
91. HE, Z. et al. Sky-blue thermally activated delayed fluorescence material employing a diphenylethyne acceptor for organic light-emitting diodes. In: *Journal of Materials Chemistry C* [interaktyvus]. 2018. Vol. 6, no. 1, p. 36–42. Prieiga per internetą: <<http://xlink.rsc.org/?DOI=C7TC02763J>>.
92. ZHAN, X. et al. Electron Affinities of 1,1-Diaryl-2,3,4,5-tetraphenylsiloles: Direct Measurements and Comparison with Experimental and Theoretical Estimates. In: [interaktyvus]. 2005. Prieiga per internetą: <<https://pubs.acs.org/doi/abs/10.1021/ja051139i>>.
93. QIAO, Y. et al. Synthesis, experimental and theoretical characterization, and field-effect transistor properties of a new class of dibenzothiophene derivatives: From linear to cyclic architectures. In: *J. Mater. Chem.* [interaktyvus]. 2012. Vol. 22, no. 4, p. 1313–1325. Prieiga per internetą:

- per internetą: <<http://xlink.rsc.org/?DOI=C1JM13962B>>.
94. KAAFARANI, B.R. et al. Bis(carbazolyl) derivatives of pyrene and tetrahydropyrene: synthesis, structures, optical properties, electrochemistry, and electroluminescence. In: *Journal of Materials Chemistry C* [interaktyvus]. 2013. Vol. 1, no. 8, p. 1638. Prieiga per internetą: <<http://xlink.rsc.org/?DOI=c2tc00474g>>.
95. MIYAMOTO, E. et al. Ionization Potential of Organic Pigment Film by Atmospheric Photoelectron Emission Analysis. In: *Electrophotography* [interaktyvus]. 1989. Vol. 28, no. 4, p. 364–370. Prieiga per internetą: <<http://www.ndsl.kr/ndsl/search/detail/article/articleSearchResultDetail.do?cn=NART57603717>>.
96. KOHN, W. - SHAM, L.J. Self-Consistent Equations Including Exchange and Correlation Effects. In: *Physical Review* [interaktyvus]. 1965. Vol. 140, no. 4A, p. A1133–A1138. Prieiga per internetą: <<https://link.aps.org/doi/10.1103/PhysRev.140.A1133>>.
97. BECKE, A.D. Density-functional thermochemistry. III. The role of exact exchange. In: *The Journal of Chemical Physics* [interaktyvus]. 1993. Vol. 98, no. 7, p. 5648–5652. Prieiga per internetą: <<http://aip.scitation.org/doi/10.1063/1.464913>>.
98. GROSS, E.K.U. et al. Density Functional Theory of Time-Dependent Systems. In: [interaktyvus]. [s.l.]: Springer, Boston, MA, 1995. p. 149–171. Prieiga per internetą: <http://link.springer.com/10.1007/978-1-4757-9975-0_7>.
99. STAKHIRA, P. et al. Characteristics of organic light emitting diodes with copper iodide as injection layer. In: *Thin Solid Films* [interaktyvus]. 2010. Vol. 518, no. 23, p. 7016–7018. Prieiga per internetą: <<https://www.sciencedirect.com/science/article/pii/S0040609010008965?via%3Dihub>>.
100. QIAN, Y. et al. A new spiro[fluorene-9,9'-xanthene]-based host material possessing no conventional hole- and electron-transporting units for efficient and low voltage blue PHOLED via simple two-step synthesis. In: *Organic Electronics* [interaktyvus]. 2012. Vol. 13, no. 11, p. 2741–2746. Prieiga per internetą: <<https://www.sciencedirect.com/science/article/pii/S1566119912003758>>.
101. TSAI, M.-H. et al. Highly Efficient Organic Blue Electrophosphorescent Devices Based on 3,6-Bis(triphenylsilyl)carbazole as the Host Material. In: *Advanced Materials* [interaktyvus]. 2006. Vol. 18, no. 9, p. 1216–1220. Prieiga per internetą: <<http://doi.wiley.com/10.1002/adma.200502283>>.
102. WU, C.-C. et al. Efficient Organic Blue-Light-Emitting Devices with Double Confinement on Terfluorenes with Ambipolar Carrier Transport Properties. In: *Advanced Materials* [interaktyvus]. 2004. Vol. 16, no. 1, p. 61–65. Prieiga per internetą: <<http://doi.wiley.com/10.1002/adma.200305619>>.
103. VOLYNIUK, D. et al. Highly Efficient Blue Organic Light-Emitting Diodes Based on Intermolecular Triplet–Singlet Energy Transfer. In: *The Journal of Physical Chemistry C* [interaktyvus]. 2013. Vol. 117, no. 44, p. 22538–22544. Prieiga per internetą: <<http://pubs.acs.org/doi/10.1021/jp407397y>>.
104. LAURENCE M. HARWOOD, C.J.M. *Experimental organic chemistry : principles and practice - Ghent University Library* [interaktyvus]. . 1990. ISBN 0632020164.
105. BREITENBACH, J.W. - POLACZEK, J. Über die Bromierung von 9-Vinylcarbazol. In: *Monatshefte für Chemie - Chemical Monthly* [interaktyvus]. 1971. Vol. 102, no. 3, p. 711–717. Prieiga per internetą: <<http://link.springer.com/10.1007/BF01167248>>.
106. GILMAN, H. - KIRBY, R.H. CARBAZOLE. I. SELECTIVE METALATION. In: *The Journal of Organic Chemistry* [interaktyvus]. 1936. Vol. 01, no. 2, p. 146–153. Prieiga per internetą: <<http://pubs.acs.org/doi/abs/10.1021/jo01231a003>>.
107. DOBARRO, A. et al. Synthesis of symmetric and asymmetric carbazolyl monomers

- and their siloxane polymers. Effect of the 2,3,6,7,9-substitution in the carbazole unit on its mesomorphic behaviour. In: *Macromolecular Chemistry and Physics* [interaktyvus]. 1997. Vol. 198, no. 8, p. 2563–2581. Prieiga per internetą: <<http://doi.wiley.com/10.1002/macp.1997.021980816>>.
108. YUNING LI, † et al. Synthesis and Properties of Random and Alternating Fluorene/Carbazole Copolymers for Use in Blue Light-Emitting Devices. In: [interaktyvus]. 2004. Prieiga per internetą: <<https://cdn-pubs.acs.org/doi/abs/10.1021/cm030069g?src=recsys>>.
109. NEUGEBAUER, F.A. - FISCHER, H. tert.-Butyl-substituierte Carbazole. In: *Chemische Berichte* [interaktyvus]. 1972. Vol. 105, no. 8, p. 2686–2693. Prieiga per internetą: <<http://doi.wiley.com/10.1002/cber.19721050829>>.
110. GRUZDEV, M.S. et al. Synthesis and photochemical properties of 3,6-di-tert-butyl-9H-carbazole derivatives. In: *Russian Journal of General Chemistry* [interaktyvus]. 2015. Vol. 85, no. 6, p. 1431–1439. Prieiga per internetą: <<http://link.springer.com/10.1134/S1070363215060122>>.
111. MINAEV, B. et al. Principles of phosphorescent organic light emitting devices. In: *Phys. Chem. Chem. Phys.* [interaktyvus]. 2014. Vol. 16, no. 5, p. 1719–1758. Prieiga per internetą: <<http://xlink.rsc.org/?DOI=C3CP53806K>>. <<http://www.hindawi.com/journals/amse/2012/794674/>>.
112. SUN, J. et al. Synthesis and characterization of heteroatom substituted carbazole derivatives: potential host materials for phosphorescent organic light-emitting diodes. In: *New Journal of Chemistry* [interaktyvus]. 2013. Vol. 37, no. 4, p. 977. Prieiga per internetą: <<http://xlink.rsc.org/?DOI=c2nj40900c>>.
113. BLAZYS, G. et al. Phenothiazinyl-containing aromatic amines as novel amorphous molecular materials for optoelectronics. In: *Journal of Photochemistry and Photobiology A: Chemistry* [interaktyvus]. 2005. Vol. 174, no. 1, p. 1–6. Prieiga per internetą: <<http://linkinghub.elsevier.com/retrieve/pii/S1010603005000729>>.
114. ORTIZ, R.P. et al. Rational design of ambipolar organic semiconductors: is core planarity central to ambipolarity in thiophene-naphthalene semiconductors? In: *Chemistry (Weinheim an der Bergstrasse, Germany)* [interaktyvus]. 2012. Vol. 18, no. 2, p. 532–43. Prieiga per internetą: <<http://www.ncbi.nlm.nih.gov/pubmed/22161811>>.
115. BUCINSKAS, A. et al. Structure–property relationship of isomeric diphenylethenyl-disubstituted dimethoxycarbazoles. In: *RSC Advances* [interaktyvus]. 2015. Vol. 5, no. 61, p. 49577–49589. Prieiga per internetą: <<http://xlink.rsc.org/?DOI=C5RA09161F>>.
116. KOOPMANS, T. Über die Zuordnung von Wellenfunktionen und Eigenwerten zu den Einzelnen Elektronen Eines Atoms. In: *Physica* [interaktyvus]. 1934. Vol. 1, no. 1–6, p. 104–113. Prieiga per internetą: <<https://www.sciencedirect.com/science/article/pii/S0031891434900112>>.
117. TOMKEVICIENE, A. et al. Impact of Linking Topology on the Properties of Carbazole Trimers and Dimers. In: *The Journal of Physical Chemistry C* [interaktyvus]. 2011. Vol. 115, no. 11, p. 4887–4897. Prieiga per internetą: <<http://pubs.acs.org/doi/10.1021/jp111333v>>.
118. BREDAS, J.-L. Mind the gap! In: *Mater. Horiz.* [interaktyvus]. 2014. Vol. 1, no. 1, p. 17–19. Prieiga per internetą: <<http://xlink.rsc.org/?DOI=C3MH00098B>>.
119. YOSHIDA, H. - YOSHIZAKI, K. Electron affinities of organic materials used for organic light-emitting diodes: A low-energy inverse photoemission study. In: [interaktyvus]. Prieiga per internetą: <<http://citeseerx.ist.psu.edu/viewdoc/download?doi=10.1.1.822.254&rep=rep1&type=pdf>>.
120. DANDRADE, B. et al. Relationship between the ionization and oxidation potentials of

- molecular organic semiconductors. In: *Organic Electronics* [interaktyvus]. 2005. Vol. 6, no. 1, p. 11–20. Prieiga per internetą: <<http://linkinghub.elsevier.com/retrieve/pii/S1566119905000030>>.
121. SHIH, C.-H. et al. A Universal Electron-Transporting/Exciton-Blocking Material for Blue, Green, and Red Phosphorescent Organic Light-Emitting Diodes (OLEDs). In: *ACS Applied Materials & Interfaces* [interaktyvus]. 2015. Vol. 7, no. 19, p. 10466–10474. Prieiga per internetą: <<http://pubs.acs.org/doi/10.1021/acsami.5b01872>>.
122. MALAGOLI, M. - BRÉDAS, J.L. Density functional theory study of the geometric structure and energetics of triphenylamine-based hole-transporting molecules. In: *Chemical Physics Letters* [interaktyvus]. 2000. Vol. 327, no. 1–2, p. 13–17. Prieiga per internetą: <<https://www.sciencedirect.com/science/article/abs/pii/S0009261400007570>>.
123. BRUNNER, K. et al. Carbazole Compounds as Host Materials for Triplet Emitters in Organic Light-Emitting Diodes: Tuning the HOMO Level without Influencing the Triplet Energy in Small Molecules. In: *Journal of the American Chemical Society* [interaktyvus]. 2004. Vol. 126, no. 19, p. 6035–6042. Prieiga per internetą: <<http://www.ncbi.nlm.nih.gov/pubmed/15137768>>.
124. O'BRIEN, D.F. et al. Improved energy transfer in electrophosphorescent devices. In: *Applied Physics Letters* [interaktyvus]. 1999. Vol. 74, no. 3, p. 442. Prieiga per internetą: <<https://aip.scitation.org/doi/abs/10.1063/1.123055>>.
125. ADACHI, C. et al. Efficient electrophosphorescence using a doped ambipolar conductive molecular organic thin film. In: *Organic Electronics* [interaktyvus]. 2001. Vol. 2, no. 1, p. 37–43. Prieiga per internetą: <<https://www.sciencedirect.com/science/article/pii/S1566119901000106>>.
126. ADACHI, C. et al. Endothermic energy transfer: A mechanism for generating very efficient high-energy phosphorescent emission in organic materials. In: *Applied Physics Letters* [interaktyvus]. 2001. Vol. 79, no. 13, p. 2082–2084. Prieiga per internetą: <<http://aip.scitation.org/doi/10.1063/1.1400076>>.
127. HOLMES, R.J. et al. Blue organic electrophosphorescence using exothermic host–guest energy transfer. In: *Applied Physics Letters* [interaktyvus]. 2003. Vol. 82, no. 15, p. 2422–2424. Prieiga per internetą: <<http://aip.scitation.org/doi/10.1063/1.1568146>>.
128. KIM, D. et al. Design of Efficient Ambipolar Host Materials for Organic Blue Electrophosphorescence: Theoretical Characterization of Hosts Based on Carbazole Derivatives. In: *Journal of the American Chemical Society* [interaktyvus]. 2011. Vol. 133, no. 44, p. 17895–17900. Prieiga per internetą: <<http://www.ncbi.nlm.nih.gov/pubmed/21942419>>.
129. SHIN, M.-G. et al. A new N-fluorenyl carbazole host material: Synthesis, physical properties and applications for highly efficient phosphorescent organic light emitting diodes. In: *Organic Electronics* [interaktyvus]. 2011. Vol. 12, no. 5, p. 785–793. Prieiga per internetą: <<https://www.sciencedirect.com/science/article/pii/S1566119911000644>>.
130. JEON, S.-O. et al. 100% internal quantum efficiency and stable efficiency roll-off in phosphorescent light-emitting diodes using a high triplet energy hole transport material. In: *Applied Physics Letters* [interaktyvus]. 2008. Vol. 93, no. 6, p. 063306. Prieiga per internetą: <<http://aip.scitation.org/doi/10.1063/1.2969786>>.
131. CUI, L.-S. et al. Bipolar host materials for high efficiency phosphorescent organic light emitting diodes: tuning the HOMO/LUMO levels without reducing the triplet energy in a linear system. In: *Journal of Materials Chemistry C* [interaktyvus]. 2013. Vol. 1, no. 48, p. 8177. Prieiga per internetą: <<http://xlink.rsc.org/?DOI=c3tc31675k>>.
132. HOLMES, R.J. et al. Efficient, deep-blue organic electrophosphorescence by guest charge trapping. In: *Applied Physics Letters* [interaktyvus]. 2003. Vol. 83, no. 18, p. 3818–

3820. Prieiga per internetą: <<http://aip.scitation.org/doi/10.1063/1.1624639>>.
133. SU, S.-J. et al. Tuning Energy Levels of Electron-Transport Materials by Nitrogen Orientation for Electrophosphorescent Devices with an ‘Ideal’ Operating Voltage. In: *Advanced Materials* [interaktyvus]. 2010. Vol. 22, no. 30, p. 3311–3316. Prieiga per internetą: <<http://doi.wiley.com/10.1002/adma.200904249>>.
134. CAO, X. et al. Alkyl effects on the optoelectronic properties of bicarbazole/cyanobenzene hybrid host materials: Double delayed fluorescent host/ dopant systems in solution-processed OLEDs. In: *Dyes and Pigments* [interaktyvus]. 2017. Vol. 136, p. 543–552. Prieiga per internetą: <https://ac.els-cdn.com/S0143720816306441/1-s2.0-S0143720816306441-main.pdf?_tid=8b5817c0-ca09-11e7-bac2-00000aacb360&acdnat=1510752981_eecefc13c58c848b44dc87dbe3519709>.
135. ZHANG, D. et al. Highly efficient and color-stable hybrid warm white organic light-emitting diodes using a blue material with thermally activated delayed fluorescence. In: *J. Mater. Chem. C* [interaktyvus]. 2014. Vol. 2, no. 38, p. 8191–8197. Prieiga per internetą: <<http://xlink.rsc.org/?DOI=C4TC01289E>>.
136. DIAS, F.B. et al. Triplet Harvesting with 100% Efficiency by Way of Thermally Activated Delayed Fluorescence in Charge Transfer OLED Emitters. In: *Advanced Materials* [interaktyvus]. 2013. Vol. 25, no. 27, p. 3707–3714. Prieiga per internetą: <<http://doi.wiley.com/10.1002/adma.201300753>>.
135. ZHOU, J. et al. Charge-transfer-featured materials—promising hosts for fabrication of efficient OLEDs through triplet harvesting via triplet fusion. In: *Chem. Commun.* [interaktyvus]. 2014. Vol. 50, no. 57, p. 7586–7589. Prieiga per internetą: <<http://xlink.rsc.org/?DOI=C4CC00576G>>.
136. ZHANG, T. et al. Efficient Triplet Application in Exciplex Delayed-Fluorescence OLEDs Using a Reverse Intersystem Crossing Mechanism Based on a $\Delta E S-T$ of around Zero. In: *ACS Applied Materials & Interfaces* [interaktyvus]. 2014. Vol. 6, no. 15, p. 11907–11914. Prieiga per internetą: <<http://pubs.acs.org/doi/10.1021/am501164s>>.
137. TOMOAKI KOZAKI, SHOTA KOGA, NAOHIRO TODA, HIROKI NOGUCHI, A.Y. Effects of short wavelength control in polychromatic light sources on nocturnal melatonin secretion. In: *Neuroscience Letters* [interaktyvus]. 2008. Vol. 439, no. 3, p. 256–259. Prieiga per internetą: <<http://www.sciencedirect.com/science/article/pii/S0304394008006757>>.
138. CHERPAK, V. et al. Efficient “Warm-White” OLEDs Based on the Phosphorescent bis-Cyclometalated iridium(III) Complex. In: *The Journal of Physical Chemistry C* [interaktyvus]. 2014. Vol. 118, no. 21, p. 11271–11278. Prieiga per internetą: <<http://pubs.acs.org/doi/10.1021/jp503437b>>.
139. DAMIT, E.F. et al. Synthesis of Novel Derivatives of Carbazole-Thiophene, Their Electronic Properties, and Computational Studies. In: *Journal of Chemistry* [interaktyvus]. 2016. Vol. 2016, p. 1–14. Prieiga per internetą: <<http://www.hindawi.com/journals/jchem/2016/9360230/>>.
140. DIMITRAKOPOULOS, C.D. - MALENFANT, P.R.L. Organic Thin Film Transistors for Large Area Electronics. In: *Advanced Materials* [interaktyvus]. 2002. Vol. 14, no. 2, p. 99–117. Prieiga per internetą: <<http://doi.wiley.com/10.1002/1521-4095%2820020116%2914%3A2%3C99%3A%3AAID-ADMA99%3E3.0.CO%3B2-9>>.
141. REIG, M. et al. Molecular order of air-stable p-type organic thin-film transistors by tuning the extension of the π -conjugated core: the cases of indolo[3,2-b]carbazole and triindole semiconductors. In: *Journal of Materials Chemistry C* [interaktyvus]. 2015. Vol. 3, no. 3, p. 506–513. Prieiga per internetą: <<http://xlink.rsc.org/?DOI=C4TC01692K>>.
142. XIN GUO, MARTIN BAUMGARTEN, K.M. Designing π -conjugated polymers for organic electronics. In: *Progress in Polymer Science* [interaktyvus]. 2013. Vol. 38, no. 12,

p. 1832–1908. Prieiga per internetą:

<<http://www.sciencedirect.com/science/article/pii/S0079670013001196>>.

143. CAO, X. et al. CN-Containing donor–acceptor-type small-molecule materials for thermally activated delayed fluorescence OLEDs. In: *Journal of Materials Chemistry C* [interaktyvus]. 2017. Vol. 5, no. 31, p. 7699–7714. Prieiga per internetą:

<<http://xlink.rsc.org/?DOI=C7TC02481A>>.

144. DOBARRO, A. et al. Synthesis of symmetric and asymmetric carbazolyl monomers and their siloxane polymers. Effect of the 2,3,6,7,9-substitution in the carbazole unit on its mesomorphic behaviour. In: *Macromolecular Chemistry and Physics* [interaktyvus]. 1997. Vol. 198, no. 8, p. 2563–2581. Prieiga per internetą:

<<http://doi.wiley.com/10.1002/macp.1997.021980816>>.

145. LI, Y. et al. Synthesis and Properties of Random and Alternating Fluorene/Carbazole Copolymers for Use in Blue Light-Emitting Devices. In: *Chem. Mater.* [interaktyvus]. 2004. Vol. 16, no. 11, p. 2165–2173. Prieiga per internetą:

<<https://pubs.acs.org/doi/abs/10.1021/cm030069g>>.

146. GRUZDEV, M.S. et al. Synthesis and Photochemical Properties of 3,6-Di-tert-butyl-9H-carbazole Derivatives. In: *ISSN Russian Journal of General Chemistry* [interaktyvus]. 2015. Vol. 85, no. 6, p. 1070–3632. Prieiga per internetą:

<<https://link.springer.com/content/pdf/10.1134%2FS1070363215060122.pdf>>.

147. LI, J.-C. et al. A Thiophene, Benzothiadiazole, and Carbazole-Based Copolymer: Synthesis and Characterization. In: *Bulletin of the Korean Chemical Society* [interaktyvus]. 2009. Vol. 30, no. 4, p. 951–954. Prieiga per internetą:

<<http://koreascience.or.kr/journal/view.jsp?kj=JCGMCS&py=2009&vnc=v30n4&sp=951>>.

148. KIKUGAWA, Y. et al. Synthesis of Carbazoles from N-(N,N-Diarylamino)phthalimides with Aluminum Chloride via Diarylnitrenium Ions. In: [interaktyvus]. 2001. Vol. 66, no. 25, p. 8612–8615. Prieiga per internetą:

<<https://pubs.acs.org/doi/abs/10.1021/jo016124r>>.

149. RUDNICK, A.A. et al. The influence of torsion on excimer formation in bipolar host materials for blue phosphorescent OLEDs. In: *The Journal of Chemical Physics* [interaktyvus]. 2016. Vol. 144, no. 21, p. 214906. Prieiga per internetą:

<<http://aip.scitation.org/doi/10.1063/1.4953102>>.

150. ZHANG, Q. et al. Efficient blue organic light-emitting diodes employing thermally activated delayed fluorescence. In: *Nature Photonics* [interaktyvus]. 2014. Vol. 8, no. 4, p. 326–332. Prieiga per internetą:

<<http://www.nature.com/doi/10.1038/nphoton.2014.12>>.

151. MIMAITE, V. et al. Can hydrogen bonds improve the hole-mobility in amorphous organic semiconductors? Experimental and theoretical insights. In: *Journal of Materials Chemistry C* [interaktyvus]. 2015. Vol. 3, no. 44, p. 11660–11674. Prieiga per internetą:

<<http://xlink.rsc.org/?DOI=C5TC02534F>>.

152. FISHCHUK, I.I. et al. Transition from trap-controlled to trap-to-trap hopping transport in disordered organic semiconductors. In: *Physical Review B* [interaktyvus]. 2006. Vol. 73, no. 11, p. 115210. Prieiga per internetą:

<<https://link.aps.org/doi/10.1103/PhysRevB.73.115210>>.

153. SANTOS, P.L. et al. Engineering the singlet–triplet energy splitting in a TADF molecule. In: *J. Mater. Chem. C* [interaktyvus]. 2016. Vol. 4, no. 17, p. 3815–3824. Prieiga per internetą: <<http://xlink.rsc.org/?DOI=C5TC03849A>>.

154. WONG, M.Y. - ZYSMAN-COLMAN, E. Purely Organic Thermally Activated Delayed Fluorescence Materials for Organic Light-Emitting Diodes. In: *Advanced Materials* [interaktyvus]. 2017. Vol. 29, no. 22, p. 1605444. Prieiga per internetą:

- <<http://doi.wiley.com/10.1002/adma.201605444>>.
155. GOUSHI, K. et al. Organic light-emitting diodes employing efficient reverse intersystem crossing for triplet-to-singlet state conversion. In: *Nature Photonics* [interaktyvus]. 2012. Vol. 6, no. 4, p. 253–258. Prieiga per internetą: <<http://www.nature.com/articles/nphoton.2012.31>>.
156. ADACHI, C. et al. Nearly 100% internal phosphorescence efficiency in an organic light-emitting device. In: *Journal of Applied Physics* [interaktyvus]. 2001. Vol. 90, no. 10, p. 5048–5051. Prieiga per internetą: <<http://aip.scitation.org/doi/10.1063/1.1409582>>.
157. ETHERINGTON, M.K. et al. Revealing the spin–vibronic coupling mechanism of thermally activated delayed fluorescence. In: *Nature Communications* [interaktyvus]. 2016. Vol. 7, p. 13680. Prieiga per internetą: <<http://www.ncbi.nlm.nih.gov/pubmed/27901046>>.
158. DANYLIV, Y. et al. Derivatives of carbazole and chloropyridine exhibiting aggregation induced emission enhancement and deep-blue delayed fluorescence. In: *Dyes and Pigments* [interaktyvus]. 2018. Vol. 149, p. 588–596. Prieiga per internetą: <<https://www.sciencedirect.com/science/article/pii/S0143720817318144>>.
159. HU, J. et al. Linkage modes on phthaloyl/triphenylamine hybrid compounds: Multi-functional AIE luminogens, non-doped emitters and organic hosts for highly efficient solution-processed delayed fluorescence OLEDs. In: *Dyes and Pigments* [interaktyvus]. 2017. Vol. 137, p. 480–489. Prieiga per internetą: <<https://www.sciencedirect.com/science/article/pii/S014372081630763X>>.
160. GUO, J. et al. Achieving High-Performance Nondoped OLEDs with Extremely Small Efficiency Roll-Off by Combining Aggregation-Induced Emission and Thermally Activated Delayed Fluorescence. In: *Advanced Functional Materials* [interaktyvus]. 2017. Vol. 27, no. 13, p. 1606458. Prieiga per internetą: <<http://doi.wiley.com/10.1002/adfm.201606458>>.
161. WANG, H. et al. Novel Thermally Activated Delayed Fluorescence Materials-Thioxanthone Derivatives and Their Applications for Highly Efficient OLEDs. In: *Advanced Materials* [interaktyvus]. 2014. Vol. 26, no. 30, p. 5198–5204. Prieiga per internetą: <<http://doi.wiley.com/10.1002/adma.201401393>>.
162. FURUE, R. et al. Aggregation-Induced Delayed Fluorescence Based on Donor/Acceptor-Tethered Janus Carborane Triads: Unique Photophysical Properties of Nondoped OLEDs. In: *Angewandte Chemie International Edition* [interaktyvus]. 2016. Vol. 55, no. 25, p. 7171–7175. Prieiga per internetą: <<http://www.ncbi.nlm.nih.gov/pubmed/27145481>>.
163. SUN, K. et al. Novel aggregation-induced emission and thermally activated delayed fluorescence materials based on thianthrene-9,9',10,10'-tetraoxide derivatives. In: *RSC Advances* [interaktyvus]. 2016. Vol. 6, no. 26, p. 22137–22143. Prieiga per internetą: <<http://xlink.rsc.org/?DOI=C6RA03281H>>.
164. HUANG, BIN et al. Simple aggregation–induced delayed fluorescence materials based on anthraquinone derivatives for highly efficient solution–processed red OLEDs. In: *Journal of Luminescence* [interaktyvus]. 2017. Vol. 187, p. 414–420. Prieiga per internetą: <<https://www.sciencedirect.com/science/article/pii/S002223131631777X>>.
165. GUO, J. et al. Robust Luminescent Materials with Prominent Aggregation-Induced Emission and Thermally Activated Delayed Fluorescence for High-Performance Organic Light-Emitting Diodes. In: *Chemistry of Materials* [interaktyvus]. 2017. Vol. 29, no. 8, p. 3623–3631. Prieiga per internetą: <<http://pubs.acs.org/doi/10.1021/acs.chemmater.7b00450>>.
166. HUANG, B. et al. Bicolour electroluminescence of 2-(carbazol-9-yl)anthraquinone based on a solution process. In: *Journal of Materials Chemistry C* [interaktyvus]. 2017. Vol. 5, no. 46, p. 12031–12034. Prieiga per internetą:

<<http://xlink.rsc.org/?DOI=C7TC04444E>>.

167. CHERPAK, V.V. et al. 3,6-Di(9-carbazolyl)-9-(2-ethylhexyl)carbazole based single-layer blue organic light emitting diodes. In: *Synthetic Metals* [interaktyvus]. 2011. Vol. 161, no. 13–14, p. 1343–1346. Prieiga per internetą:

<<https://www.sciencedirect.com/science/article/abs/pii/S0379677911001779>>.

168. MÉHES, G. et al. Influence of host matrix on thermally-activated delayed fluorescence: Effects on emission lifetime, photoluminescence quantum yield, and device performance. In: *Organic Electronics* [interaktyvus]. 2014. Vol. 15, no. 9, p. 2027–2037. Prieiga per internetą:

<<https://www.sciencedirect.com/science/article/pii/S1566119914002067>>.

7. LIST OF PUBLICATIONS ON THE SUBJECT OF THE THESIS

1. **Grybauskaite-Kaminskiene, G.**, Ivaniuk, K., Bagdziunas, G., Turyk, P., Stakhira, P., Baryshnikov, G., Volyniuk, D., Cherpak, V., Minaev, B., Hotra, Z., Ågren, H., Grazulevicius, J.V. (2018). Contribution of TADF and exciplex emission for efficient “warm-white” OLEDs // Royal Society of Chemistry. 2018, vol. 6, pp. 1543-1550.
2. **Grybauskaite-Kaminskiene, G.**, Volyniuk, D., Mimaite, V., Bezvikonny, O., Bucinskas, A., Bagdziunas, G., Grazulevičius, J.V. (2018). Aggregation enhanced emission and thermally activated delayed fluorescence of derivatives of 9-phenyl-9H-carbazole: effects of methoxy and tert-butyl substituents // Chemistry – A European Journal. 2018, vol. 24, pp. 9581-9591.
3. Bagdziunas, G., **Grybauskaite-Kaminskiene, G.**, Kostiv, N., Ivaniuk, K., Volyniuk, D., Lazauskas, A. (2016). Green and red phosphorescent organic light emitting diodes with ambipolar hosts based on phenothiazine and carbazole moieties: photoelectrical properties, morphology and efficiency // RSC Advances. 2016, vol. 6, pp. 61544-61554.

8. LIST OF PRESENTATIONS AT INTERNATIONAL CONFERENCES

1. **Grybauskaite-Kaminskiene, G.**, Bagdziunas, Kostiv, N., Volyniuk, D., Grazulevicius, J.V. Synthesis of derivatives based on phenothiazine and carbazole moieties for optoelectronics // Advanced materials and technologies: book of abstracts of the 17th international conference-school, August 27-31, 2015, Palanga, Lithuania. Kaunas: Kauno technologijos universitetas. ISSN 1822-7759. 2015, p. 76.
2. **Grybauskaite-Kaminskiene, G.**, Bagdziunas, Kostiv, N., Volyniuk, D., Grazulevicius, J.V. Donor-acceptor derivatives of phenothiazine and carbazole as semiconductors for oleds // Baltic polymer symposium 2015 : Sigulda, Latvia, September 16-18 : programe and proceedings / Riga Technical University Institute of Polymer Materials. Riga: Riga Technical University Institute of Polymer Materials, 2015, ISBN 9789934542121. p. 99.
3. **Grybauskaite-Kaminskiene, G.**, Bagdziunas, G., Ivaniuk, K., Cherpak, V., Stakhira, P., Volyniuk, D., Gražulevičius, J.V. New efficient 3,3'-bicarbazole derivatives for light emitting devices: photophysical, photoelectrical and electroluminescent properties // Baltic polymer symposium 2016 : Klaipeda, September 21-24, 2016 : programme and abstracts / Kaunas University of Technology, Vilnius University, Klaipeda University. Kaunas: Kaunas University of Technology, 2016, ISBN 9786090212356. p. 90.
4. **Grybauskaite-Kaminskiene, G.**, Bagdziunas, G., Ivaniuk, K., Cherpak, V., Stakhira, P., Volyniuk, D., Gražulevicius, J.V. Efficient 3,3'-bicarbazole derivative based OLED with interfacial exciplex emission // ElecMol2016 : 8th international conference on molecular electronics, August 22-26, 2016, Paris, France : book of abstracts. Paris: Université Pierre et Marie Curie, 2016. p. 153.

5. **Grybauskaite-Kaminskiene, G.**, Bucinskas, A., Grazulevicius, J.V. Silicon-based electroactive compounds containing different donor moieties as potential hosts for organic light emitting diodes // Promising materials and processes in applied electrochemistry: monograph. Kyiv: KNUTD, 2017, pp. 3-3. ISBN 9789667972790.
6. **Grybauskaite-Kaminskiene, G.**, Bezikonnyi, O., Volyniuk, D., Bucinskas, A., Grazulevicius, J.V. Trifluoromethylbenzotrile substituted carbazoles for blue organic light emitting diode based on thermally activated delayed fluorescence. In: ERPOS 2017: 14th International Conference on Electrical and Related Properties of Organic Solids, July 9-13, 2017, University of St. Andrews, Scotland: programme and abstracts.
7. **Grybauskaite-Kaminskiene, G.**, Bezikonnyi, O., Volyniuk, D., Bucinskas, A., Grazulevicius, J.V. Novel bipolar molecules for efficient blue TADF organic light-emitting diodes. In: State of the Art in Organic-only TADF OLEDs. From Theory to Applications. XXIInd International Krutyn Summer School 2017 Krutyń, Masurian Lake District, Poland, May 21-27, 2017.

9. ACKNOWLEDGEMENTS

Prof. habil. dr. Juozas Vidas Gražulevičius is sincerely thanked for the consultations, useful advice and the opportunity to carry out the work at the Department of Polymer Chemistry and Technology.

All the colleagues of the research group are kindly thanked for the help and motivating working atmosphere.

My beloved husband and family are wholeheartedly thanked for the endless support.

SL344. 2019-07-05, 14,25 leidyb. apsk. l. Tiražas 12 egz. Užsakymas 155.
Išleido Kauno technologijos universitetas, K. Donelaičio g. 73, 44249 Kaunas
Spausdino leidyklos „Technologija“ spaustuvė, Studentų g. 54, 51424 Kaunas